

Faculty of Science, Charles University
Institute of Geochemistry, Mineralogy and Mineral Resources



USE AND LIMITATIONS OF LASER ABLATION ICP-MS IN GEOSCIENCE APPLICATIONS

Jitka Míková

Dissertation

Supervisor: Doc. RNDr. J. Košler, Ph.D.
Faculty of Mathematics and Natural Sciences, University of Bergen

Prague 2010

Statement of originality

The research presented in this dissertation is the result of my original scientific work, in collaboration with my supervisor and other colleagues. This dissertation represents work during my PhD. study at the Faculty of Science, Charles University.

To the best of my knowledge and belief, I declare that the results presented in my dissertation have not been published or presented by someone else. This dissertation has not been submitted for any other academic degrees at other university or educational institution.

Jitka Míková
Prague, October 2010

Statement on behalf of co-authors

On behalf of the co-authors I declare that scientific papers that constitute the present thesis submitted for Ph.D. degree by Jitka Míková are solely the work of those named in the respective lists of authors. The authors on each paper are named in the order that reflects their individual contributions to the scientific work of which the paper is a result (i.e., the principal author is always named as first in the list).

Jan Košler
2nd August 2010

Acknowledgments

I would like to thank to my supervisor Jan Košler who introduced me to the ICP-MS spectrometry, allowed me to work in the ICP-MS laboratory at Department of Geochemistry, Charles University and provided me scientific support during the whole course of my PhD. study. I also would like to thank him for giving me in cooperation with Rolf-Birger Pedersen the opportunity to join the ICP-MS lab with great team of geoscientists housed at University of Bergen in Norway.

I am also greatly indebted to Henry J. Longerich and Michael Wiedenbeck. I am grateful to Henry for his permanent interest in the fundamentals of laser ablation and numerous valuable remarks as well as for financial support. Michael is acknowledged for his kind approach and patience during introduction into the Secondary Ion Mass Spectrometry, for providing analytical data, and effective scientific collaboration.

I would like to thank to ICP-MS lab chief engineer Ole Tumyr and clean lab manager Yuval Ronen for their help with troubleshooting during my stays in Bergen. Of course, there are many others, my close colleagues in Prague and group of PhD students and post-docs in Bergen were fantastic and I thank all of them for sharing their time and ideas with me. Especially without Claudia Kruber and Heidi-Elisabeth Hansen it would not be such a pleasure to work on my doctorate at University of Bergen.

Last but not least, I would like to thank my family for their everlasting support. This thesis belongs to them in a great part.

Table of contents

Abstract	4
Chapter 1: Introduction	6
1.1 Laser ablation system.....	7
1.1.1 Laser	8
1.1.2 Ablation cell and transport system	9
1.1.3 Inductively coupled plasma (ICP)	10
1.2 Objectives of this study	11
Chapter 2: Chemical and phase composition of particles produced by laser ablation of silicate glass and zircon—implications for elemental fractionation during ICP-MS analysis	14
2.1 Abstract	14
2.2 Introduction	15
2.3 Experimental	17
2.3.1 Laser ablation ICP-MS	17
2.3.2 Particle size measurements and imaging	17
2.3.3 Measurements of particle chemical and phase composition	19
2.4 Results	20
2.4.1 Size distribution of ablated particles	20
2.4.2 Phase and major element composition of ablated particles	22
2.4.3 Trace element composition of particles in the ejecta blanket	24
2.4.4 Phase and chemical composition of zircon adjacent to the ablation pit	27
2.4.5 Effect of particle size selection on fractionation during laser ablation ICP-MS analysis	28
2.5. Discussion	30
2.5.1 Mechanism of Pb/U fractionation during laser ablation of zircon	31
2.5.2 Particle size selection for accurate laser ablation-ICP-MS analysis	32
2.6 Concluding remarks	33
2.7 Acknowledgements	34

Chapter 3: Fractionation of alkali elements during laser ablation ICP-MS	
analysis of silicate geological samples	35
3.1 Abstract	35
3.2 Introduction	36
3.3 Experimental	37
3.3.1 Sample preparation	37
3.3.2 Electron probe characterization of the albite samples	40
3.3.3 Laser ablation experiments	40
3.3.4 Secondary ion mass spectrometry experiments	41
3.4 Results	44
3.4.1 Laser ablation measurements	44
3.4.2 Ion probe measurements	46
3.4.2.1 <i>Analysis of the ejecta blanket</i>	46
3.4.2.2 <i>Depth profile analysis</i>	48
3.5. Discussion	51
3.5.1 Depth profile analyses	52
3.5.2 Ejecta blanket analyses	53
3.5.3 Laser ablation analyses	54
3.5.4 Effect of the crystallographic orientation	55
3.5.5 Correction for ablation yield	56
3.6 Concluding remarks	57
3.7 Acknowledgements	57
Chapter 4: Evaluation of matrix effects during laser ablation ICP-MS	
analysis of boron isotopes in tourmaline samples	58
4.1 Abstract	58
4.2 Introduction	59
4.3 Samples and experimental	61
4.3.1 Tourmaline samples	61
4.3.2 Laser parameters	62
4.3.3 MC ICP-MS parameters	63

4.3.4 SIMS parameters	64
4.4 Results	65
4.5 Discussion	72
4.5.1 Laser ablation MC ICP-MS.....	72
4.5.2 SIMS	76
4.5.3 Relative Merits of Laser ablation and SIMS	77
4.6 Conclusion	79
4.7 Acknowledgements	79
Chapter 5: Summary and outlook	80
References	83
Curriculum Vitae	93
Additional materials (<i>Full text articles are attached on CD</i>)	95

Abstract

This dissertation contributes to applications of laser ablation plasma source mass spectrometry (LA ICP-MS) in Earth sciences. The primary goal of the thesis is to address some of the fundamental processes related to laser ablation of solid samples that result in decoupling of elements during laser ablation ICP-MS analysis. Better understanding of mechanisms that cause the elemental fractionation and matrix effects is necessary before the accuracy and precision of laser ablation ICP-MS analyses can be improved.

The chemical and phase compositions of particles produced by laser ablation (266 nm Nd:YAG) of silicate NIST glasses and zircon were studied by SIMS and HR-TEM techniques with a particular focus on Pb/U fractionation. This is of great importance in geology as the Pb/U elemental fractionation hampered the precision and accuracy of the measured accessory mineral ages. The data suggest that chemical composition and mineralogy of particles produced at the ablation site during laser ablation differs from the original sample and varies with their size. This can result in elemental fractionation (non-stoichiometric sampling) in material delivered to the ICP-MS for quantitative analysis. Evidence of the element fractionation is preserved in chemically zoned ejecta deposited around the ablation pit. Evidence of the phase changes of zircon to baddeleyite and SiO₂ is preserved in the wall of the ablation pit, and may be responsible for the commonly observed increase in Pb/U ratio during laser ablation ICP-MS analysis. It implies that a matrix-matched external calibration is essential for achieving highly precise and accurate laser (266 nm wavelength) ablation ICP-MS analysis of Pb and U in silicate samples because mechanisms of Pb/U elemental fractionation are dependent on the phase and chemical composition of the ablated material.

Laser ablation ICP-MS and SIMS were used to determine differences in sample composition before and after laser interaction with the silicate reference glasses (NIST-610, BCR-2G, alkali element-doped andesite glasses), and crystalline mineral albite (NaAlSi₃O₈) with a particular focus on alkali elements fractionation. It has importance in the study of geological materials including geochronology (Rb–Sr, K–Ar) and thermobarometry. The fractionation trends of the alkali elements are different from those of other lithophile elements, and the rate of fractionation varies for different sample matrices and for different alkali elements in the same matrix. Data from SIMS analyses of the ejecta blanket suggest a matrix dependent fractionation of alkali

elements in different particle size fractions at ablation site. The extent of fractionation varies for different alkali elements and is independent of their ionic radii. SIMS depth profiling into the bottom of laser craters showed laser ablation-induced chemical changes in the sample that involved alkali elements and major matrix elements including Si and Ca. This suggests that a combination of thermally-driven diffusion and size-dependent particle fractionation is responsible for the observed fractionation of alkali elements during laser ablation of silicate samples.

Laser ablation MC ICP-MS and SIMS were used to determine the boron isotopic compositions of several natural tourmaline group minerals with variable chemical composition. This study evaluates the effects of laser ablation ICP-MS instrument parameters and sample matrix composition on data precision and accuracy. Isotopic composition of boron is a powerful tracer of various types of geochemical transfer and mixing processes. It was demonstrated that the tourmaline matrix affects significantly the obtained $\delta^{11}\text{B}$ values and impacts on data accuracy if a non matrix-matched reference material is used to calibrate ICP-MS analyses. Also the ICP-MS instrument parameters influence the measured $^{11}\text{B}/^{10}\text{B}$ ratios if the signal intensity varies between sample and reference material and by interference of $^{40}\text{Ar}^{4+}$ peak tail on ^{10}B mass. The relation of offset between the measured and expected $\delta^{11}\text{B}$ values to the composition of the reference material matrix remains same for all studied samples, suggesting a systematic matrix effect related to composition differences between the unknown tourmaline sample and reference tourmaline material. In case of matrix-matched calibration, the accuracy of LA MC ICP-MS boron isotopic data is comparable to the previously published values obtained by the TIMS technique. SIMS accuracy in this specific study is biased compare to TIMS values. The measurement precision associated with the average $\delta^{11}\text{B}$ values achieved by LA MC ICP-MS are about double compare to TIMS and are estimated between 0.2 and 0.5‰ (1s). SIMS precision in this specific study is estimated at 1.3‰ (1s).

Chapter 1: Introduction

Geological materials are complex, heterogeneous mixtures of minerals, often small grained and each with a different and variable composition. Study of these materials often demands an instrument capable of providing spatially resolved, *in situ* elemental or isotopic analyses with high sensitivity and multi-element capability. The laser ablation inductively coupled plasma mass spectrometry (LA ICP-MS) is adequate to the task and rivals other microbeam techniques such as the electron probe micro analysis (EPMA), secondary ion mass spectrometry (SIMS, or the "ion probe"), micro-particle-induced x-ray emission (micro-PIXE), synchrotron-x-ray fluorescence (SXRF), and accelerator mass spectrometry (AMS).

The first attempts to analyse solid samples with an infra-red ruby laser attached to an inductively coupled plasma mass spectrometer were made by Alan Gray (Gray, 1985) in the mid 1980s. Alan Gray's publication showed not only the great potential of the LA ICP-MS technique with respect to its detection capabilities and spatial resolution, but also its limitations, namely in analytical precision and accuracy. The landmark paper in application of laser ablation in the Earth sciences was the first comprehensive work on the use of LA ICP-MS for analysis of trace elements in minerals published by Jackson *et al.* (1992). They pointed out the important limitations of the ultra-violet laser wavelength for minerals with a variety of optical properties and outlined the most suitable calibration strategy for element concentration measurements. This approach was further developed by Longerich *et al.* (1996b), who presented calculation procedures that are routinely used today. These studies (Jackson *et al.*, 1992; Longerich *et al.*, 1996b) demonstrated that significant improvements in laser technology and ICP mass spectrometry as well as entirely new calibration strategies would have to be developed in order to achieve the precision and accuracy required for applications such as isotopic analysis of geological samples.

Nowadays the LA ICP-MS is one of the most frequently used techniques for in-situ analysis and is considered to be a routine method for element and isotope-specific analyses of various solid samples (Becker *et al.*, 2000; Becker, 2002; Becker and Dietze, 2000; Durrant, 1999; Gunther *et al.*, 1999; Horn *et al.*, 2006; Poitrasson *et al.*, 2003). The broad interest in LA ICP-MS is mainly due to its capability of direct micro-analysis, conceptual simplicity, a high degree of

flexibility and the technological progress in laser and ICP–MS instrumentation during the last two decades.

1.1 Laser ablation system

The laser ablation sampling is based on interactions of focused short pulsed high power laser beam with a solid, *e.g.*, geological sample. The sample is eroded and vaporized during a complex process that involves formation and ejection of atoms, ions, molecules, melt droplets and solid particles (Darke and Tyson, 1993; Durrant, 1999). The laser ablated aerosol is transported to the ICP discharge for atomization and ionization followed by analysis of these ions in a mass spectrometer.

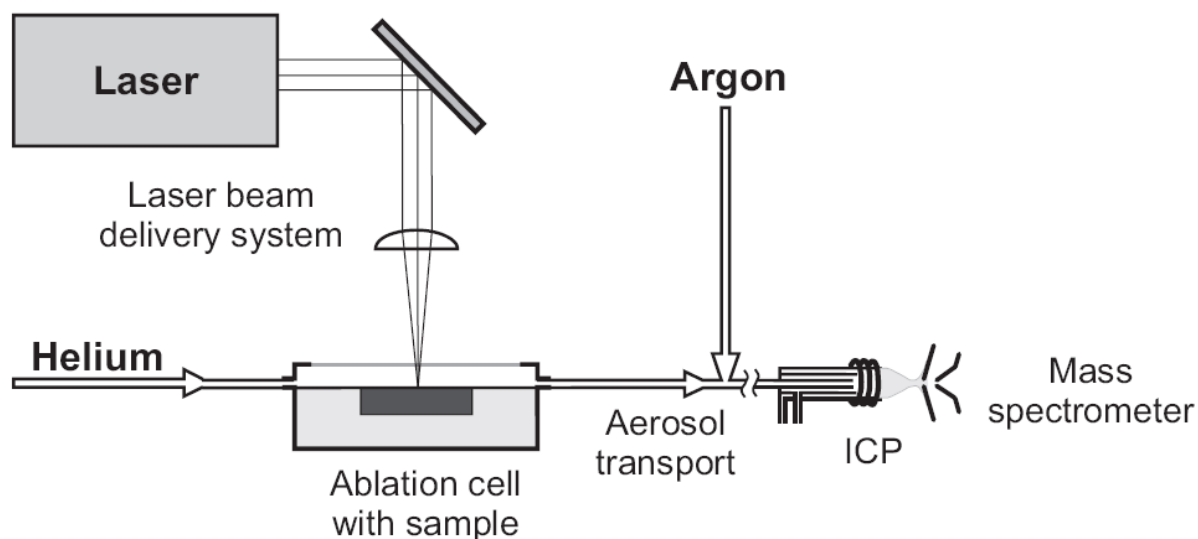


Fig. 1.1: Schematics of a laser ablation system

Most laser ablation systems consist of four parts (Fig. 1.1): (i) a laser (light amplification by stimulated emission of radiation) source that generates a beam of high energy photons; (ii) laser beam delivery system that modifies the laser wavelength, energy, shape and diameter of the beam and focuses it on to the sample surface; (iii) ablation cell where the laser beam interacts with the solid target (sample), producing an aerosol of particles; and (iv) a transport system for transferring the ablated aerosol to the ICP source of a mass spectrometer.

1.1.1 Laser

A laser consists of a laser gain medium (material with properties that enable light amplification by stimulated emission) inside a highly reflective optical cavity and energy supply to the laser gain medium. Lasers used commonly in geological applications are based on light amplification in gaseous or solid-state laser gain media. The light of a specific wavelength that passes through the gain medium is amplified by interaction with atoms or molecules whose excitation state in the active gain media is maintained by external pumping of light (*i.e.* forming an inverse population of atoms). Absorption of photons with energy that is equal to the difference between the excited and ground state triggers decay and emission of photons with the same energy and direction. This process is called stimulated emission and it results in amplification of a highly directed light (lasing effect).

The most frequently used gas laser in LA ICP-MS is the excimer (excited dimmer gas molecule) (Günther et al., 1997; Horn et al., 2000; Loucks et al., 1995). Its operation is based on electronic transitions in diatomic molecules of noble gases and halides. The important dimmer molecules and their fundamental wavelengths are Xe-F (351 nm), Xe-Cl (308 nm), Kr-F (248 nm), Ar-F (193 nm) and F-F (157 nm); however, only the 193 nm Ar-F excimer laser has been widely used for laser ablation ICP-MS of geological samples (Horn et al., 2000; Sylvester and Ghaderi, 1997).

The most widely used are solid state lasers, especially the yttrium-aluminum garnet ($\text{Y}_3\text{Al}_5\text{O}_{12}$) doped with ca 1% Nd^{3+} (Nd: YAG) because they require little maintenance and are easily incorporated into small commercial ablation systems. The fundamental wavelength of the Nd: YAG laser is 1064 nm (IR), which is not suitable for sampling of most geological materials because this wavelength is poorly absorbed by many geological sample matrices (Jackson et al., 1992). The conversion to shorter UV wavelengths is achieved by passing the laser light through harmonic generators (optically nonlinear crystals) that can be combined in a series to produce output wavelengths of 532, 355, 266, 213 and 193 nm. The choice of wavelength for LA has been widely discussed in the literature (Geertsen et al., 1994; Gonzalez et al., 2002; Guillong et al., 2003a; Horn et al., 2001; Jeffries et al., 1995). Generally, it is the amount of laser energy absorbed by the sample surface (or near-surface volume), that controls the ablation yield and hence the analytical response while absorption of laser energy by sample is laser wavelength

dependent. Nd: YAG systems employing wavelengths of 266 nm, 213 nm and, increasingly, 193 nm have been used most widely for geological applications.

Not only the laser wavelength but also the laser pulse duration is an important parameter influencing analytical performance. Several authors have recently reported on the use of femtosecond lasers (*c.* 100 femtosecond pulse duration) for ablation of geological samples (Horn and von Blanckenburg, 2005; Poitrasson et al., 2005). Compared to nanosecond lasers, ablation with a femtosecond laser minimizes the volume of heat affected zone of the sample, which reduces melting and other thermal reactions at the ablation site, resulting in a more homogeneous particle size distribution, more stable analytical signals and reduction of elemental and isotopic fractionation (time-dependent decoupling of elemental and isotopic pairs in the analytical signal during the ablation process).

1.1.2 Ablation cell and transport system

The ablation cell with sample is often mounted on an adjustable platform which allows for positioning of the sample in the X, Y and Z directions under computer control. The laser beam enters the cell through a non-absorbing transparent window to interact with the sample surface and to produce a fine aerosol of ablated particles. The cell is flushed with an inert gas to transport the ablated sample to the ICP. Efficient transport of aerosol through the ablation cell is important for achieving a stable and high intensity signal in ICP-MS. Hence the use of different gases (*e.g.* He, Ar-N₂ and Ar-He mixtures) to flush the ablated sample from the cell has been tested. It has been demonstrated that ablation in gases with low density and high thermal conductivity and ionization potential, such as He, reduces elemental fractionation in the ablation cell and improves the aerosol transport properties (Garcia et al., 2008; Horn and Günther, 2003; Mank and Mason, 1999; Russo, 1995).

Also a variety of different ablation cell designs have been developed and tested in the past (Garcia et al., 2007; Günther et al., 2000; Gurevich and Hergenröder, 2007; Monticelli et al., 2009). The ablation chamber geometry and the connective transport tubing play an important role as they can influence the flow characteristics of the carrier gas. They affect the overall transport efficiency and the measured signal profile. The whole setup should minimize aerosol losses and allow for rapid aerosol transport from the ablation site to the ICP source. The effect of setup geometry on the signal profile was experimentally studied by several authors (Bleiner, 2002;

Bleiner and Günther, 2001; Leach and Hieftje, 2002; Moenke-Blankenburg, 1993; Moenke-Blankenburg et al., 2010; Ruzicka and Hansen, 1988). Based on experimental data from a number of cell designs, theoretical models of transport efficiency and temporal intensity distribution of measured signal were proposed (Bleiner, 2002; Bleiner and Bogaerts, 2006; Bleiner and Bogaerts, 2007; Bleiner and Gunther, 2001; Gackle and Merten, 2004; Gackle and Merten, 2005; Garcia et al., 2007; Koch et al., 2004a; Plotnikov et al., 2002). They can be used to assist in further development and optimization of laser ablation systems.

1.1.3 Inductively coupled plasma (ICP)

The ablated sample aerosol is converted to atoms and ions at temperatures of 8000-10 000 K in the ICP and the abundances of elements and isotopes are detected by a mass spectrometer.

It has been shown that the size, phase and chemical composition and structure of the ablated particles have significant influence on the vaporization, atomization and ionization within the ICP (Aeschliman et al., 2003; Kuhn and Günther, 2004). Accordingly, the size dependent composition and incomplete vaporization of particles within the ICP can result in elemental (and isotopic) fractionation effects. Based on this, matrix matched calibration (Guillong and Günther, 2002; Jackson et al., 2004; Košler et al., 2005b) or matching in particle size distribution (by similar absorbance of sample and standard) has been proposed for precise and accurate quantification. The incomplete conversion of particles into ions in the plasma is an important effect which occurs in the ICP. However, sample matrix-induced changes in signal intensities (enhancement or suppression) are yet another source of uncertainty influencing the analytical performance which has been reported for LA ICP-MS (Jackson et al., 2004; Košler et al., 2005b). The matrix effects are generally defined as a change in signal intensity of analytes as a function of abundance of concomitant ions in the ICP. These effects are normally corrected for using internal standardization (Vandecasteele et al., 1988; Vanhaecke et al., 1992). Standard addition and isotope dilution have also been applied to reduce the influence of the matrix (Heumann, 2004; Riondato et al., 2000). A review containing almost 400 references to the pioneering studies of matrix effects in ICP-MS can be found in Evans and Giglio (1993). However, the fundamental reasons for the matrix effects in ICP-MS are not well understood. Some insight into the occurrence of matrix effects in laser ablation sampling were provided by study of mass load induced matrix effects within the plasma (Krosiakova and Günther, 2007). It has been shown that

these effects were most severe for elements with low melting points and that the matrix effects become less severe after aerosol dilution. Changes in mass load can influence ion sampling efficiency and accordingly, accurate quantitative analyses should only be carried out using identical laser parameters for standards and samples while similar absorptivity of sample and standard will not only provide a similar particle size distribution, but also a similar mass load of the plasma.

1.2 Objectives of this study

Several authors (Borisov et al., 2000; Cromwell and Arrowsmith, 1995; Jackson et al., 2004; Košler et al., 2005b; Kuhn and Günther, 2003; Kuhn and Günther, 2004; Liu et al., 2005; Liu et al., 2000; Mank and Mason, 1999; Outridge et al., 1996; Outridge et al., 1997; Poitrasson et al., 2003; Poitrasson et al., 2005; Russo et al., 2000; Saetveit et al., 2008) have reported on non-representative sampling or temporal changes in elemental responses during LA which were found to affect accuracy of the measurements. This effect commonly referred to as “elemental fractionation”, represents a limiting factor for precision and accuracy of analyses based on non-matrix-matched calibration.

The process of non-stoichiometric sampling during high-power irradiation has triggered an interest in the fundamentals of laser-assisted micro-sampling. Increasingly more studies are devoted to the investigation of laser-induced particle formation, their size distribution and composition, fractionation processes and matrix effects (Bleiner et al., 2005; Bleiner, 2005; Guillong et al., 2003a; Guillong et al., 2003b; Guillong and Günther, 2002; Horn and Günther, 2003; Koch et al., 2004b; Košler et al., 2005b; Kuhn and Günther, 2004; Liu et al., 2005; Marton et al., 2003; Motelica-Heino et al., 2001).

The aim of this study was to investigate influence of fractionation and matrix effects for some geologically important applications of LA ICP-MS and to address some of the fundamental processes related to laser ablation of solid samples that result in decoupling of elements during laser ablation ICP-MS analysis.

Isotopic determination of accessory mineral ages, especially dating based on radioactive decay of uranium to lead in the accessory mineral zircon (ZrSiO_4) is of great importance in geosciences. Since the first attempts to use LA ICP-MS for isotopic dating of zircons (Feng et al.,

1993; Fryer et al., 1993; Hirata and Nesbitt, 1995; Jackson et al., 1996), the effects the Pb/U elemental fractionation hampered the precision and accuracy of the measured ages. Various approaches have been tested to reduce the Pb/U elemental fractionation (Hirata, 1997; Hirata, 2003; Parrish et al., 1999) but they did not succeed in eliminating it completely. Clearly, a better understanding of mechanisms that cause the elemental fractionation is necessary before the accuracy and precision of laser ablation ICP-MS U-Pb dating can be improved.

Chapter 2 reports on a study of chemical and phase composition of particles produced by laser ablation of silicate reference glass NIST 610 and zircon, with a particular focus on Pb/U fractionation. An important observation was that laser ablation of different silicate samples under identical experimental conditions produced aerosols with different size distributions of particles. These particles can vary in their phase and chemical composition and the elimination of the different particle size fractions from analysis can significantly influence the elemental fractionation. The mechanisms of Pb/U elemental fractionation are dependent on the phase and chemical composition of the ablated material.

Determination of alkali elements is of great importance in the study of geological materials including geochronology (Rb–Sr, K–Ar) and thermobarometry. The alkali elements (Li, Na, K, Rb, and Cs) are commonly present as major or minor constituents in silicate minerals and natural and synthetic glasses. The first comprehensive description of elemental fractionation in LA ICP-MS was published in 1995 (Fryer et al., 1995), describing the time dependent behaviour of intensity ratios (relative to Ca intensity) and defining the fractionation index as a relative measure of fractionation. It has been also demonstrated that fractionation behaviour of elements generally follows the geochemical classification of elements (Longerich et al., 1996a), with the exception of alkali elements (esp. Li, Rb, and Cs) which do not fractionate similar to other lithophile elements. A study that addresses some of the phenomena affecting alkali elements fractionation in LA ICP-MS is described in the Chapter 3. Understanding alkali element fractionation during laser ablation ICP-MS is important not only for improving the precision and accuracy of alkali element determinations, but also because alkali elements can be used as internal standards to correct for variations in ablation yield during analysis of other elements.

This study reveals that a significant part of the fractionation of alkali elements takes place on the ablation site and that the concentration of individual alkali elements has an effect on the rate of elemental fractionation. The important conclusion of this study is that spatial distribution of

elements used for corrections of ablation yield (isotopes of Si and Ca) is strongly influenced by thermal effects introduced to the sample by the ablation process.

Isotopic composition of boron is a powerful tracer of various types of geochemical transfer and mixing processes. Difficulties associated with sample decomposition and ion exchange separation of boron prior to mass spectrometric measurement, as well as the requirement for high spatial resolution in some geological applications, lead to development of laser ablation multicollector ICP-MS for boron isotope ratio measurements (le Roux et al., 2004; Tiepolo et al., 2006). The technique has been applied only to natural and synthetic glasses so far, and further work was required on rocks and minerals in order to evaluate possible matrix effects (le Roux et al., 2004). Tourmaline as important boron reservoir in many crustal rocks was chosen for the study presented in Chapter 4.

This study revealed that matrix effects play an important role in laser ablation analyses of boron isotopic composition of tourmalines and the analytical results are influenced by the chemical matrix and structure of the samples. In addition, the ICP-MS instrument parameters can influence the measured $^{11}\text{B}/^{10}\text{B}$ ratios if the signal intensity is different for sample and reference material and by interference of $^{40}\text{Ar}^{4+}$ peak tail on ^{10}B mass.

Chapter 2: Chemical and phase composition of particles produced by laser ablation of silicate glass and zircon—implications for elemental fractionation during ICP-MS analysis

Jan Košler ¹, Michael Wiedenbeck ², Richard Wirth ², Jan Hovorka ¹, Paul Sylvester ³

Jitka Míková ¹

¹ *Charles University, CZ-128 43 Prague, Czech Republic*

² *GeoForschungsZentrum Potsdam, D-14473 Potsdam, Germany*

³ *Earth Sciences Department, Memorial University, St John's, NL, Canada A1B 3X5*

Status: Published in *Journal of Analytical Atomic Spectrometry*, 2005, 20, 1-8

2.1 Abstract

The chemical and phase compositions of particles produced by laser ablation (266 nm Nd:YAG) of silicate NIST glasses and zircon were studied by SIMS and HR-TEM techniques. The data suggest that the formation of phases of different mineralogy and/or chemical composition from the original sample at the ablation site can result in elemental fractionation (non-stoichiometric sampling) in material delivered to the ICP-MS for quantitative analysis. Evidence of the element fractionation is preserved in chemically zoned ejecta deposited around the ablation pit. The chemical composition and mineralogy of particles varies with particle size so that the efficiency of transport of particles also plays a role in elemental fractionation. During the first 250 pulses in a typical ablation experiment using a 266 nm laser, particle sizes are mainly <2.5 μm ; thereafter they decrease to <0.3 μm . Pb and U are fractionated significantly during the ablation of both silicate glass and zircon. During the ablation of glass, both micron-sized, melt-derived, spherical particles, and nm-sized, condensate-derived particle clusters, are produced; the very smallest particles (<0.04 μm) have anomalously high Pb/U ratios. For zircon, both larger (0.2–0.5 μm) spherical particles and agglomerates of smaller (~0.005 μm) particles produced by ablation are mixtures of amorphous and crystalline materials, probably zircon, baddeleyite (ZrO_2)

and SiO₂. Evidence for thermal decomposition of zircon to baddeleyite and SiO₂ is preserved in the wall of the ablation pit, and may lead to the commonly observed increase in Pb/U recorded during laser ablation ICP-MS analysis. It follows that a matrix-matched external calibration is essential for achieving highly precise and accurate laser (266 nm wavelength) ablation ICP-MS analysis of Pb and U in silicate samples.

2.2 Introduction

During laser ablation ICP-MS analysis, there is a progressive change in the ratios of measured signals of certain element pairs with increasing number of laser pulses applied to the sample. This phenomenon is referred to as elemental fractionation, and is most severe for pairs of elements that have large differences in volatility (boiling or melting points) or geochemical affinity: (Fryer et al., 1995; Kuhn and Günther, 2003; Outridge et al., 1997) however, other sample properties, such as the phase composition, and mechanisms such as phase transformations and zone refinement during the ablation, may also contribute to the observed elemental fractionation (see discussion in Outridge *et al.* (1997)). The accuracy and precision of measurements for certain applications of laser ablation ICPMS are compromised by element fractionation. In particular, in the earth sciences, Pb/U fractionation may affect the reliability of geochronological determinations based on radioactive decay of uranium to lead in the accessory mineral zircon (ZrSiO₄) (Košler and Sylvester, 2003). Complex corrections and sampling strategies are often required to reduce the effect of Pb/U elemental fractionation and to obtain accurate geochronological results (Horn et al., 2000; Jackson et al., 2004; Košler et al., 2002a).

The complexity of the physical and chemical processes related to laser ablation of solid samples has so far prevented a detailed understanding of mechanisms that result in decoupling of particular elements during laser ablation ICP-MS analysis. Fractionation may occur at the ablation site, during the transport of ablated material to the plasma source of ICPMS, and in the plasma itself (by incomplete volatilization of delivered particles). The size distribution of particles produced during laser ablation is thought to exert a significant control on the nature and size of elemental fractionation (Aeschliman et al., 2003; Guillong et al., 2003a; Guillong et al., 2003b; Guillong and Günther, 2002; Jackson and Günther, 2003; Kozlov et al., 2003; Kuhn et al., 2004; Kuhn and Günther, 2003; Kuhn and Günther, 2004). Major factors affecting the size

distribution of particles reaching the ICP are: the fluence (Horn et al., 2001; Jeong et al., 1999), wavelength (Guillong et al., 2003a; Jeffries et al., 1998), and pulse duration of laser radiation (Koch et al., 2004b; Russo et al., 2002); the aspect ratio of laser pit (Eggins et al., 1998; Mank and Mason, 1999), the composition of the sample carrier gas (Günther and Heinrich, 1999; Horn and Günther, 2003; Košler et al., 2002b); and the size-dependent transport efficiency of the ablated particles (Jackson and Günther, 2003). Particles with diameters below 0.5 μm are transported with high efficiency to the ICP and are thus most completely atomized and ionized in the plasma. It has also been suggested that the critical size of particles that are completely atomized and ionized in the ICP varies with their composition (Kuhn et al., 2004; Kuhn and Günther, 2003). Temperatures of particle atomization are largely determined by their boiling temperatures; it can be anticipated that the critical particle size of copper particles in He^3 (0.6–0.9 μm , boiling at 2575 °C) will be similar to the critical particle size of aerosol produced by ablation of silicate glass (SiO_2 boiling at 2230 °C). Similarly, the critical particle size of aerosol produced by ablation of zircon would probably be smaller as ZrSiO_4 decomposes to ZrO_2 and SiO_2 at *ca.* 1540 °C, and ZrO_2 boils off at 4275 °C. Coarse particles (>1.0 μm) may be deposited as a thin deposit (ejecta blanket) on the sample surface around the pit, or most effectively trapped in the sample transport system (Koch et al., 2002). An outstanding issue is whether the chemical and phase compositions of ablated particles vary with their size distribution (Košler et al., 2004; Kuhn et al., 2004; Kuhn and Günther, 2004; Liu et al., 2005) and which mechanisms may cause such variations (Košler et al., 2004). A better understanding of particle properties will help identify the dominant processes responsible for elemental fractionation.

Here we report the results of a study of phase and chemical compositions of different size fractions of particles produced by laser ablation of NIST 610/612 silicate glasses and 91 500 zircon, focusing particularly on Pb/U fractionation. Various micro-beam techniques were used to determine the composition of particles deposited on the sample surface and of particles collected in the sample carrier gas tube before the ICP in order to evaluate the effects of elemental fractionation at the ablation site and during the transport of ablated aerosol to the ICP. In addition, the phase and chemical composition of the inner walls of an ablation pit were examined by high resolution transmission electron microscopy (HR-TEM), using a Ga-focused ion beam technique (FIB) (Bleiner and Gasser, 2004; Overwijk et al., 1993). Ablations were carried out using a laser emitting with a 266 nm wavelength because previous studies have shown that lasers with shorter

wavelengths may produce less pronounced element fractionation phenomenon (Horn et al., 2001; Telouk et al., 2003).

2.3 Experimental

2.3.1 Laser ablation ICP-MS

The laser ablation system used in this study was a 266 nm Nd:YAG Continuum Minilite laser that is part of a VG Elemental Microprobe 1 ablation system. The laser was focused 100 μm above the sample surface and fired at 10 Hz repetition rate. The laser energy was 1 mJ per pulse (measured before the laser beam entered the objective of the microscope) and the laser pit size varied from 40–60 μm .

The sample was mounted in a PTFE holder that was placed in a 25 cm^3 quartz glass cell mounted on the motorized stage of the microscope. Helium gas (99.9999% purity, the flow rate through the ablation cell varied between 1–1.4 l min^{-1} , subject to the experimental setup) was used to flush the sample cell; it was then brought in a PFA tube to a T-piece mounted at the back end of the ICP torch, where it was mixed with Ar (0.9 l min^{-1}) before forming the plasma. The ICP-MS instrument used in this study was the VG Elemental PlasmaQuad 3 at Charles University. It was operated in peak jumping mode with one point measured per peak for masses 206 (Pb), 208 (Pb), 232 (Th) and 238 (U). Data were acquired in time resolved mode with quadrupole settling and dwell times of 1 and 10.24 ms, respectively.

2.3.2 Particle size measurements and imaging

For simultaneous measurement of U, Th and Pb signal intensities and particle size distribution, the laser He-gas line (1.4 l min^{-1}) was split in a Y-piece, with one line going to the ICP (1 l min^{-1}) and the other to a particle sizer attached to a particle counter (0.4 l min^{-1}). To achieve the optimum gas flow for the particle sizer (*ca.* 5.2 l min^{-1}), a zero air filter and a mass flow controller were connected via a T-piece to the gas line between the Y-piece and the particle sizer (Fig. 2.1). The He/air ratio was lower than 0.08; the increase of the gas viscosity and temperature conductivity due to the presence of He, which influence the particle size-separation characteristics of the particle sizer and increase the efficiency of the particle detection, were very small and, accordingly, no correction for the presence of He was employed.

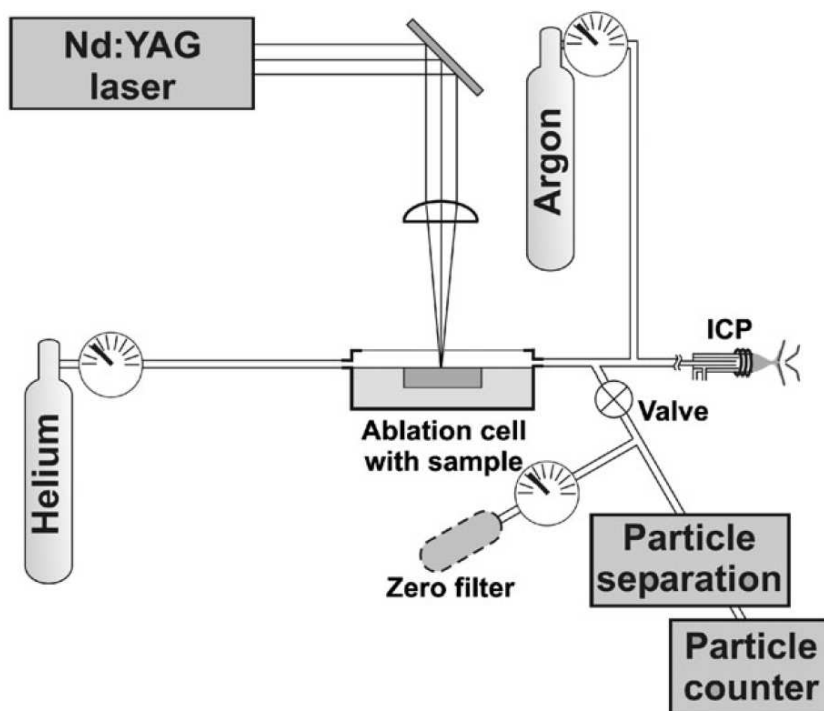


Fig. 2.1: Schematic diagram of experimental setup for simultaneous particle counting and ICP-MS analysis.

Temporal variations of mass concentrations of particles in three different size ranges ($<1.0 \mu\text{m}$, $<2.5 \mu\text{m}$, $<10 \mu\text{m}$) were successively determined by a Thermo-Systems Inc. (TSI) DustTrak 8520 laser photometer. The size distribution of particles between $0.003\text{--}0.2 \mu\text{m}$ was determined using a previously calibrated TSI Model 3040 Diffusion Battery coupled to a TSI 3025A Ultrafine Condensation Particle Counter. Thus, a broad size spectrum of particles (nm- to μm -sized) could be detected. Commercially available particle selection devices were used to study the effect of particle size on the slope of the Pb/U fractionation trend. In these experiments, the lower size cut-off of particles was controlled by a TSI 376060 Particle Size Selector. The upper particle cut-off was controlled by a stainless steel impactor such as is used in the TSI Scanning Mobility Particle Sizer. Both the lower and the upper cut-offs were of 50% efficiency. Nevertheless, the impactor penetration curve is very steep and the penetration of a particle larger than the upper cut-off has a very low probability. For the upper cut-off of $0.35 \mu\text{m}$ this was also confirmed by measurements of close to zero counts using a laser photometer that has a real lower detection limit of $0.2 \mu\text{m}$. The particle measurements used did not take into account the shape of

particles (or their clusters) in the aerosol and spherical or near-spherical particles were assumed throughout this study. We have also considered the potential agglomeration of particles due to a pressure build-up at the impactor. However, the increase in pressure was too small to cause significant particle agglomeration; such small pressure variations may induce large variation of aerosol size characteristics only in the early stages of aerosol formation, up to 0.1 s after the laser pulse, due to the gas cooling (Friedlander, 2000; Ullmann et al., 2002). To induce subsequent changes in the aerosol sizes, much higher changes of pressure would be required (Sasaki et al., 1998).

Shape and size of ablated particles were studied by imaging individual particles or their clusters collected on a TEM membrane placed in the He carrier gas line *ca.* 100 cm after the ablation cell. A scanning electron microscope (DSM-962/Zeiss) and Philips CM200 high-resolution transmission electron microscope at GFZ Potsdam were used to image the collected particles.

2.3.3 Measurements of particle chemical and phase composition

The Cameca ims 6f SIMS in Potsdam was used to conduct point profiles extending from immediately at the edge of the laser ablation pit, radially outwards to beyond the edge of the ejecta deposit. Sample preparation involved sputtering a ~50 nm thick, high purity gold coat directly onto the ejecta. This procedure did not cause any visible change in the ejecta deposit, which remained clearly visible after the gold coat. Despite the granular nature of the ejecta, this approach provided adequate electrical conductivity for the subsequent SIMS analyses.

The SIMS measurements employed a 5 nA, 12.5 kV $^{16}\text{O}^-$ primary beam that was focused to a *circa* 20 μm diameter spot. A 3 min, unrastered preburn was conducted prior to each measurement in order to penetrate the gold coat and establish equilibrium sputtering conditions. In the case of the NIST 610 glass sample, the mass spectrometer was operated at $m/\delta m \approx 4100$, whereas in the case of 91 500 zircon, $m/\delta m \approx 4900$ was employed, so as to eliminate the molecular interferences inherent to the zircon Pb mass spectrum. A single spot analysis lasted 44 min in the case of the glass and 29 min in the case of zircon. However, only the data from the first 22 min of the NIST glass analysis were considered for further evaluation. Given the conditions used and the duration of the data acquisition, a crater depth of less than 1 μm would be

expected for both silicate materials analyzed in this study. After each analysis was completed the stage stepping motors automatically moved the sample 25 μm , and the next analysis was performed. This stepping sequence was continued until the edge of the ejecta was reached and traversed by several additional analyses. At this point a large step of several hundred micrometers was made in order to conduct the final analyses on the clearly pristine sample surface.

Changes in mineralogy and chemical composition due to the thermal effect produced by laser radiation adjacent to the ablation pit were studied by TEM on a thin slice of zircon sampled using a focused ion beam (FIB) technique. The FIB technique (Overwijk et al., 1993) uses accelerated Ga-ions to sputter material from the target. We used an FEI FIB200 instrument operated with an acceleration voltage of 30 kV at the GFZ Potsdam to cut electron transparent foils ($20 \times 10 \times 0.12 \mu\text{m}$) from the zircon reference sample 91 500. The foils were cut tangentially to the edge of the laser ablation pit in such a way that they included both the rim/inner wall of the pit and the pristine zircon away from the pit. The foils were then removed from the sample and placed onto a perforated TEM carbon grid. The TEM study was performed using a Philips CM200 electron microscope operated at 200 kV with a LaB_6 electron source and with no additional sample coating. Chemical analyses were carried out with an energy dispersive EDAX X-ray analyzer in STEM mode. The spot size was *ca.* 4 nm, the depth of the excitation was equal to the thickness of the sample (*ca.* 50–80 nm) and the acquisition time was 200 s. The uncertainty of individual major element analyses (at 20 wt% element content) of individual particles or particle clusters was better than 5% (1 RSD).

2.4 Results

2.4.1 Size distribution of ablated particles

The laser photometric measurements of particle size distribution in this and in previous studies suggest that the particles generated by laser ablation of silicates show a systematic change in their size distribution during the ablation (Guillong and Günther, 2002; Jackson and Gunther, 2003). Our measurements of particle mass concentration for three size fractions ($<10 \mu\text{m}$, $<2.5 \mu\text{m}$ and $<1 \mu\text{m}$) using a DustTrak laser photometer suggest that approximately 50% of the mass of material transported to the ICP during the first 250 pulses in a typical laser ablation experiment is present as particles that are smaller than 1 μm . The particle size of the remaining 50% of

ablated mass varies between 1–2.5 μm . Following the release of coarse particles during the initial 250 laser pulses, the average particle size decreases to less than 0.3 μm . SEM imaging of particles larger than 0.3 μm collected on an impaction plate of the DustTrak laser photometer suggests that they are mostly spherical to oval melt droplets and fragments derived directly from the ablated sample (Fig. 2.2).

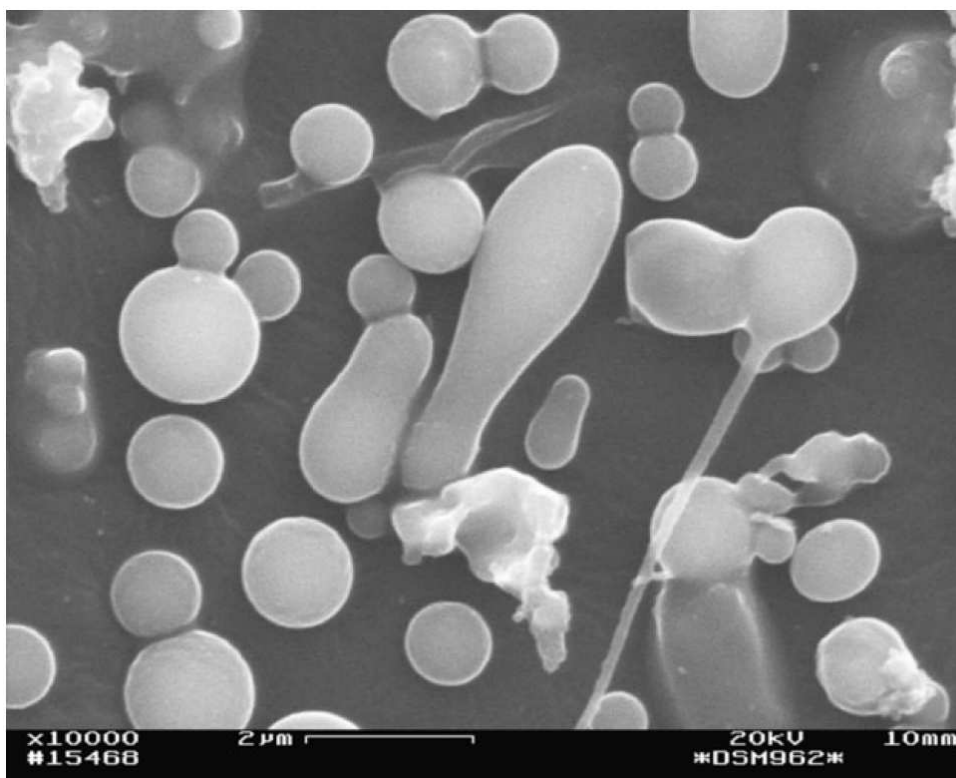


Fig. 2.2: SEM image of particles larger than 0.3 μm produced by laser ablation of the NIST 612 silicate glass. The particles were collected on an impaction plate of the DustTrak laser photometer ca. 100 cm from the ablation cell.

The size distribution of particles smaller than 0.3 μm was measured by a condensation particle counter attached to a diffusion battery. The measurements suggest the presence of several particle size maxima at 0.005, 0.025 and 0.1 μm (Fig. 2.3A). Our data from more than 50 particle size distribution measurements of ablated aerosol from the NIST 612 glass suggest that the reproducibilities of the peak height and position were better than 12.5 and 5% (1 RSD), respectively. A cluster of particles from the smallest fraction was collected on a TEM membrane and its TEM image (Fig. 2.3B) shows that the small individual particles are also spherical to oval

with a diameter of *ca.* 0.005 μm . This may be the size of most primary particles, corresponding to the size distribution maxima at 0.005 μm . The TEM observations also suggest that the primary particles aggregate to form larger clusters that vary in size from 0.0X μm to few micrometres (see Fig. 2.4B). However, as a result of particle agglomeration on the TEM membrane, the maximum size of the agglomerates observed in the TEM is likely to be larger than the size of agglomerates that form in the ablated aerosol. The size maxima at 0.025 and 0.100 μm may therefore reflect the presence of particle clusters formed by the primary particles. Unlike the larger particles formed by sample melting (melt splashing), the nanometer-sized particles are likely to have formed as condensates from the vapor phase produced during the ablation process (Kozlov et al., 2003).

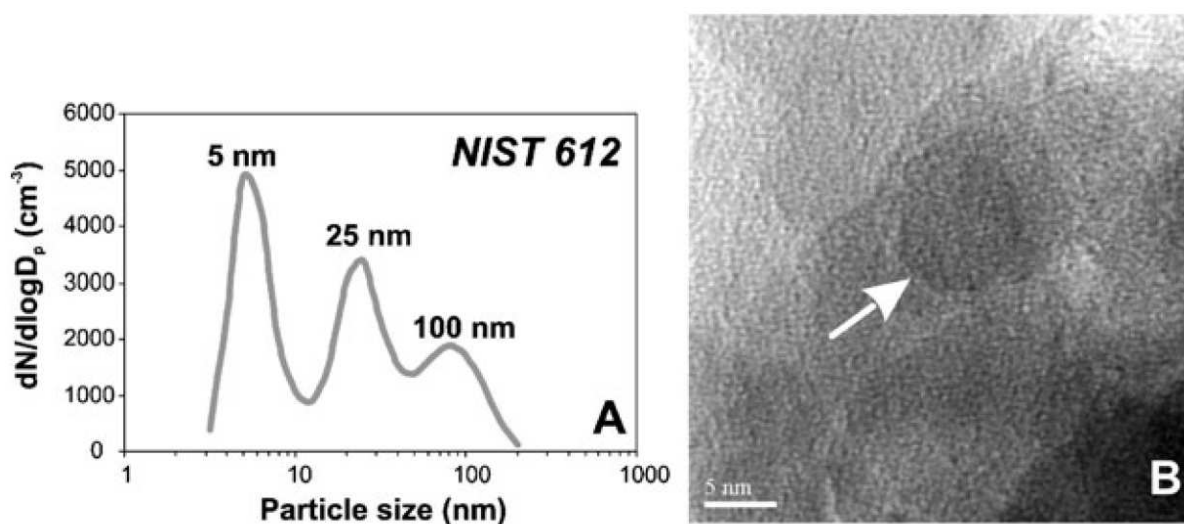


Fig. 2.3: **A**, Aerosol number size distribution plot for particles smaller than 0.3 mm produced by laser ablation of the NIST 612 silicate glass. N corresponds to the number of particles, D_p is their aerodynamic diameter. The total number of counts was 3.64×10^4 , reproducibility of the peak height and position were 12.5% and 5%, respectively (1 RSD). Data are from the measurement by a condensation particle counter attached to a diffusion battery. **B**, A TEM image of particle cluster showing an individual particle collected on a TEM membrane *ca.* 100 cm from the ablation cell.

2.4.2 Phase and major element composition of ablated particles

The high resolution transmission electron microscope study of the phase and chemical compositions of ablated particles suggests that laser ablation of the silicate NIST 612 glass produced two different types of particles (Fig. 2.4).

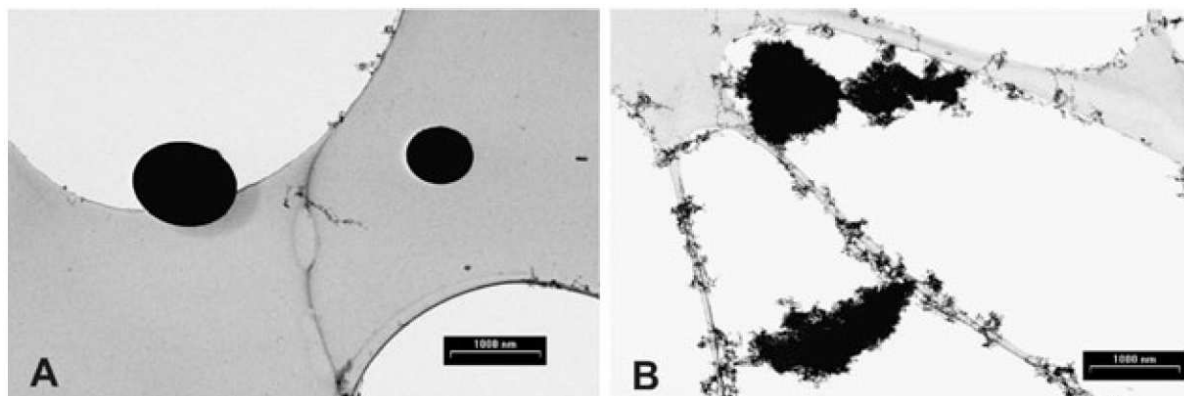


Fig. 2.4: STEM bright field images of particles produced by laser ablation of the NIST 612 silicate glass. The particles were collected *ca.* 100 cm from the ablation cell.

The larger spherical to oval particles collected on a TEM membrane in the He carrier gas line *ca.* 100 cm after the ablation cell vary in size between *ca.* 0.5 and 2 μm . Much smaller particles collected on the same membrane are only several nm in diameter and form up to 2 μm large particle clusters. The oval to spherical particles are amorphous and there are differences between the major element composition of individual particles that vary as follows (number of analyses $n = 6$): SiO_2 53–78 wt% (mean = 64.9 wt%), Al_2O_3 2.4–5.5 wt% (mean = 4.1 wt%), CaO 15–41 wt% (mean = 28.2 wt%) and Na_2O 0.7–7.3 wt% (mean = 2.8 wt%). This is significantly different from the composition of the NIST 612 glass (SiO_2 72 wt%, Al_2O_3 2 wt%, CaO 12 wt% and Na_2O 14 wt%). The ultrafine (nm sized) particles are also amorphous on the scale of the electron beam but have a major element composition (SiO_2 71.7 wt%, Al_2O_3 2.2 wt%, CaO 11.6 wt% and Na_2O 14.5 wt%) that corresponds well with that of the NIST 612 glass.

Spherical particles (0.2–0.5 μm) produced by laser ablation of zircon 91 500 reference material represent a mixture of amorphous and crystalline material. Most are pure or nearly pure ZrO_2 (baddeleyite) with attached amorphous Si phase on the surface (Bleiner and Gasser, 2004). Their bulk compositions ($n = 5$) range from 32 wt% SiO_2 , 68 wt% ZrO_2 to 2 wt% SiO_2 , 98 wt% ZrO_2 . The composition of agglomerates of crystalline spherical particles (0.005–0.05 μm in diameter) varies between ($n = 2$) 8–9 wt% SiO_2 and 91–92 wt% ZrO_2 . Agglomerates of even smaller amorphous and crystalline particles (~ 0.005 μm in diameter) contain 41–50 wt% SiO_2 and 50–59 wt% ZrO_2 ($n = 5$). As with the particles produced by laser ablation of the silicate NIST glass, only some particles produced by the ablation of zircon have a chemical composition

corresponding to that of the original solid sample (*i.e.*, natural ZrSiO_4 contains 32.8 wt% SiO_2 and 67.2 wt% ZrO_2). Ablation of zircon clearly produces particles that vary not only in their chemical compositions, but also in their phase properties.

2.4.3 Trace element composition of particles in the ejecta blanket

The ejecta blanket (Fig. 2.5) is a circular thin deposit of particles that surrounds the ablation crater on the sample surface and has a radius between *ca.* 200 and 400 μm .

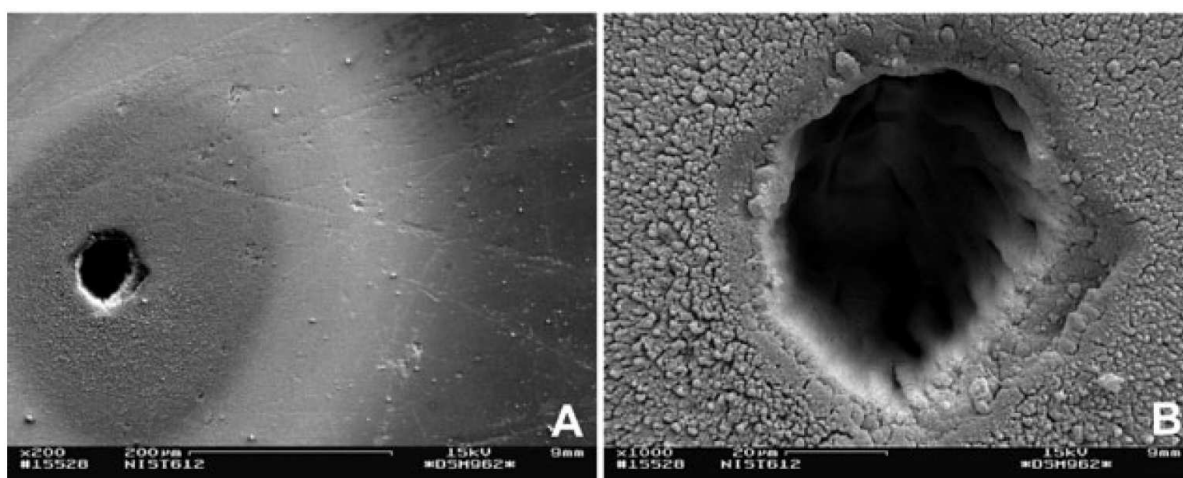


Fig. 2.5: SEM images of ejecta blanket formed around a laser pit in the NIST 612 silicate glass.

Its thickness (measured by a Dektrak profilometer) increases towards the crater and does not exceed 2 μm , except for the innermost zone adjacent to the crater, where the particles are blended with the melt sheets. Here the blanket may be elevated several tens of μm above the sample surface. The shape of the ejecta blanket can be affected by the dynamics of the gas flow during the ablation but it commonly maintains a structure that consists of larger ($\sim 5 \mu\text{m}$) particles being concentrated adjacent to the ablation crater and smaller (sub- μm or nm sized) particles being deposited in the outer part of the blanket. Lasers with an ns pulse width and a non-even (Gaussian) distribution of energy across the laser beam commonly produce a variable amount of melt in the vicinity of the ablation crater and even inside the crater (Fryer et al., 1995).

Ion probe analyses of particles in a *ca.* 600 μm traverse across the ejecta blanket around an ablation pit in the silicate NIST 610 glass show a strong variation in the U, Th and Pb elemental

composition. The concentrations of all three elements relative to Si are similar to the NIST 610 bulk composition in the vicinity of the ablation pit but the ratios increase two to five fold at a distance of *ca.* 350 μm from the crater rim. They then drop down again at *ca.* 600 μm from the crater rim to a value that is similar to the NIST 610 bulk composition. Significant variations were also observed in Pb/U and Pb/Th ratios (each with 3-fold decreases away from the pit rim) while the U/Th ratio was almost constant across the ejecta blanket (Fig. 2.6).

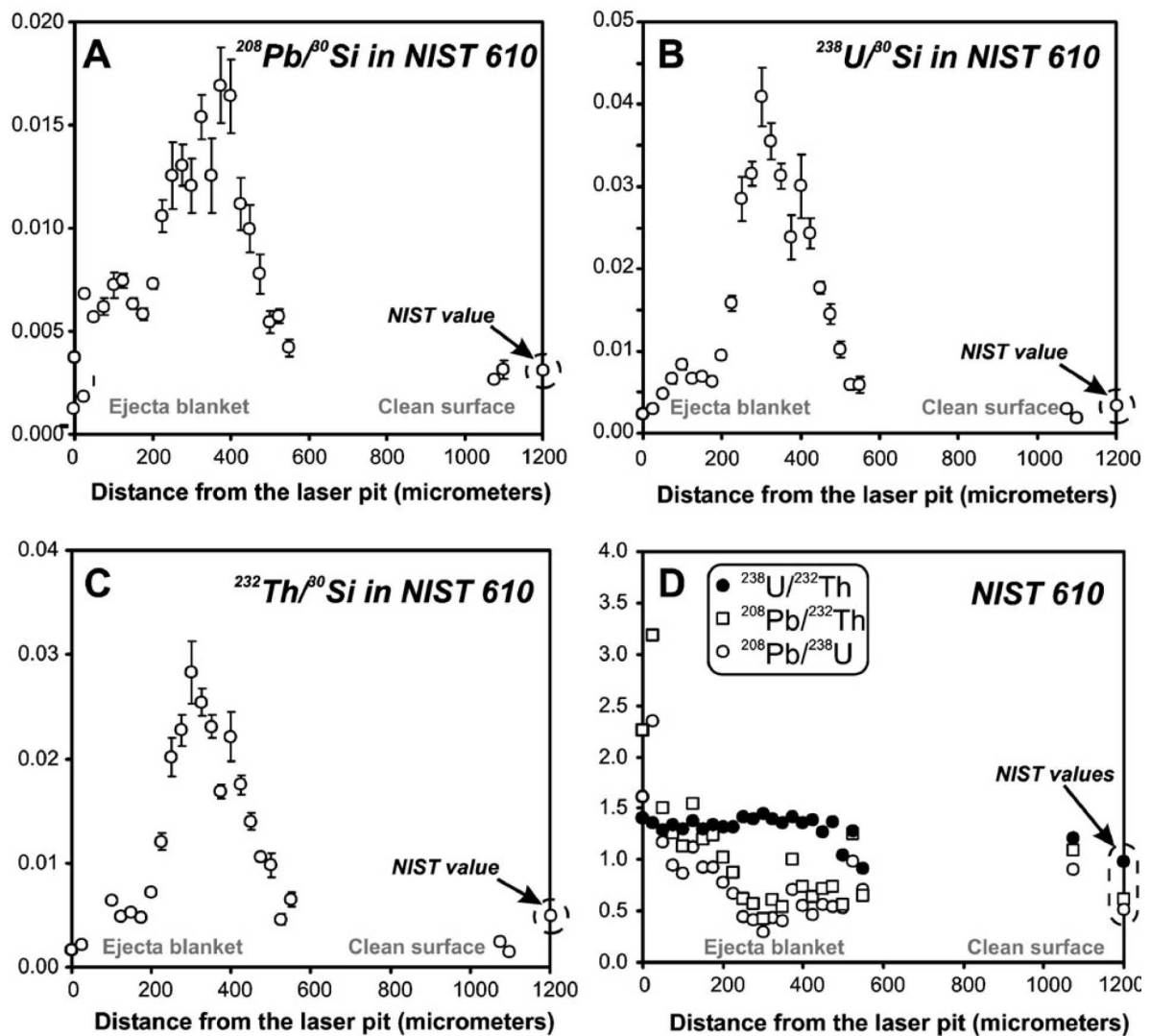


Fig. 2.6: SIMS data collected from a traverse across the ejecta blanket in the NIST 610 silicate glass. The traverse runs from immediately at the edge of the laser ablation pit radially outwards to beyond the edge of the ejecta deposit. Analytical uncertainties in plots A–C are 1 sigma, the error bars in plot D are not shown for the sake of clarity but the uncertainties for individual analyses vary between 5–10%.

Chemical variations on a similar scale were also observed in data obtained from the ion probe traverse across the ejecta blanket deposited adjacent to a laser pit in the zircon 91 500 reference sample. The chemical profiles in Fig. 2.7 show a variation in major elements Zr and Si across the ejecta blanket with Zr being depleted relative to Si close to the ablation pit. The Zr/Si ratio increases by ~25% at *ca.* 250 μm from the rim of the ablation pit followed by a slow and steady decrease of the Zr/Si ratio towards the outer part of the ejecta blanket. The observed variation in Zr and Si content is not compatible with presence of only single phase zircon but rather it points to at least two different phases in the ejecta blanket, zircon and baddeleyite + quartz, as was seen earlier in the collection of ablated particles. There is a strong decoupling of minor elements Pb and U in particles deposited in the ejecta blanket as well. The Pb/U ratio increases by ~25% during the first 250 μm from the rim of the ablation pit, followed by a decrease to the Pb/U value which is lower than the value adjacent to the rim. If the high-Zr/Si ejecta present between 250 and 750 μm from the rim of the ablation pit reflects the formation of baddeleyite, at least some of the baddeleyite has strongly fractionated Pb/U ratios relative to the target zircon.

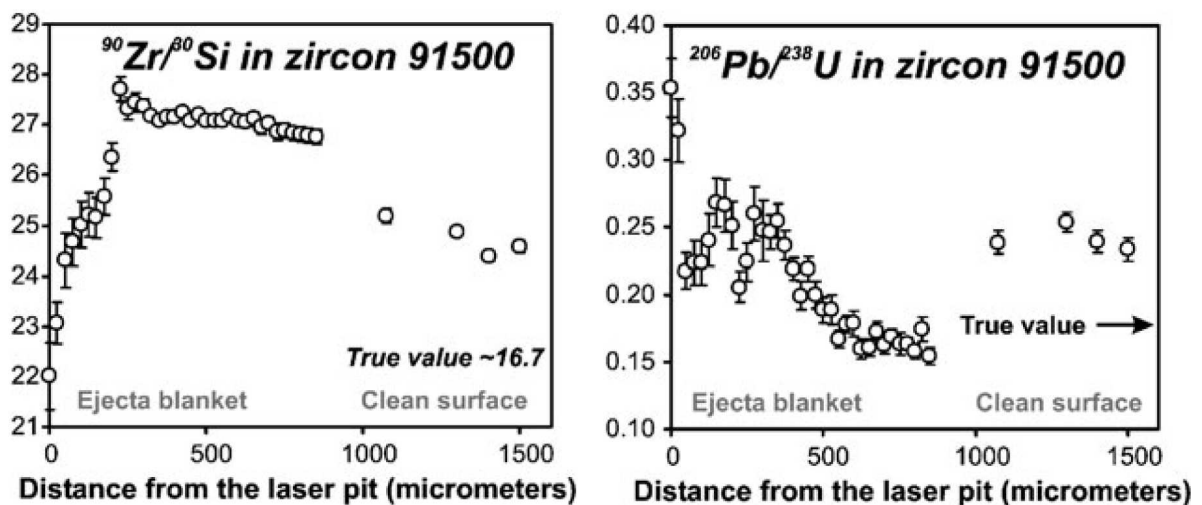


Fig. 2.7: SIMS data collected from a traverse across the ejecta blanket in the zircon 91 500 reference sample. The traverse runs from immediately at the edge of the laser ablation pit radially outwards to beyond the edge of the ejecta deposit. Analytical uncertainties are 1 sigma.

The grain size of the ejected material (up to few micrometres) is much smaller than the diameter of the primary ion beam; the surface roughness should not therefore have a significant effect on the production and extraction of the secondary ions. Also, no charging of the ejecta

dominated areas was observed, suggesting that the conductivity of the gold coating of the ejecta was sufficient to produce reliable data. Large differences in the sensitivity for U, Th, and Pb are clearly visible in the data as shown by the “true values” (Figs. 2.6 and 2.7) which differ from the observed ratios measured by SIMS on the pristine domains. These differences are determined largely by the chemical composition of the material analyzed (matrix effect). The bulk chemistry of the material contained in the 20 μm diameter SIMS beam did not vary greatly (*i.e.*, all material was silicate dominated), the trends in the data which are seen are therefore most readily interpreted as being due to real variations in the concentration of the target elements. In conclusion, the data suggest that the composition of the ejecta blanket is clearly different from that of the clean sample surface.

2.4.4 Phase and chemical composition of zircon adjacent to the ablation pit

Thin foils for a HR-TEM study were prepared directly from the 91 500 zircon reference material by using the focused ion beam (FIB) technique. The foils were cut from the sample adjacent to a laser pit in order to study changes in the phase and chemical composition of zircon that result from the laser ablation process. The foils sampled the zircon up to a distance of ~ 20 μm away from the inner wall of the laser pit. TEM data from the foils show a strong variation in the phase and chemical composition of the sample adjacent to the pit (Fig. 2.8). Close to the pit, at a distance of *ca.* 0.5 μm from the ablation pit wall, the sample was composed mostly of baddeleyite, with some amorphous SiO_2 and a minor amount of zircon. Further away, to a distance of 1–1.5 μm from the pit wall, the sample was dominated by a coarse tetragonal and monoclinic ZrO_2 (baddeleyite). The transition from tetragonal to monoclinic ZrO_2 occurs around 1150 $^\circ\text{C}$ at atmospheric pressure (Butterman and Foster, 1967). Crystalline ZrO_2 and ZrSiO_4 (baddeleyite and zircon), together with a small amount of high temperature SiO_2 , formed the outer parts of the studied foils (between 1.5–2 μm from the laser pit) before reaching into the pristine zircon.

The observed phase and chemical changes are most likely due to thermal effects caused by interactions of the non-homogenized UV laser with the zircon sample. Thermal decomposition of zircon to various phases of ZrO_2 (including baddeleyite) and SiO_2 is very common in nature and it has been previously described from various environments (Heaman and Lecheminant, 1993).

Lead loss may occur in zircon during the breakdown to baddeleyite and SiO_2 in nature (Chapman and Roddick, 1994). This reaction is utilized in measurements of Pb isotopes liberated from zircon crystals in the laboratory during their decomposition in thermal ionization source mass spectrometry (Chapman and Roddick, 1994; Klotzli, 1997).

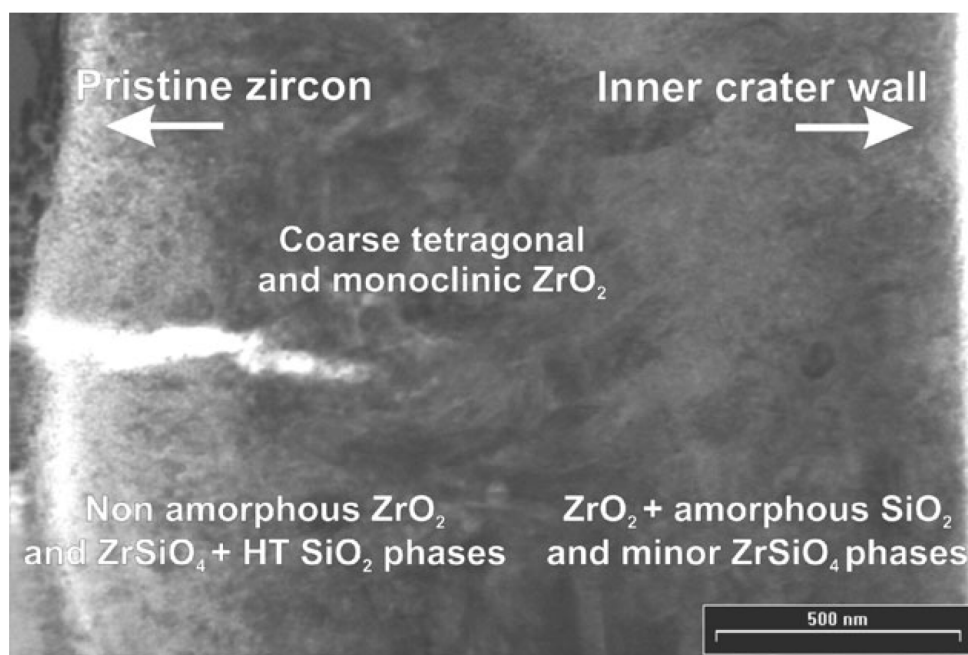


Fig. 2.8: TEM bright field image of a thin foil that was cut from the zircon 91 500 reference sample adjacent to a laser pit using a Ga focused ion beam.

2.4.5 Effect of particle size selection on fractionation during laser ablation ICP-MS analysis

We explored the possibility of using commercially available and calibrated particle separators to control the particle size window that reaches the ICP by screening out both large and small particles. We have used a single-stage stainless steel TSI impactor to remove the large particles. A particle sizer consisting of a number of stainless steel screens, similar to those used in the TSI diffusion battery, was used to remove the nanoparticles. For a given He gas flow, the upper cut-off was varied by changing the diameter of the jet in the impactor while the lower cut-off was controlled by the number of screens in the particle sizer. The selected size fraction of particles was transported to the ICP source of the mass spectrometer where the Pb and U signals were measured. The results of this experiment are shown in Fig. 2.9.

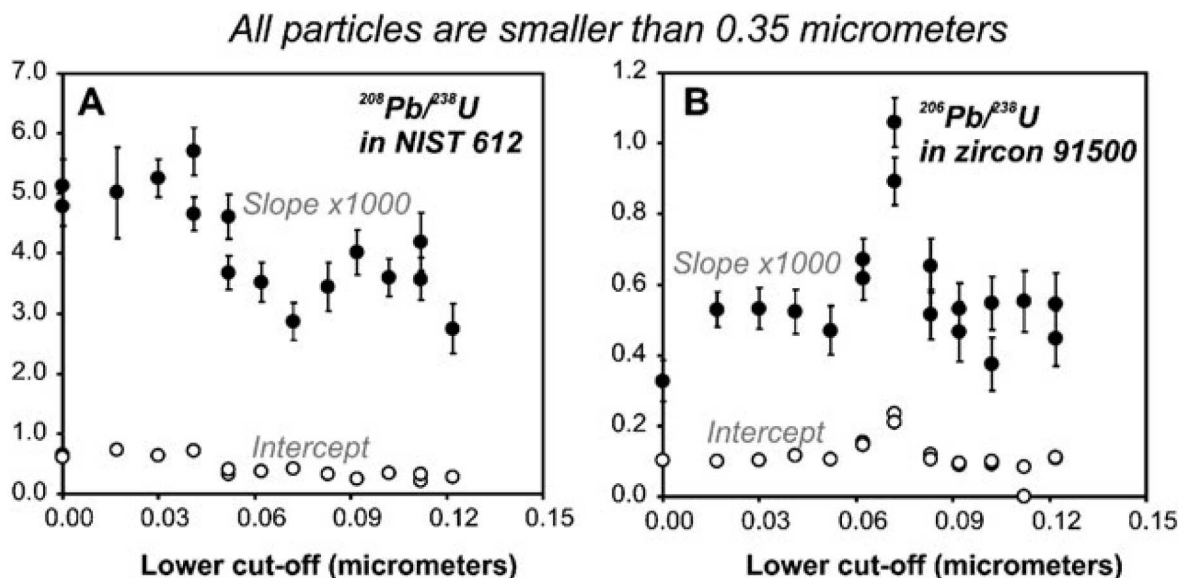


Fig. 2.9: ICP-MS data for different size fractions of particles produced by laser ablation of the NIST 612 silicate glass and the zircon 91 500 reference sample. The elemental fractionation of the respective major Pb isotopes and ^{238}U is expressed as the slope of the line fitted through the fractionating isotopic ratio plotted against the number of applied laser pulses. The intercept value corresponds to the isotopic ratio calculated as the intercept of this line with the y-axis at the start of the laser ablation. The uncertainties are 1 sigma or within the size of displayed symbols.

The Pb/U ratios in ablated silicate samples systematically increase with the increasing depth/diameter ratio of the laser crater (number of applied laser pulses). The extent of Pb/U elemental fractionation during the ablation of silicate NIST 612 glass and zircon 91 500 is expressed as the slope of the line fitted through the fractionating $^{208}\text{Pb}/^{238}\text{U}$ and $^{206}\text{Pb}/^{238}\text{U}$ ratios, respectively, plotted against the number of applied laser pulses (total of 1150 pulses per measurement). The slope of the regression line is proportional to the rate of Pb/U fractionation. Also plotted in Fig. 2.9 are the ratio values calculated as the intercept of this line with the y-axis at the start of the ablation (0 laser pulses applied to the sample). During this experiment the upper cut-off was set to 0.35 μm to ensure a maximum particle atomization in the ICP (Jackson and Günther, 2003) and the lower cut-off was varied between 0–0.12 μm by changing the number of screens in the particle sizer. This effectively produced size windows of analysed particles that could be varied from 0–0.35 to 0.12–0.35 μm by using the appropriate number of screens in the particle sizer. The rate of Pb/U fractionation varies with the size range of the analysed particles (*i.e.*, with the number of screens used in the particle sizer: Fig. 2.9).

Data for the NIST 612 glass (Fig. 2.9A) show a significant decrease in the slope and the intercept of the fractionating Pb/U ratio following the removal of particles smaller than $\sim 0.04 \mu\text{m}$. Further removal of particles $>0.04 \mu\text{m}$ from the aerosol had no significant effect on the elemental fractionation. Not only has the removal of the fine and ultrafine particle fractions ($<0.04 \mu\text{m}$) from the aerosol produced by ablation of the NIST 612 glass reduced the Pb/U elemental fractionation, but it has also shifted the intercept value (*i.e.*, the measured $^{208}\text{Pb}/^{238}\text{U}$ ratio at the start of ablation) from ~ 0.8 towards the NIST value of ~ 0.55 . This suggests that very small particles produced from the NIST glass are enriched in Pb relative to U.

Removal of fine and ultrafine particles from the aerosol produced by laser ablation of zircon 91 500 resulted in a different fractionation pattern compared with the ablation of the NIST 612 glass (Fig. 2.9B). The elimination of particles smaller than $0.060 \mu\text{m}$ had no significant effect on the slope and intercept of the Pb/U fractionation trend. However, the additional removal of particles between 0.060 and $0.075 \mu\text{m}$ from the aerosol significantly increased the slope of the Pb/U elemental fractionation and the intercept value (*i.e.*, the measured $^{206}\text{Pb}/^{238}\text{U}$ ratio at the start of ablation) from being slightly below the recommended value (Wiedenbeck et al., 1995) for zircon 91 500 (~ 0.18) to a value of >0.2 . Further removal of particles between 0.075 – $0.090 \mu\text{m}$ (*i.e.*, all particles smaller than 0.090 and larger than $0.35 \mu\text{m}$ were not allowed to the ICP) again caused a decrease of the slope and intercept to values similar to the analysis of the bulk particle fraction (*i.e.*, all particles smaller than $0.35 \mu\text{m}$). The results of this experiment suggest that for the experimental conditions used in this study, the particle size fraction between 0.060 – $0.075 \mu\text{m}$ had a significantly different Pb/U ratio compared with the rest of the particles present in the aerosol, which gave a more accurate Pb/U ratio.

The observed contrast between the Pb/U fractionation patterns of NIST silicate glass and zircon can be attributed to the different size, phase and chemical composition of the particles produced during the ablation of these samples.

2.5 Discussion

The evidence presented in this paper contributes to the ongoing discussion on whether the elemental fractionation during laser ablation ICP-MS analysis takes place at the ablation site, in the ablation cell, during the transport of ablated material to the ICP and, or, in the ICP source of the mass spectrometer (Eggins et al., 1998; Guillong and Gunther, 2002; Koch et al., 2002;

Kozlov et al., 2003; Kuhn et al., 2004; Kuhn and Gunther, 2003; Mank and Mason, 1999). We have shown that particles comprising the ejecta blanket, and in the carrier gas line *ca.* 100 cm after the ablation cell, have variable chemical compositions in both the NIST silicate glass and the zircon reference sample. The particles derived from the zircon consist of variable phases. Moreover, phase changes occur adjacent to ablation pits in zircon. These inhomogeneities point to elemental fractionation at the ablation site and probably in the ablation cell. Elemental fractionation at the ablation site has previously been demonstrated for the laser ablation of brass (Koch et al., 2002; Kuhn and Günther, 2003), but until now only limited evidence was available for a corresponding process during the ablation of silicate samples (Košler et al., 2004; Kuhn and Günther, 2004) and for the mechanisms of elemental fractionation during the ablation of silicates (Košler et al., 2004).

Although the link between the formation of different phases and elemental fractionation can be demonstrated for crystalline samples, such as in the zircon, this relationship remains difficult to prove for amorphous materials such as the NIST silicate glasses, where the phase composition of ablated particles may be the same as that of the original sample.

2.5.1 Mechanism of Pb/U fractionation during laser ablation of zircon

Thermal decomposition of zircon to baddeleyite and SiO₂ resulting from UV laser ablation can explain the time-dependent elemental fractionation of Pb and U observed during ICP-MS analysis. Despite a small difference in ionic radii, U⁴⁺ (1.00 Å) may substitute for Zr⁴⁺ (0.84 Å) in the 8-fold coordinated site of the tetragonal ZrSiO₄. Natural zircon thus contains a significant amount of U, typically at levels from ppm to low % (Heaman and Parrish, 1991). Lead, on the other hand, does not normally enter the ZrSiO₄ lattice because most of the Pb in rocks is present in the 2⁺ oxidation state (Watson et al., 1997) and its incorporation into the zircon lattice requires a charge balance, usually by P⁵⁺ or H⁺. Most of the Pb that is present in natural zircon forms in situ by radioactive decay of ²³⁸U, ²³⁵U and, to a smaller extent, ²³²Th. Unlike U, Pb is not strongly bound in the ZrSiO₄ structure; rather it occupies domains in the zircon lattice that have suffered radiation damage due to the alpha-recoil from the radioactive decay of U and Th isotopes. Similarly, U and Th are compatible with the structure of ZrO₂ (baddeleyite), while Pb is normally not present in large quantities (Heaman and Lecheminant, 1993).

It is likely that the formation of baddeleyite by thermal decomposition of zircon results in strong partitioning of U into baddeleyite particles, while significant quantities of the Pb would be excluded from either ZrO_2 or from the thermally affected ZrSiO_4 . High-Zr/Si ejecta found around the zircon pit, and presumably enriched in baddeleyite, tends to have lower Pb/U ratios than the target zircon (Fig. 2.7), which is consistent with this interpretation. We speculate that much of the excluded Pb is transported efficiently to the ICP as a volatile species whereas the U is locked largely in particles of baddeleyite, which are transported less efficiently from the ablation site. The rate of ZrO_2 formation is related to the surface area affected by thermal effects of the laser beam. Accordingly, elemental fractionation becomes increasingly pronounced with increasing surface area of the wall of the laser pit (*i.e.* increasing depth of the pit). This interpretation is consistent with the observed increase of the Pb/U ratio (elemental fractionation) during laser ablation ICP-MS analyses of zircon (Hirata and Nesbitt, 1995; Horn et al., 2000; Košler and Sylvester, 2003).

Similar elemental fractionation of Pb and U has also been observed during the ablation of other U-bearing accessory minerals (*e.g.*, REE phosphate—monazite (Košler et al., 2001) and Ca, REE, Al, Fe silicate hydroxide—allanite (Cox et al., 2003)) and during the ablation of other samples containing U and Pb, such as are the amorphous NIST silicate glasses. It follows that the mechanisms of Pb/U elemental fractionation are dependent on the phase and chemical composition of the ablated material. As a result, non-matrix matched external calibration during laser ablation ICP-MS analysis can lead to inaccurate results for this element pair.

2.5.2 Particle size selection for accurate laser ablation-ICP-MS analysis

Several previous studies have attempted to use particle separation devices to improve ICP-MS signal stability and to obtain more accurate measurements of elemental ratios in the ICP-MS (Guillong et al., 2003b; Guillong and Günther, 2002). These devices utilized differences in the physical/mechanical properties of the particles to achieve separation. However, it has proved difficult to achieve a clean separation of the required particle fraction; *e.g.*, filtering off the coarse particles by mechanical filters, such as glass wool, inevitably results not only in the mechanical retention of the coarse particles, but also in the retention of a large proportion of the ultrafine, nanometer-sized particles. The behavior of nanoparticles is fundamentally different from that of larger, micrometer-sized particles in that nanoparticles are usually charged and their diffusion

rates in gases are much faster (Preining, 1998). Therefore they rapidly coagulate to form clusters or they adhere to the surfaces of the cell, tubing or any obstacles such as mechanical filters that may be present in the sample carrier tube. Particle separation devices based on centrifugal forces (Guillong et al., 2003b) have the advantage that the upper size cut-off can be continuously adjusted by varying the inner surface of the centrifugal tube (*i.e.* by changing its length and diameter) and by adjusting the gas flow.

In this study we have demonstrated that different sized particles produced during laser ablation can have different phases and chemical compositions. It is therefore important to select the size fraction of particles that most closely matches the bulk composition of the target sample in order to avoid large elemental fractionation and to improve the accuracy of laser ablation ICP-MS analyses.

2.6 Concluding remarks

In contrast with the previous work, which focused mostly on the role of coarse particles in elemental fractionation (Guillong and Günther, 2002; Jackson and Günther, 2003; Kozlov et al., 2003; Wiedenbeck et al., 1995), this study shows that the elimination of the fine and ultrafine particle fractions can also have a significant effect on the elemental fractionation rates during laser ablation of silicate samples. A corresponding effect of removal of ultrafine particle fraction from ablated aerosol has already been demonstrated for isotopic fractionation of iron during the ablation of Fe metal and Fe sulfides (Košler et al., 2005a). An important observation is that laser ablation of different silicate samples under identical experimental conditions can produce aerosols with different size distributions of particles. These particles can vary in their phase and chemical composition. Because laser ablation can form different phases at the ablation site, the ablated sample has to be transported to the ICP in a quantitative or representative fashion. In some cases, a representative population of particles may be selected for transport and analysis in the ICPMS using screening devices. The results of this study point to the importance of matrix matched external calibration in cases where highly precise and accurate laser ablation ICP-MS data are required for element pairs of differing chemical affinity for the target material such as Pb and U in zircon.

2.7 Acknowledgements

Helpful comments provided by two anonymous referees are gratefully acknowledged. This study was financially supported by GACR project 205/03/0220. The ICP-MS facility at Charles University was funded by PHARE.

Chapter 3: Fractionation of alkali elements during laser ablation ICP-MS analysis of silicate geological samples

Jitka Míková^{1,2}, Jan Košler¹, Henry P. Longerich³, Michael Wiedenbeck⁴, John M. Hanchar³

¹ *Centre for Geobiology and Department of Earth Science, University of Bergen, Allegaten 41, Bergen, N-5007, Norway*

² *Czech Geological Survey, Klárov 3, Prague 1, CZ-118 21, Czech Republic*

³ *Earth Sciences Department, Memorial University, St John's, NL, Canada A1B 3X5*

⁴ *Helmholtz-Zentrum Potsdam, Deutsches GeoForschungsZentrum, Potsdam, D-14473, Germany*

Status: Published in *Journal of Analytical Atomic Spectrometry*, 2009, 24, 1244-1252

3.1 Abstract

Data on elemental fractionation of alkali elements during laser ablation ICP-MS analysis of silicate reference glasses (NIST-610, BCR-2G, alkali element-doped andesite glasses), and crystalline mineral albite ($\text{NaAlSi}_3\text{O}_8$) are reported. Laser ablation ICP-MS and SIMS were used to determine differences in sample composition before and after laser interaction with the samples. The fractionation trends of the alkali elements are different from those of other lithophile elements, such as Ca and the rare earth elements (REEs). The rate of fractionation varies for different sample matrices and for different alkali elements in the same matrix. Data from SIMS analyses of the ejecta blanket deposited adjacent to the laser ablation crater in silicate NIST-610 glass and crystalline albite suggest a matrix dependent fractionation of alkali elements for different particle size fractions in the ablated aerosol. The extent of fractionation varies for different alkali elements and is independent of their ionic radii. Ion probe depth profiling into the bottom of laser craters showed laser ablation-induced chemical changes in the sample that involved alkali elements and major matrix elements including Si and Ca. This suggests that a combination of thermally-driven diffusion and size-dependent particle fractionation are responsible for the observed fractionation of alkali elements during laser ablation of silicate samples.

3.2 Introduction

Determination of alkali elements is of great importance in the study of geological materials. The alkali elements (Li, Na, K, Rb, and Cs) are commonly present as major or minor constituents in silicate minerals and natural and synthetic glasses, but they can be difficult to determine using Laser Ablation Inductively Coupled Plasma Mass Spectrometry (LA ICP-MS). LA ICP-MS is capable of quantifying all of the alkali elements, but it is best suited for the trace elements, Li, Rb, and Cs. Sodium can be present in geological samples at high concentrations which are not practical to be measured by ICP-MS, and the determination of K by ICP-MS is difficult due to high Ar^+ background and interferences of polyatomic ions from the argon gas near mass 40.

Interaction of solid samples with a laser beam can result in element redistribution in the samples and non-stoichiometric ablation, which affects the measurement precision and accuracy of many elements (Longerich et al., 1996a), including importantly the alkali elements. The mechanism and scale of element redistribution in solids are not well understood, but involve various diffusion mechanisms and phase separation (Bleiner and Gasser, 2004; Košler et al., 2005b), and are thought to be the primary cause of element decoupling. Diffusion behaviour of elements is a function of the ionic radii and the charge of the elements (ions), as well as the chemical composition and structure of the sample (Giletti and Shanahan, 1997) and the thermal gradient induced by sample–beam interaction.

Difficulties with the determination of the alkali elements, especially the major element, Na, have long been recognized in Electron Probe Micro Analysis (EPMA). This problem is especially notable in albite feldspar and Na-rich glasses in which the measured Na signal quickly decreases asymptotically during the course of a typical EPMA analysis (*e.g.*, ~ 2 minutes). This effect has been reported not only for sodium, but also for the other alkali ions (Humphreys et al., 2006) and it has been attributed to ion migration under the electron beam. The rate of migration has been shown to depend on the electron current density (*e.g.*, counts/time/beam current) (Gedeon and Jurek, 2004) and the nature of the material being analyzed. While most previous EPMA studies tried to minimize this effect, only a few attempts have been made to identify the mechanisms that cause the alkali element fractionation during electron microbeam analysis (Gedeon et al., 2000; Gedeon and Jurek, 2004; Hanson et al., 1996; Humphreys et al., 2006; Jones et al., 2004; Jurek and Gedeon, 2003; Lin and Yund, 1972; Pederson, 1982; Stormer et al., 1993).

The precision and accuracy of LA ICP-MS analysis often suffers from a change in the ratios of measured isotope signal intensities with an increasing number of laser pulses (time) applied to the sample. This is referred to as laser induced elemental fractionation (Košler et al., 2005b) or more simply as fractionation. Fractionation is defined here as a progressive change of element or isotope ratios with time, with out any implication as to the mechanism causing the fractionation or the location where such fractionation takes place. Significantly less than 100% of the ablated material is transferred to the ICP. The amount of ablated sample transported to the ICP under experimental conditions used in this study was estimated to be ca. 10% (Bleiner and Bogaerts, 2007; Horn and Günther, 2003; Kuhn et al., 2004). Differential transport of particles that vary in size and composition are responsible for some of the observed fractionation (Horn et al., 2001; Košler et al., 2005b; Longerich et al., 1996a). The ablation behaviour of samples depends on the laser wavelength used (Guillong et al., 2003a; Jeffries et al., 1998), fluence (Horn et al., 2001), pulse duration (Koch et al., 2004b), and upon bulk and defect absorption of the laser radiation (Cramer et al., 2002). A better understanding of the mechanisms responsible for the sample conversion into the ablated particles (Guillong et al., 2003a; Horn et al., 2001; Koch et al., 2004b; Košler et al., 2005b) is crucial for controlling the laser ablation process.

While the fractionation behaviour of many elements reflects their geochemical affinities (lithophile, siderophile, chalcophile), the alkali elements Li, Rb, and Cs generally do not behave similar to the rest of the lithophile elements during laser ablation ICP-MS analysis (Longerich et al., 1996a). Thermally driven diffusion of alkali elements due to sample heating by laser-sample interaction may contribute to this different fractionation of alkali elements compared to other lithophile elements. However, no systematic study of alkali element fractionation during laser ablation ICP-MS analysis has been previously reported.

The fractionation behaviour of alkali elements during analysis is important in geological applications including geochronology (Rb-Sr, K-Ar) and thermobarometry. Understanding of alkali element fractionation during laser ablation ICP-MS is important not only to improve the precision and accuracy of alkali element determinations, but also because of the use of alkali elements in correcting for variations in ablation yield (as internal standards) in analyses of other lithophile elements.

The combination of external calibration with internal standardization using a naturally occurring element is the most commonly used strategy for quantification in LA ICP-MS analysis.

Synthetic reference silicate glasses such as the NIST-600 series are used for external standardization in multi-element LA ICP-MS analysis to calibrate the instrument response, and analytically suitable, naturally occurring major element or elements having known concentrations in the sample and calibration materials (*e.g.* Ca in silicate, phosphate, and carbonate minerals) are commonly used as internal standards to correct for ablation yield and other multiplicative factors. This was considered when selecting samples for this study. Results from a laser ablation ICP-MS and ion probe (SIMS) study of synthetic silicate reference glasses, natural crystalline mineral albite, and synthetic haplo (*i.e.*, simplified composition and Fe free)-andesite composition glasses doped with alkali elements (Li, Na, K, Rb) are presented in this report. This study was designed to help to reveal the mechanisms that cause the observed fractionation of alkali elements during laser ablation sampling.

3.3 Experimental

3.3.1 Sample preparation

Synthetic reference silicate glasses (NIST-610 and BCR-2G) that are commonly used for calibration in the analysis of geological samples using LA ICP-MS, a natural mineral albite (crystalline $\text{NaAlSi}_3\text{O}_8$), and synthetic glasses with a haplo (*i.e.*, iron free) andesite composition were used in this study. The NIST (National Institute of Standards and Technology)-610 silicate glass is spiked with sixty-one elements at nominal concentrations of 500 $\mu\text{g/g}$. The BCR-2G (U.S. Geological Survey Columbia River Basalt reference glass material) was prepared from BCR-2 powder by the USGS from a basalt collected in the Bridal Veil Flow Quarry, Oregon, USA (Wilson, 1997). The albite sample was obtained from a single crystal (2 cm in diameter) from the mineral collection of Charles University in Prague. This grain was divided into two parts, mounted and analyzed in two different crystallographic orientations with planes (010) and (001) parallel to the sample surface. This was to examine potential effects of differential diffusion rates of alkali elements, especially for expected faster diffusion parallel to the (010) plane (Jones et al., 2004; Lin and Yund, 1972), and to look for effects of differential ablation on elemental fractionation in the two crystallographic orientations.

Synthetically prepared silicate glasses with an andesite bulk composition were doped with variable amounts of alkali elements (Li, Na, K, and Rb; Tab. 3.1) in order to study the effects of

alkali element concentrations on their fractionation behaviour during laser ablation ICP-MS analysis. The following method was used for each glass synthesis. High purity carbonate and oxide starting materials were dried in an oven at 100°C and then mixed under ethanol in an agate mortar. Carbonates were used for Ca, Li, Na, K, and Rb because of the hygroscopic nature of the oxides of those elements. After drying under a heat lamp, the mixed oxide powders were transferred to an uncovered 25 ml platinum crucible. The mixture was then suspended using Pt wire from an alumina rod in the “hot spot” of a Deltech MoSi₂ furnace at 700°C in the experimental geochemistry facility at Memorial University. The furnace was then ramped to 1340°C at a moderate rate of 50°C per hour to minimize spattering during decarbonation of the Ca, Li, Na, K, and Rb compounds. The crucible was held at 1400°C for four hours and was then quickly quenched in water. The quenched and fractured glass was removed from the crucible and pulverized in an agate mortar. The ground powder was then remelted at 1400 °C, quenched, and pulverized, three more times to ensure homogenization of the glasses. The quenched glass fragments (*ca.* 4-5 mm) were broken out of the crucible. The glass samples from each synthesis were inspected optically using a binocular microscope and powder X-ray diffraction to look for evidence of minerals that may have formed during the fusion or quenching of the glass. No evidence of either type of crystals was found in the samples.

Tab. 3.1: *Nominal composition of the synthetic haplo-andesite glasses (values in wt %).*

	A-1	A-2	A-3	A-4	A-7	A-9	A-10	A-11
SiO ₂	59.0	59.0	60.0	59.0	59.0	60.0	60.0	59.0
Al ₂ O ₃	17.0	17.0	19.0	17.0	17.0	19.0	19.0	17.0
CaO	10.0	10.0	11.5	10.0	10.0	11.5	11.5	10.0
MgO	7.0	7.0	8.5	7.0	7.0	8.5	8.5	7.0
K ₂ O	7.0	3.5	0.5	—	—	—	—	—
Na ₂ O	—	3.5	0.5	—	7.0	—	—	—
Rb ₂ O	—	—	—	—	—	1.0	—	7.0
Li ₂ O	—	—	—	7.0	—	—	1.0	—

All samples were mounted in epoxy resin and polished to obtain flat smooth surfaces suitable for EPMA, Secondary Ion Mass Spectrometry (SIMS, ion probe), and LA ICP-MS microanalysis.

3.3.2 Electron Probe characterization of the albite samples

A CamScan CS3200 scanning electron microscope (SEM) equipped with an electron backscatter diffraction (EBSD) system (Nordlys II detector + Channel 5 Software, Oxford Instruments HKL) and an energy dispersive spectrometry (EDS) system (Link-ISIS, Oxford Instruments) at the Czech Geological Survey in Prague was used to verify the crystallographic orientation of albite samples. Samples were carbon coated prior to the analysis. The primary beam accelerating voltage was 20 kV, and the probe current was 5 nA. The sample mount was tilted 70 degrees during the analysis.

The EDS system was used to examine the homogeneity of the major element composition of the albite. During this test, the primary beam accelerating voltage was 15 kV, the probe current was 3 nA, with a 1 μm spot size, and data were acquired for 120s. Following the EBSD and EDS analyses, the samples were re-polished to remove the carbon coating (that can contain significant concentrations of trace elements) prior to laser ablation ICP-MS analysis.

3.3.3 Laser ablation experiments

A 213 nm UV Nd:YAG (New Wave, UP213) laser coupled to a Thermo Finnigan Element2 single collector ICP-MS at Bergen University was used for the ablation. The laser was fired at a 10 Hz repetition rate with an energy density of 5 J/cm^2 , with a laser spot diameter of 30 μm . Samples were ablated in a He atmosphere (1 l min^{-1} flow). A gas blank was measured for an initial 30 s of each acquisition followed by 120 s of the ablation signal. Data were acquired using low mass resolution in time resolved mode with 1 reading and 10 ms dwell time on each mass. Data were acquired at masses ^6Li (fly-back mass to allow for additional magnet settling time), ^7Li , ^{23}Na , ^{29}Si , ^{30}Si , ^{43}Ca , ^{44}Ca , ^{85}Rb , and ^{133}Cs . Following the ablation, the samples were carefully handled in an effort to preserve the thin layer of particles (the ejecta blanket) on the sample surface adjacent to the laser pit for subsequent analysis using SIMS, and for secondary electron imaging using the SEM.

The data were processed off-line. Following the correction of signal intensities for the gas blank, a measure of elemental fractionation was calculated as the slope of the isotope ratio vs. time (Košler et al., 2002b). This parameter was calculated using a least square linear fit to the signal intensity ratios plotted versus the number of laser pulses applied to the samples. An

identical length of signal corresponding to 600 laser pulses (60 seconds of ablation) was used to calculate fractionation slope for all analyses to ensure a valid inter-element and inter-sample comparison as well as low uncertainty of the calculated fractionation slope. In calculating the slope and its uncertainties we used the method of Sylvester and Ghaderi (1997) that assumes a zero uncertainty in x (number of laser pulses equivalent to time) and a constant uncertainty in y . This approach allows for comparison of fractionation behaviour of signal ratios in different samples with different concentrations of the measured elements, provided that data for these samples were obtained using identical analytical conditions.

Laser ablation pits for subsequent depth-profiling using SIMS were produced by firing 5 or 10 shots on each sample. The laser parameters were 1 Hz repetition rate, with an energy density of 5 J/cm^2 and a $80 \text{ }\mu\text{m}$ laser spot diameter.

3.3.4 Secondary ion mass spectrometry experiments

A Cameca ims 6f SIMS at the Helmholtz-Zentrum Potsdam was used to measure the elemental composition of particles deposited in the ejecta blanket adjacent to the crater on the surface of the NIST-610 and albite samples. The ejecta blanket is the thin deposit of particles on the sample surface surrounding the ablation crater. The shape of the ejecta blanket is affected by the dynamics of gas flow during the ablation. It commonly consists of larger (*e.g.*, μm sized) particles which are mainly adjacent to the ablation crater and smaller (*e.g.*, sub- μm or nm sized) particles which are deposited in the outer part of the blanket (Bleiner et al., 2005; Košler et al., 2005b; Kuhn and Günther, 2003) shown in Fig. 3.1. Several point profiles (300 μm length, 10 μm step between measurements) were made, which extend from the edge of the laser ablation pit radially outwards to beyond the edge of the ejecta deposit. Analyses of a clean sample surface away from the ablation sites were acquired for comparison to evaluate the difference between sample material originating from the laser pit and sample not affected by the ablation. The first points of the ejecta blanket point profile, placed immediately on the rim of the laser pit, were not taken into account because of possible artefacts associated with incidental deflection of the SIMS primary beam on the laser crater edge.

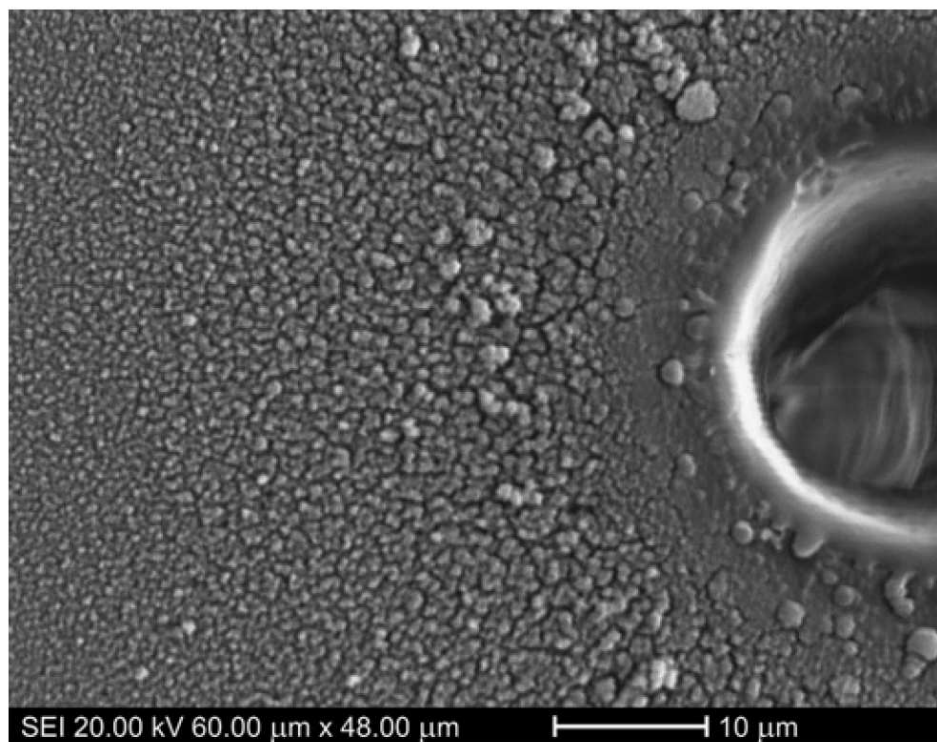


Fig. 3.1: Secondary Electron Image of the structure of the ejecta blanket on the surface of the artificial andesite glass A-2 (3.5% K_2O + 3.5% Na_2O).

Sample preparation involved sputtering a *ca.* 50 nm thick, high purity gold coating directly onto the sample surface. Based on microscopic observation, this procedure did not cause any visible change in the ejecta deposit. The primary beam accelerating voltage was 22.5 kV with an ion current of 500 pA. The beam spot size was 5 μm with a secondary extraction voltage of 10 kV. Masses acquired using the SIMS were ^7Li , ^{23}Na , ^{28}Si , ^{39}K , ^{40}Ca , ^{85}Rb , and ^{133}Cs . A single spot analysis consisting of ten measurement cycles with a 5 min unrastered preburn lasted 17 min. The penetration depth of ion beam was kept short to minimize penetration of the ejecta layer. Estimation of penetration depth from analytical conditions used for analysis would not have exceeded more than 200 nm. The depth of penetration of the Cs^+ probe could not be quantified using the profilometer as the SIMS pit diameter was comparable to that of the stylus. However, only the data from the first 5 cycles were considered for further evaluation. The second five cycles were acquired merely to ensure that acquired data were only representative of the ejecta blanket.

Additionally, a series of SIMS depth profile measurements were performed at the bottom of some ca. 80 μm wide laser ablation pits to evaluate the compositional changes in the samples caused by the interaction with the laser beam. The primary beam (accelerating voltage 22.5 kV and ion beam current of 5 nA) was rastered over the sample area (raster size 70x70 μm), while secondary ions (extraction voltage of 10 kV) were collected only from the part of the raster corresponding to the centre of the flat-bottomed ablation pit (30 μm field-of-view defined by a mechanical field stop). Roughness of the laser crater bottoms and crater depth before and after the SIMS analyses was determined using a Dektrak3 stylus profilometer. The time-resolved SIMS signals were converted to depth profiles assuming a constant rate of sputtering during the time of the analyses.

Four depth profile analyses were made on each sample. The first and last depth profile were on a clean sample surface that was not affected by the laser while the remaining two acquisitions were conducted at the bottom of laser pits produced previously by firing 5 or 10 laser shots. Importantly, we normalized each depth profile data obtained from within the laser pits to the mean of the two equivalent bracketing measurements from the clean sample surface; this procedure suppressed the near-surface artefacts which could affect the interpretation. For further calculations and interpretation we used depth profile signals from the point where rapid change of Si response indicates that the ion beam penetrated through the gold coating (the first 6 readings were usually removed). The SIMS depth profile analyses reached ca. 250 nm below the bottom of laser craters. The number of cycles was constant for all samples, but the thickness of analysed material varied between 180 to 300 nm, depending on the number of determined elements and their concentrations in the samples, both of which control the integration time in each cycle. The sputtering rate was assumed to be constant during single analysis, and accordingly, it was calculated by linear interpolation of analysis time and depth of SIMS crater determined by Dektrak3 stylus profilometer.

Also, scanning ion images of laser crater in one synthetic andesite glass doped with alkali elements (Fig. 3.2) were acquired to qualitatively estimate the element distribution in the vicinity of the laser pits.

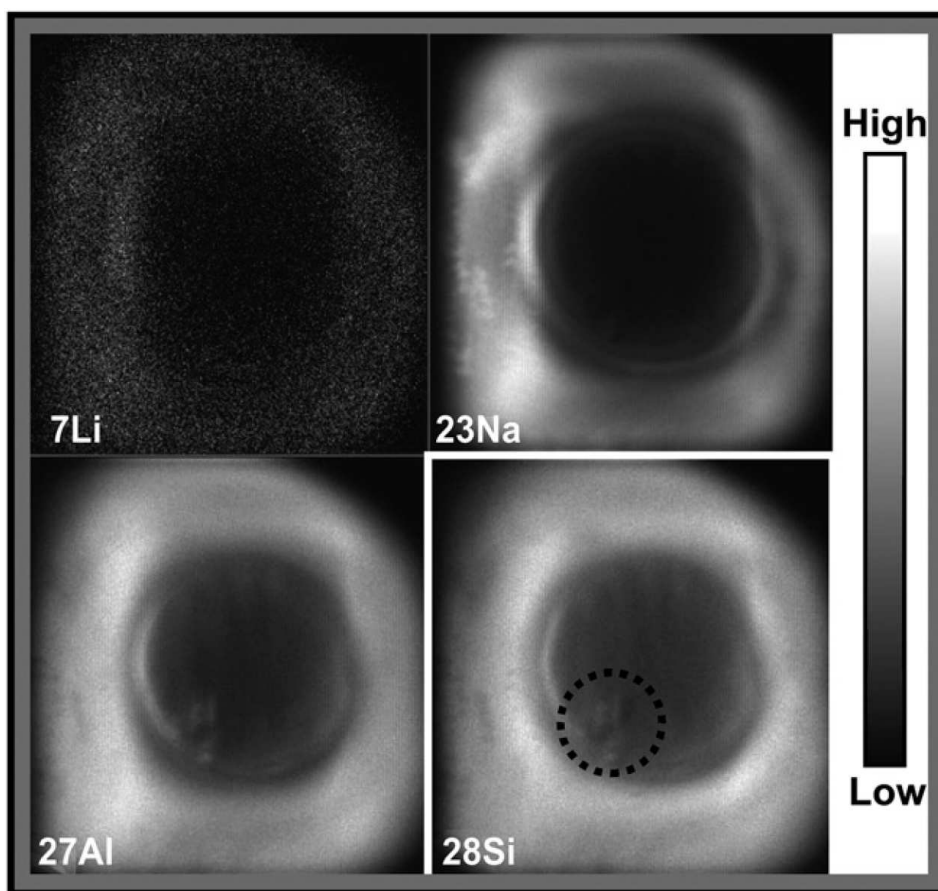


Fig. 3.2: Scanning ion image maps (SIMS) showing qualitative element distribution within a laser crater and the adjacent area in the synthetic andesite glass A-7 (7% Na₂O). The gray scale reflects the relative isotope (element) concentrations, showing variations in element abundances across the surface of the sample affected by laser ablation.

3.4 Results

3.4.1 Laser ablation measurements

Alkali elements often show elemental fractionation (systematic change of element intensity ratios with an increasing number of laser pulses) during LA ICP-MS acquisition. The observed fractionation varies from progressive alkali-depletion to alkali-enrichment when normalized to Si and Ca and the fractionation patterns are often related to the composition of sample matrix (Fig. 3.3).

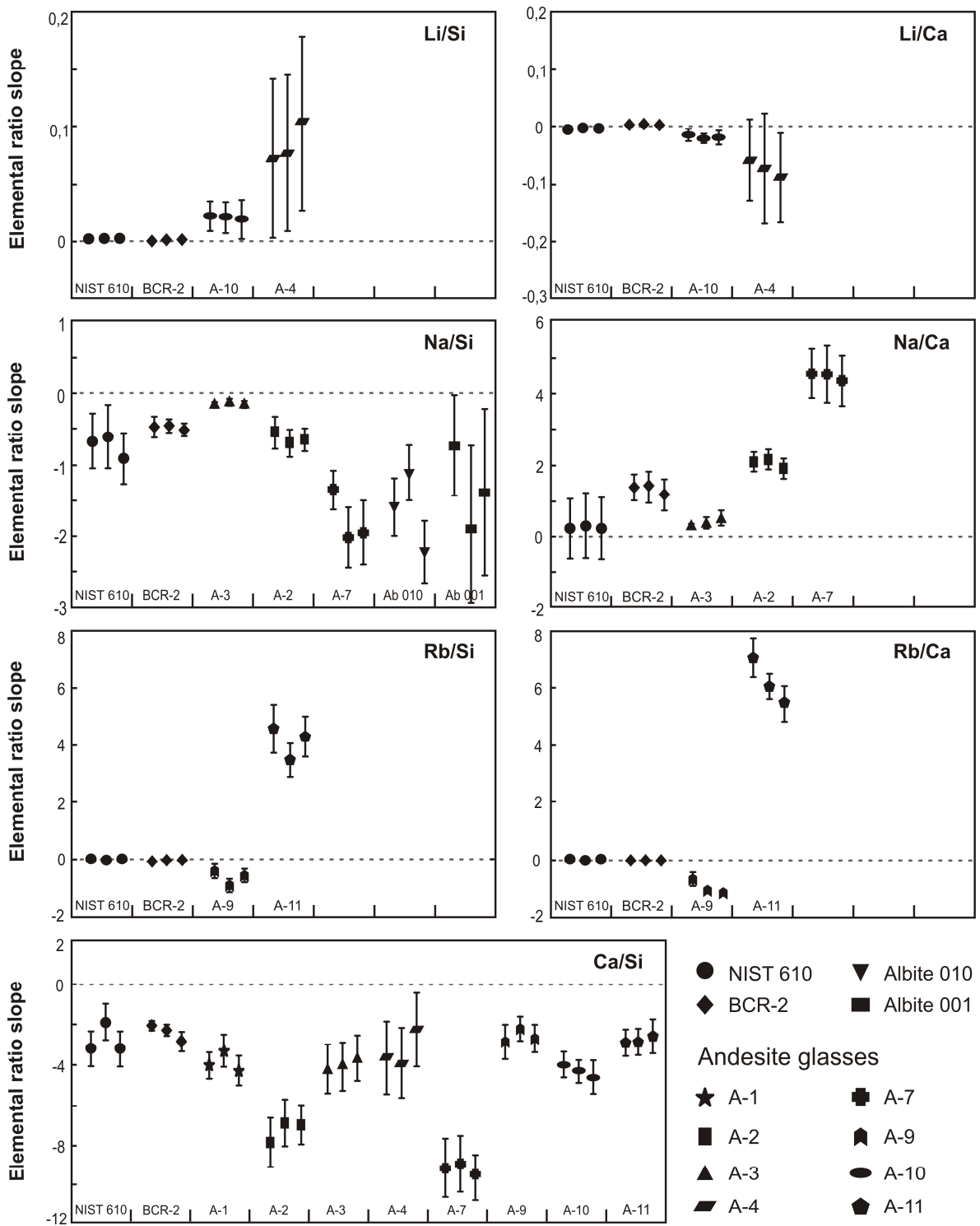


Fig. 3.3: Laser ablation TRA (time-resolved acquisition) signals for three replicate analyses of studied samples expressed using slope as a measure of the fractionation trend [24]. The uncertainties for individual measurements are 1 sigma or less than the size of the symbols. The synthetic andesite glasses are arranged in the order of increasing alkali element concentrations.

The ablation of NIST-610 glass shows differences in the fractionation trends for different alkali elements. The ratios Li/Ca, Na/Si, and Ca/Si have negative slopes of the fractionation trend as a function of ablation time while the Li- and Rb/Si and Na- and Rb/Ca show positive slopes of the fractionation trends.

Signals obtained from ablation of BCR-2G glass show negative fractionation slopes for Na, Rb, and Ca when normalized to Si, and positive slopes of fractionation for Li relative to Si and Li, Na, and Rb when normalized to Ca.

Both samples of albite that were ablated in different crystallographic orientations (Albite (010) and Albite (001)) have negative slopes of Na/Si fractionation.

The synthetic andesite glasses show a positive fractionation slope for Li relative to Si and negative slope relative to Ca in samples A-4 (7% Li₂O) and A-10 (1% Li₂O). Contrary to Li, Na shows negative fractionation trends relative to Si and a positive fractionation relative to Ca in samples A-2 (3.5% K₂O + 3.5% Na₂O), A-3 (0.5% K₂O + 0.5% Na₂O) and A-7 (7% Na₂O); the rate of fractionation relative to Si and Ca increased with increasing concentration of sodium in the glasses. Rubidium shows a negative fractionation slope relative to Si and Ca for sample A-9 (1% Rb₂O), while sample A-11 (7% Rb₂O) has a positive fractionation slope for Rb relative to Si and Ca. The Ca/Si ratio shows a negative fractionation for all analysed samples.

3.4.2 Ion probe measurements

3.4.2.1 Analysis of the ejecta blanket

The composition of the ejecta blanket on the surface of NIST-610 glass and on the albite was studied using 300 μm ion probe traverses starting at the crater rim (large ejecta particles) and proceeded away from the crater through the smaller ejecta particles and on to a clean sample surface. The results show systematic changes in the composition of the particles with increasing distance from the laser pit (Fig. 3.4).

The signal intensity ratios of alkali elements (Li, Na, K, and Rb) and Ca to Si in the NIST-610 glass show significant variations across the ejecta blanket. The Li/Si and Ca/Si ratios decrease outwards from the crater rim and approach the value measured on the clean sample surface. The Na/Si ratios show non-systematic variations across the ejecta blanket and the K/Si and Rb/Si ratios gradually increase in the traverse away from the crater rim.

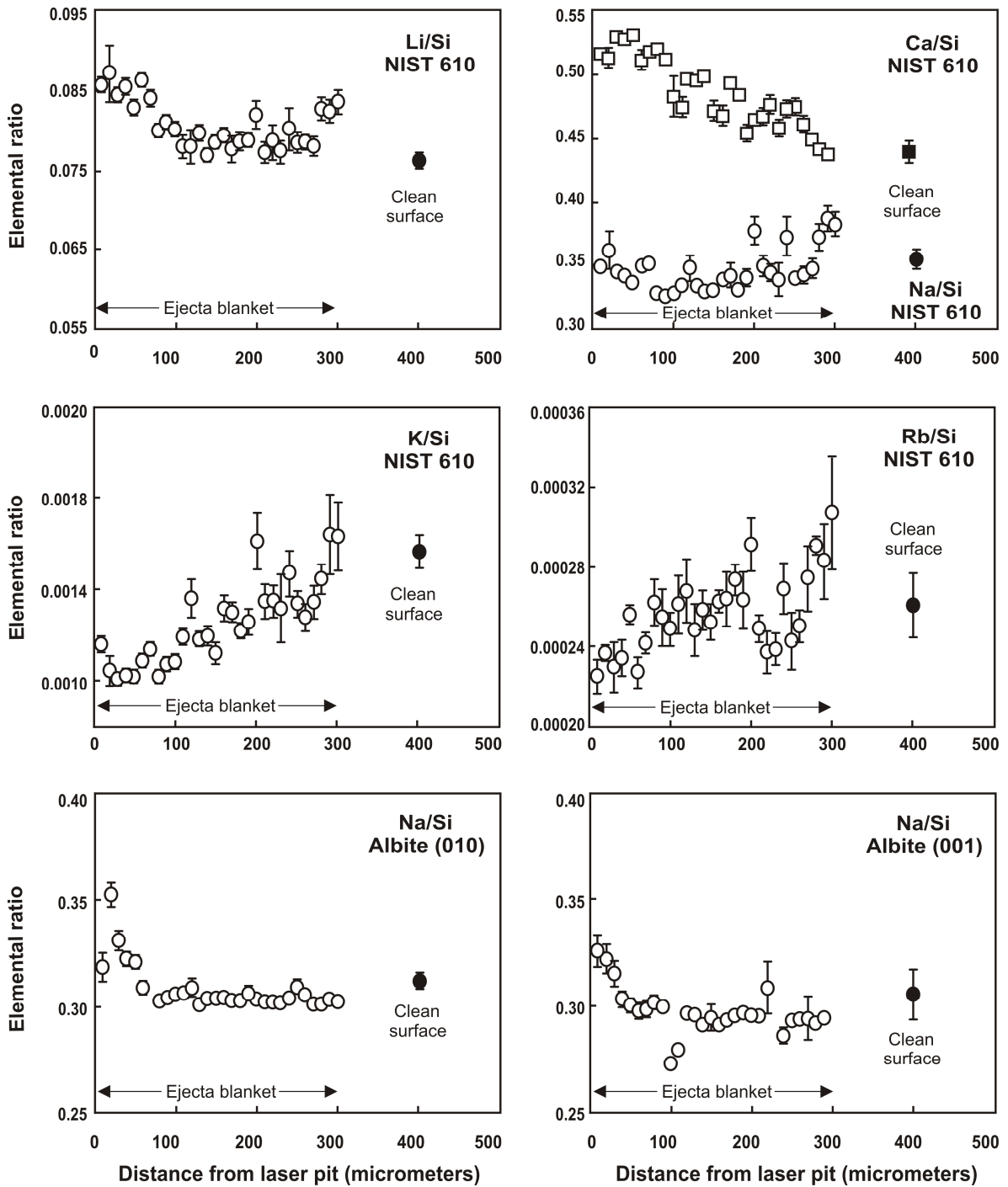


Fig. 3.4: Ion probe traverses from the rim of the laser ablation crater radially outwards to beyond the edge of the ejecta blanket deposited on the sample surface (data are not corrected for instrument mass discrimination). Uncertainties are 1 sigma.

Comparison of NIST-610 glass data for the first 5 cycles of SIMS measurement (Fig. 3.4) is in a good agreement (within analytical uncertainty) with values of the second 5 cycles for the first 200 μm of traverse. During the last 100 μm of the traverse there is a small shift of the second 5 cycles block values towards clean surface value. This is interpreted as an effect of slow ion beam penetration through the ejecta blanket and analysis of mixture of ejecta particles with the underlying sample. Small (nm-sized) particles are deposited in this part of ejecta blanket and the thickness of the ejecta decreases further away from the crater rim.

The Albite (010) sample also shows a significant variation in the measured Na/Si ratio across the ejecta blanket. The value of the ratio, near the edge of the laser crater, increases until reaching ca. 20 μm from the crater rim. This is followed by a decrease until the ratio stabilizes near its original value at ca. 80 μm from the crater rim (Fig. 3.4).

Results obtained from a traverse of the ejecta blanket on Albite (001) are similar to Albite (010), but do not show an initial Na/Si increase adjacent to the crater rim. Two measurements at ca. 100 μm from the crater rim yield lower Na/Si values compared to the remaining part of the traverse.

Comparison of the first and second 5-cycle blocks of Albite SIMS analysis revealed that ejecta blanket is present just within ca 100 μm from the laser crater.

Collectively, data from traverses across the ejecta blanket on the NIST-610 glass and on the albite show variations in the measured alkali element/Si intensity ratios that can be correlated with the systematic change in the size of particles that form the ejecta. While there is difference between the two albite samples adjacent to the crater rim, the NIST-610 and the albite differ in their Na/Si composition changes across the ejecta.

3.4.2.2 Depth profile analysis

The results from SIMS depth profile measurements in the bottom of the 80 μm wide laser ablation craters in the NIST-610, BCR-2G and andesitic glasses and in the albite reveal significant changes in the chemical composition in the first tens of nanometres below the bottom of the craters. The composition changes due to the ablation process are best observed when the depth profile data from the craters are normalized to corresponding depth profile data obtained on the fresh sample surface.

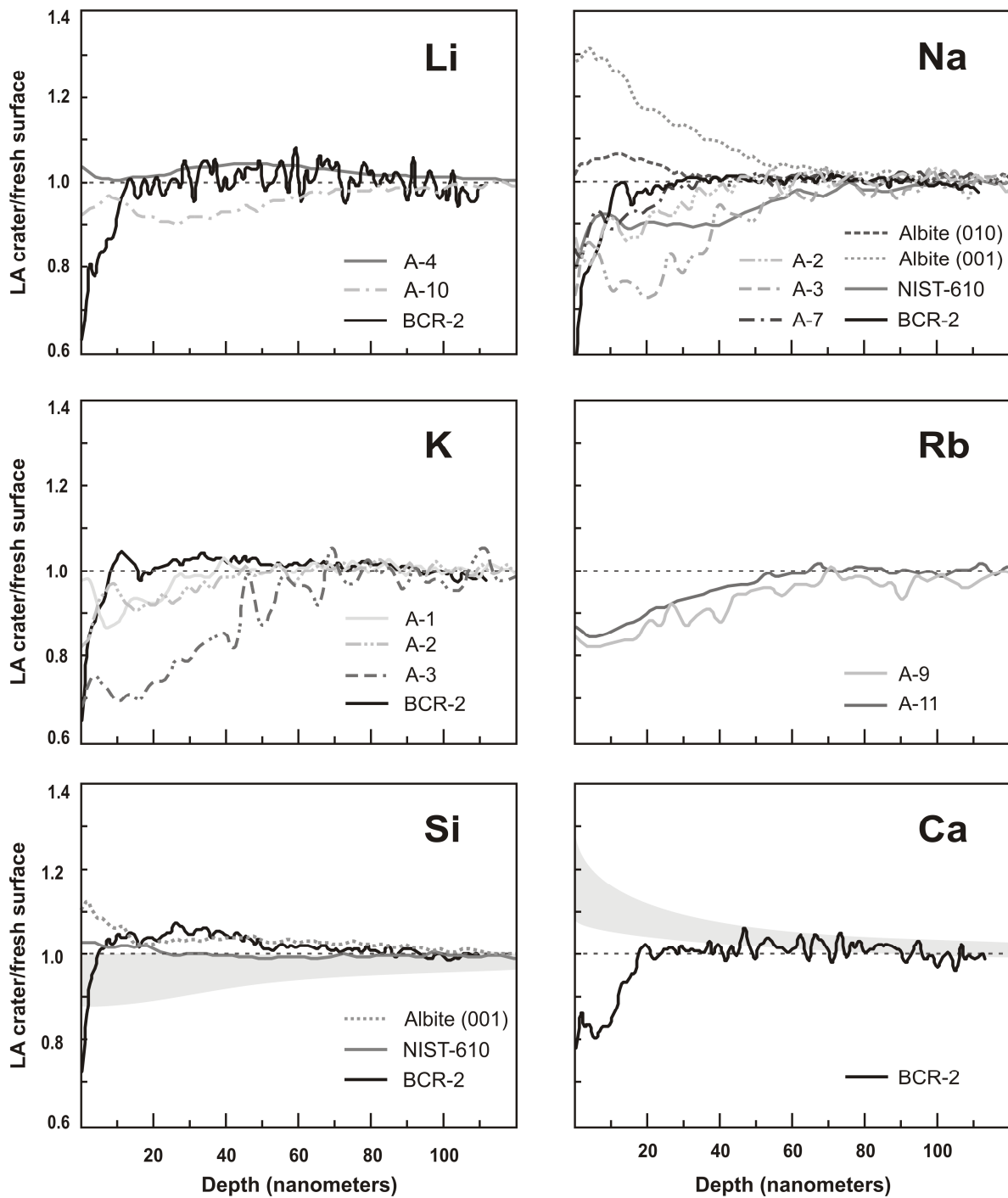


Fig. 3.5: Results of SIMS depth profile measurements of the bottom of laser craters. The craters were produced by firing 5 laser pulses. Individual mass scans are normalized to the corresponding depth profile analyses of the fresh sample surface. The shaded areas in the Si and Ca graph are fields fitting to the depth profiles of all analysed samples except for the highlighted individual ones.

The depth profile in NIST-610 glass (Fig. 3.5) shows a depletion of Na in the first 60 nm relative to the fresh sample surface. The amount of Si in the first 20 nm of the profile is very slightly increased, followed by a stable signal intensity ratio of $\text{Si}_{\text{crater}}/\text{Si}_{\text{fresh surface}}$. The signal intensity ratio of $\text{Ca}_{\text{crater}}/\text{Ca}_{\text{fresh surface}}$ suggests enrichment in the concentration of Ca down to a depth of 60 nm below the bottom of the laser crater. Sodium shows the largest difference (ca. 20%) between signal intensities measured by depth profiling on the crater floor and the fresh sample surface of the NIST-610 glass.

The results of corresponding depth profiling in BCR-2G glass suggest depletion in Li, Na, and K in the first 15 nm of the profile relative to the fresh sample surface. Silicon is depleted in a zone that is only 10 nm deep followed by a zone of weak enrichment to the depth of 50 nm, while depletion in Ca extends down to 20 nm into the sample. Maximum depletion (ca. 40%) for Li, Na, and K was observed directly below the bottom of the laser crater with the degree of depletion decreasing with increasing depth in the profile.

A maximum enrichment of up to 8% in Na, relative to clean sample surface, was observed at a depth of 15 nm below the floor of ablation crater in Albite (010), in an enrichment zone which was 30 nm thick. This sample was also depleted in Si (ca. 10% depletion) in the zone that extended to a depth of ca. 30 nm. Different observations were made in Albite (001) where the depth of maximum enrichment in Na (ca. 30%) was 10 nm while the enriched zone was 80 nm deep. Silicon was also enriched below the laser crater with the maximum enrichment in Si (ca. 10%) directly below the laser crater; with enrichment zone which was ca. 80 nm thick.

The andesite glass A-4 (7% Li_2O) was enriched in Li to a depth of 100 nm below the ablation pit bottom with two maxima directly below the bottom of the crater between 40 to 60 nm. The andesite glass A-10 (1% Li_2O) is depleted relative to the fresh sample surface in the first 100 nm below the bottom of the crater with a maximum depletion of 10% at a depth of 25 nm. The content of Na in samples A-2 (3.5% K_2O + 3.5% Na_2O), A-3 (0.5% K_2O + 0.5% Na_2O) and A-7 (7% Na_2O) was depleted in the first 50, 70, and 30 nm, respectively, of the profile relative to the fresh sample surface. Potassium in andesite glass A-1 (7% K_2O) was depleted to a depth of 30 nm with a maximum depletion of ca. 15% at 8 nm depth. Sample A-2 (3.5% K_2O + 3.5% Na_2O) was depleted in K in first 45 nm while sample A-3 (0.5% K_2O + 0.5% Na_2O) was depleted in K to a depth of 70 nm. Rubidium crater/fresh sample surface ratio in glass A-9 (1% Rb_2O) was depleted in the first 100 nm with a maximum depletion of 18% directly below the laser pit while

sample A-11 (7% Rb₂O) was depleted in the first 50 nm with a maximum depletion of 15%. All synthetic andesite glasses were depleted in Si and enriched in Ca directly below the laser crater relative to the sample unaffected by laser ablation.

All samples, except for BCR-2G glass, show enrichment in Ca below the ablation crater. The depth of enrichment varies for different sample matrices with a maximum enrichment at 120 nm in the artificial andesite glass A-11 (7% Rb₂O).

The content of Si along depth profiles in most of the studied samples was constant or slightly depleted compared to the fresh sample surface, with the exception of Albite (001), NIST-610 and BCR-2G glasses which show a weak Si enrichment directly below the bottom of the laser crater. This is consistent with the measured signal intensities during laser ablation ICP-MS analysis, where the observed elemental fractionation trends vary depending whether Ca or Si was used for signal normalization.

Lithium was depleted directly below the ablation craters in all samples, except for the andesitic glass A-4 (7% Li₂O) where Li was slightly enriched. Sodium was systematically depleted below the ablation craters in all glasses relative to parts of samples that were not affected by the laser. The depth of depletion varies from 15 to 70 nm. The zone of relative Na enrichment in the two albite samples (010 and 001) was at 30 and 80 nm, respectively. Potassium and rubidium were depleted in all samples with a depletion zone between 30 and 100 nm. Consistent with observations from the SIMS depth profiling, the SIMS scanning ion image of the laser crater in the synthetic andesitic glass A-7 (7% Na₂O, Fig. 3.2) suggests heterogeneities in the Li, Na, Al, and Si contents at the bottom of the crater. Small but significant variations of elemental distribution in the inner part of ablation pit are best observed in the marked part of the Si map on Fig. 3.2. These variations are interpreted as corresponding to fractionated material deposited on the bottom of the laser crater.

3.5 Discussion

Previous studies suggested that interactions of a laser beam with solid samples can result in phase and chemical modifications (Košler et al., 2005b), the extent of which are dependent on the sample matrix, especially its chemical composition and crystal structure. The new SIMS depth profile and scanning ion image data obtained from glass and albite samples in this study show the

laser-induced changes in chemical (*e.g.*, alkali elements) composition within, and adjacent to the ablation crater. The outstanding question is whether the observed alkali element fractionation during laser ablation ICP-MS analysis is primarily due to alkali element migration within the volume of the sample, or whether the dominant fractionation occurs during the formation of aerosol particles, their transport to the ICP, and excitation processes in the ICP torch. This issue can be addressed through careful analysis of depth profile patterns, chemical composition of the ejecta blanket adjacent to laser craters and time-resolved signal measurements by laser ablation ICP-MS.

3.5.1 Depth profile analyses

The depth profile analyses in laser ablation craters (Fig. 3.5) in synthetic andesite glasses and NIST-610 suggest that the alkali elements and Si are depleted and Ca is enriched relative to the parts of samples that were not ablated by the laser. The crystalline Albite (001) and Albite (010) samples show distinct behaviour for Na and Si. The basaltic glass BCR-2G has a different distribution of Ca and Si compared to other (andesite and NIST) glass samples. This could be due to the higher absorbance of laser radiation in the more opaque (at the laser wavelength) BCR-2G glass that could have resulted in differences in sample heating during laser ablation. This effect was also observed in depth profile patterns of alkali elements (Li, Na, and K) which are, similar to other glasses, depleted below the laser pit in BCR-2G, but with a narrow depletion zone.

The effects of laser ablation on element distribution below the bottom of the laser pits can be detected down to the depth of ~70 nm (for the laser parameters used in this study and 5 or 10 laser shots), the only exception being for Ca which was found to be enriched down to the depth of ~120 nm in synthetic andesite glass A-11 (7% Rb₂O).

Changes of Na content revealed by depth profiling can potentially be attributed to volume diffusion, such as estimated by Arrhenius equation ($D = D_0 \cdot \exp[-Q/RT]$) for series of sodium-potassium silica glasses using values of pre-exponential factor D_0 and activation energy Q published in Frischat (1971). Assuming sample surface temperature of 5000K and time of 100 ns (*i.e.* 20 times longer than laser pulse duration), the depth effect of sodium diffusion for glasses ranging in composition from pure soda to mixed soda-potash glass would be between 60 to 80 nm. Although the composition of NIST glasses used in this study does not match exactly the

glass composition used to estimate the diffusion depth, such diffusion model might assist in estimating the observed compositional variation.

The depth profile patterns did not reveal any significant effects as a function of the number of laser pulses (5 or 10) used. This is probably due to the efficient removal of laser-affected parts of the sample during the ablation. Therefore, only one set of depth profile data for craters produced by 5 laser shots is shown (Fig. 3.5). Below the zones affected by laser ablation, the compositions of the samples remain constant (the same as the fresh sample). Should volume diffusion be the dominant mechanism of chemical changes caused by sample heating during laser ablation, migration of another species in the opposite direction, or formation of depleted and enriched zone sequence, as observed for EPMA in Humphreys *et al.* (2006) would be expected to compensate for mass and ionic charge. However, the depth profile data obtained from the glass samples (NIST 610, BCR-2G, and all synthetic andesite glasses) are not indicative of such a process, suggesting that element fractionation during the formation and transport of aerosol may be a likely explanation for the alkali element fractionation observed during laser ablation ICP-MS analysis. The enrichment of Na and Si in the depth profile below the bottom of the laser crater in natural crystalline albite was different from the behaviour of these elements in glasses and may be indicative of laser-induced migration of alkali elements within the albite structure which in turn may be related to the differences in the short- and long-range order between amorphous and crystalline materials.

3.5.2 Ejecta blanket analyses

It has previously been shown that for static ablation sampling (*i.e.*, single laser pit), the aerosol particle size distribution changes systematically with the number of laser pulses applied to a sample (Guillong and Günther, 2002; Jackson and Günther, 2003). Differently sized particles can vary in phase and chemical composition that may also be different from that of the bulk sample (Košler *et al.*, 2005b; Kuhn and Günther, 2004). The ejecta blankets were composed of variably sized particles that also show variations in chemical composition (Fig. 3.4). Their composition trends towards the bulk sample composition in profiles measured across the ejecta starting at the crater rim and proceeding radially towards the clean sample surface. Given the systematic change in particle size distribution across the ejecta (*i.e.*, larger particles are deposited closer to the crater (Košler *et al.*, 2005b)), data in Fig. 3.4 show that different particle size

fractions have different chemical compositions. The larger particles close to the crater are enriched in Li, very similar in Na content and depleted in K and Rb relative to the bulk NIST-610 composition. This might be due to enhanced diffusion of light alkali elements (*e.g.*, Li) compared to heavy alkali elements (*e.g.* K, Rb) at the start of laser ablation.

Particles in the ejecta blanket also show different behaviour of Ca and Si. Ca is enriched relative to Si in droplets of molten material deposited close to the laser crater. This is in agreement with observations in Motelica-Heino *et al.* (2001) where melt droplets formed by laser ablation of glass material were depleted in Si and K and enriched in Ca. It has been shown by several studies that large (μm -sized) particles preferentially form during the early stages of single pit ablation (Guillong and Günther, 2002; Košler *et al.*, 2005b; Kuhn *et al.*, 2004). Smaller particles deposited farther from the laser crater (ca. 200-250 μm) have composition similar to the bulk NIST 610 glass (Fig. 3.4). This variation may be due to different dominant processes involved in the formation of small (condensation from vapour phase) and large (melt splashing) particles (Košler *et al.*, 2005b). The data from SIMS traverses across the NIST 610 ejecta blankets suggest a preferential incorporation of Li and Na relative to Rb and K into larger aerosol particles that form primarily by melt splashing; this observation is also consistent with the results of SIMS depth profiling into the crater floors.

3.5.3 Laser ablation analyses

The rate of fractionation for Li, Na, and Rb relative to Si and Ca in the synthetic andesite glasses shows an increase with increasing element concentration in the glass (Fig. 3.3), but no similar effect was observed for the NIST-610 and BCR-2G glasses. While the concentration effect is negligible when comparing samples with different matrices, the matrix, rather than the concentration of alkali elements, appears to have a dominant effect on the elemental fractionation during laser ablation analysis.

Fractionation of alkali elements (*i.e.*, systematic change in alkali element to Ca or Si ratio with the number of laser pulses applied to the sample) due to composition differences between larger particles released early during the ablation process and smaller particles released later should also be reflected in composition variations across the ejecta blanket. The results of this study allow for the comparison for the Li/Si, Na/Si, and Rb/Si ratios obtained in the NIST-610

glass, however, no clear correlation between the ICP-MS elemental fractionation and elemental distribution within the ejecta blanket was observed.

3.5.4 Effect of crystallographic orientation

Orientation of the diffusion path is an important factor that affects the transport of alkali ions in crystalline samples. Ions can be transported in crystalline solids by a process of activated hopping between occupied and vacant sites or by migration within channels in a crystal structure (Jones et al., 2004). The interstitial sites and large cation vacancies in alkali feldspars are mostly linked to the (010) plane and the diffusion of alkali elements in feldspars is mostly driven by the vacancy mechanism (Jones et al., 2004). The two albite samples analyzed in this study were ablated perpendicular to the (010) and to the (001) planes, to test for effects of crystallographic orientation on re-distribution of alkali elements, especially Na. Significant differences in ablation behaviour were observed for ablation in the two crystallographic orientations. Small cracks parallel with the sample surface surrounded the craters in Albite (010), while ablation craters in Albite (001) have larger diameters (despite using identical ablation conditions), irregular shape, and ragged walls. The measured Na/Si ratio during the ablation of albite decreases with the number of laser pulses applied to samples in both crystallographic orientations (Fig. 3.3), suggesting a similar composition for particles produced during ablation of the two albite samples. Analysis of the ejecta blanket shows rapid changes in the Na/Si ratio close to the ablation crater (to a distance of ca. 100 μm) in both albite samples that are followed by stable Na/Si values in the remaining part of the profile (Fig. 3.4). This effect is attributed to the ejecta blanket being present for only 100 μm from the laser crater.

Compared to Albite (010), the change in Na content below the laser crater in Albite (001) is more pronounced (Fig. 3.5), which suggests higher sodium diffusion parallel to the (010) plane in the albite structure (Jones et al., 2004; Lin and Yund, 1972). Variations of Si content below the crater floor differ for the two crystallographic orientations of albite as shown in Fig. 3.5. Depth profile in Albite (001) shows Si enrichment below the crater floor while Albite (010) shows an opposite trend. Accordingly, the slope of fractionation is not an ideal measure of these variations since it can be caused by different behaviour of the normalizing element, Si, in the two crystallographic orientations.

The data presented suggest that crystallographic orientation is an important parameter that influences element re-distribution in the thermally affected parts of the sample and affects laser-

induced elemental fractionation in LA ICP-MS analysis. Chemical changes adjacent to the laser ablation craters in albite are consistent with a previously published thermally-induced redistribution of Na by diffusion within crystal lattice.

3.5.5 Correction for ablation yield

Calibration using external standards (such as the NIST-600 glass series) with a naturally occurring internal standard correction for differences in ablation yield between calibration reference materials and unknown samples is commonly used in LA ICP-MS analysis. The ablation yield is defined as the sensitivity (signal per unit concentration) of the internal standard measured in the calibration material relative to the sensitivity in the unknown (Košler et al., 2002b; Wilson, 1997). The choice of the internal standard is based upon its concentration and homogeneity in the sample and in the calibration reference material, mass, ionization potential, and element fractionation behaviour. Geochemical applications using LA ICP-MS often use naturally occurring isotopes of Si or Ca for internal standardization when determining lithophile elements, including alkaline, rare earth, and high field strength elements in silicate materials. The use of Ca as an internal standard is preferred compared to Si because of its higher atomic mass and lower ionization potential, and because its fractionation behaviour which is more similar to alkaline earth and rare earth analytes. The results of this study highlight some significant differences in the behaviour of Ca and Si during laser ablation of silicate materials. These are evident from variations of alkali element/Ca or Si signal intensity ratios and negative fractionation slopes for Si/Ca ratio during laser ablation analysis (Fig. 3.3). This was also seen in fractionation studies of the NIST 610 series glasses (Fryer et al., 1995; Kuhn et al., 2004; Longerich et al., 1996b) where Si does not behave similar to the other lithophile elements including the alkaline earths, rare earths, and high field strength analytes.

The SIMS depth profiles (Fig. 3.5) also show differences in laser-induced redistribution of Ca and Si in most of the samples studied, with Si and the alkali elements following similar patterns (*e.g.*, depletion below the laser crater), and Ca showing an opposite trend (*e.g.*, enrichment below the floor of laser crater). Accordingly, for the sample matrices and analytical conditions used in this study, the choice of Si for internal standardization in analysis of alkali elements would be preferred compared to the use of Ca.

3.6 Concluding remarks

Laser ablation analyses and SIMS measurements of the ejecta blanket composition and data from depth profiling below the laser craters reveal that significant part of fractionation of alkali elements during laser ablation takes place on the ablation site. The concentrations of individual alkali elements in synthetic andesite glasses had important effect on the rate of elemental fractionation. However, the fractionation rate is also controlled by the sample matrix.

Thermal alteration during ablation adjacent to the laser craters was clearly demonstrated for the samples, and the analytical conditions, used in this study. Thermally driven alteration of sample results in variations in the chemical composition as a function of the size of aerosol particles (non-stoichiometric ablation), and potentially also in fractionation due to variable transport properties of the different particle size fractions. Heat transfer during ablation can also cause the diffusion of elements within the sample and variable thermal effects in different crystallographic orientations. Sample orientation may thus influence elemental fractionation during LA ICP-MS analysis of crystalline samples. The importance of this effect for other elements and the plethora of samples used in geological applications remain topics for future studies.

The important conclusion of this study is that spatial distribution of elements that are commonly used in quantitative analysis of silicate geological samples for corrections of ablation yield (isotopes of Si and Ca) is strongly influenced by thermal effects adjacent to the laser ablation craters. As the observed effects are very different for Ca and Si, the choice of the internal standard is an important factor affecting precision and accuracy of laser ablation ICP-MS analyses.

3.7 Acknowledgements

Authors thank the Natural Sciences and Engineering Research Council of Canada for funding. Two anonymous reviewers provided detailed and constructive comments which helped to improve the quality of the manuscript.

Chapter 4: Evaluation of matrix effects during laser ablation MC ICP-MS analysis of boron isotopes in tourmaline

Jitka Míková^{1,2}, Jan Košler¹, Michael Wiedenbeck³

¹ *Centre for Geobiology and Department of Earth Science, University of Bergen, Allegaten 41, Bergen, N-5007, Norway*

² *Czech Geological Survey, Klárov 3, Prague 1, CZ-118 21, Czech Republic*

³ *Helmholtz Centre Potsdam, GFZ German Research Centre for Geosciences, Telegrafenberg, 14473 Potsdam, Germany*

Status: Submitted to Journal of Analytical Atomic Spectrometry

4.1 Abstract

Laser ablation MC ICP-MS and SIMS were used to determine the boron isotopic compositions of several natural tourmaline group minerals with variable chemical compositions (elbaite, schorl and dravite). This study evaluates the effects of laser ablation MC ICP-MS instrument parameters and sample matrix composition on data trueness, reproducibility and repeatability. We demonstrate that the tourmaline matrix affects significantly the obtained $\delta^{11}\text{B}$ values and impacts on data trueness at ca. 2.5 ‰ level if a non matrix-matched reference material is used to calibrate the measurements. In the case of a matrix-matched calibration, the LA MC ICP-MS boron isotopic data are comparable to the previously published values obtained by the TIMS technique. Repeatability associated with the average $\delta^{11}\text{B}$ values is typically between 0.2 and 0.5‰ (1s) for LA MC ICP-MS and 0.8 and 1.3‰ (1s) for SIMS, where it represents one of the main sources of uncertainty.

4.2 Introduction

Isotopic compositions of boron (B) with its two stable isotopes, ^{10}B and ^{11}B , have proven to be a powerful tool for studying geochemical processes in the natural systems. Because of peculiar geochemical characteristics of boron – high solubility and mobility in aqueous solutions, incompatibility in most magmatic systems and a large variation in natural boron isotope compositions of up to 90‰ (as a consequence of large relative mass difference between ^{10}B and ^{11}B) (Hoefs, 2009), boron isotopes often record transfer and mixing processes in the Earth and planetary processes. The applications of boron isotopic studies are reviewed in Palmer and Swihart (1996) and Leeman and Sisson (1996). Boron isotope ratios are expressed in $\delta^{11}\text{B}$ notation ($\delta^{11}\text{B} \text{ ‰} = [({}^{11}\text{B}/{}^{10}\text{B})_{\text{sample}}/({}^{11}\text{B}/{}^{10}\text{B})_{\text{reference}} - 1] \times 1000$) where the zero-point is commonly based on the NIST SRM 951 reference material, boric acid with a certified $^{11}\text{B}/{}^{10}\text{B}$ value of 4.04362 ± 0.00137 (Catanzaro et al., 1970).

Many technical improvements in the determination of boron isotopic ratios in natural materials have been introduced over the last two decades (see Tonarini *et al.* (2009)). The determination of boron isotopic ratios in geological materials by different techniques gives variable degrees of analytical uncertainties ($\pm 4 \text{ ‰}$ to 0.2 ‰). These techniques include positive thermal ionisation mass spectrometry (PTIMS) (Lemarchand et al., 2002; Sahoo and Masuda, 1995; Tonarini et al., 2003); negative ion thermal ionisation mass spectrometry (NTIMS) (Hemming and Hanson, 1994; Shen and You, 2003) inductively coupled plasma mass spectrometry (ICP-MS) (Gäbler and Bahr, 1999), including multiple-collector ICP-MS (MC ICP-MS) (Aggarwal et al., 2003), secondary ion mass spectrometry (SIMS or ion probe) (Chaussidon et al., 1997; Chaussidon and Robert, 1998) and laser ablation ICP-MS (LA ICP-MS) (le Roux et al., 2004; Tiepolo et al., 2006). Tonarini *et al.* (2003) and Gonfiantini *et al.* (2003) assessed both the analytical technique derived and interlaboratory biases; their results showed a significant spread in results and poor agreement between different laboratories. The source of data variation in their study was not clear but it could be related to the specific techniques used for boron extraction and purification or to differences in instrumental set-up routine. In order to further improve data inter-comparison between laboratories, Aggarwal *et al.* (2009) carried out a round robin study of synthetic solutions. Despite large inter-laboratory differences, this study suggested no systematic bias induced by different analytical techniques (Aggarwal et al., 2009). With the exceptions of SIMS and LA ICP-MS, all above mentioned techniques normally require chemical

separation of boron from the matrix prior to the mass spectrometric measurement. The boron separation from the sample matrix must be performed with great care to prevent both sample contamination and boron isotopic fractionation, which is a major risk due to its high volatility and high relative mass difference between the two respective isotopes (Ishikawa and Nakamura, 1990; Leeman et al., 1991; Nakamura et al., 1992; Tonarini et al., 1997).

Many applications of boron isotope geochemistry, such as the investigation of mineral zoning patterns or melt inclusions, require in-situ analysis with spatial resolution on the order of tens of micrometers. SIMS analysis offers very high spatial resolution and requires no chemical pre-treatment of samples prior to analysis. Similar to SIMS, LA MC ICP-MS does not require chemical sample preparation prior to the isotopic analysis. Reported analytical uncertainties on $\delta^{11}\text{B}$ determination in geological materials with boron concentrations ranging from tens to tens of thousands $\mu\text{g/g}$ are better than $\pm 2\%$ (Tiepolo et al., 2006). Both techniques are, however, prone to matrix effects; accordingly, a matrix-matched calibration is often required to correct for instrumental mass fractionation. In-situ boron isotope determinations conducted using laser ablation multicollector ICP-MS (le Roux et al., 2004; Tiepolo et al., 2006) have so far been applied only to natural and synthetic glasses, and further work is required in order to properly assess possible matrix effects during the analysis of natural rocks and minerals (le Roux et al., 2004).

Tourmaline represents the principal mineralogical sink for B in a broad spectrum of silicate systems. It has been demonstrated that the chemical composition of tourmaline provides a record of differentiation mechanisms and evolution of magmatic hydrothermal fluids in many granites and pegmatites (Jolliff et al., 1986; London et al., 1996). The crystallochemical properties of tourmaline have been shown to reflect the environment in which it was formed (Slack (1996) and references therein). Boron isotope studies of tourmaline have mostly provided insights into the sources of boron but have also been used to constrain tectonic settings, temperature of tourmaline formation, fluid/rock ratios and metamorphic processes (Palmer and Swihart, 1996; Trumbull et al., 2009; Xavier et al., 2008). While tourmalines often are compositionally complex and difficult to digest chemically without loss of boron, laser ablation ICP-MS may overcome these difficulties and can be a method of choice for isotopic study.

This study provides a detailed description of the analysis of tourmaline by LA-MC-ICP-MS and presents a comparison of this method and SIMS isotopic analyses of tourmalines. The

primary objective of this study was to evaluate the possible presence of matrix effects during laser ablation MC ICP-MS analysis of tourmalines.

4.3 Samples and experimental

4.3.1 Tourmaline samples

We have analysed a suite of tourmaline samples of different chemical compositions that have been well characterized by previous studies (Tab. 4.1). Their B isotopic composition varies from isotopically light ($\delta^{11}\text{B} = -18.98 \text{ ‰}$) to heavy ($\delta^{11}\text{B} = 10.63 \text{ ‰}$). Three of the samples (98144 elbaite, 108796 dravite, 112566 schorl) were developed specifically for use as reference materials by Dyar *et al.* (2001) and Leeman and Tonarini (2001). The sample B4 was used for an inter-laboratory comparison study (Gonfiantini *et al.*, 2003; Tonarini *et al.*, 2003). These four tourmalines represent the best characterised materials for boron isotopes that are presently available to the geochemical community. The other four samples (EZ-272, JS-82N-1, JS-82A-1A, and EB-67-90) are from the boron isotopic study of tourmaline by (Palmer and Slack, 1989).

Tab. 4.1: Boron contents and $\delta^{11}\text{B}$ values of analysed samples

Sample	B (ppm)	Analytical technique	$\delta^{11}\text{B}$	1s	Reference
98144 elbaite	31 402	TIMS, SIMS (concentration)	-10.40	0.20	(Dyar <i>et al.</i> , 2001; Leeman and Tonarini, 2001)
108796 dravite	31 091	TIMS, SIMS (concentration)	-6.60	0.10	(Dyar <i>et al.</i> , 2001; Leeman and Tonarini, 2001)
112566 schorl	31 153	TIMS, SIMS (concentration)	-12.50	0.05	(Dyar <i>et al.</i> , 2001; Leeman and Tonarini, 2001)
B4 (schorl)	28 700	TIMS + isotope dilution	-8.85	0.17	(Tonarini <i>et al.</i> , 2003)
EZ-272		TIMS	-14.17	0.23	(Palmer and Slack, 1989)
JS-82N-1		TIMS	-1.63	0.36	(Palmer and Slack, 1989)
JS-82A-1A		TIMS	-18.98	0.38	(Palmer and Slack, 1989)
EB-67-90		TIMS	10.47	0.36	(Palmer and Slack, 1989)

All samples were mounted in epoxy resin and polished to obtain flat and smooth surfaces suitable for EPMA, SIMS, and laser ablation MC ICP-MS analysis. Sample grains were split in two sample mounts. The mount S1 contained the samples 98144 elbaite, 108796 dravite, 112566 schorl and B4; the mount S2 contained Palmer and Slack's tourmalines together with 98144

elbaite and 108796 dravite. As the ablation cell was capable of holding only one sample mount at a time and our reference materials were mounted together with samples, data obtained from each sample mount were treated separately to avoid reference material change and effects of potential variation of analytical conditions during the session. Electron microprobe data available for these samples are summarized in Tab. 4.2.

Tab. 4.2: Electron microprobe data for analysed tourmaline samples. Values are given in wt%.

	elbaite	dravite	schorl	B4	EZ-Z72	JS-82N-1	JS-82A-1A	EB-67-90
F	1.08	0.16	0.09	0.69	0.00	0.00	0.01	0.19
Na ₂ O	2.64	1.73	2.01	2.30	2.14	2.69	2.32	1.68
SiO ₂	37.65	36.14	34.85	35.68	37.90	36.66	37.02	35.75
MgO	1.19	8.35	0.20	0.97	9.49	5.61	6.65	8.15
Al ₂ O ₃	36.81	22.71	33.33	33.35	33.32	28.97	33.03	24.39
Cl	0.00	0.01	0.00	0.01	0.00	0.00	0.00	0.01
K ₂ O	0.03	0.09	0.05	0.04	0.02	0.02	0.04	0.08
CaO	0.09	2.30	0.14	0.56	1.13	0.58	0.54	2.32
TiO ₂	0.35	1.53	0.67	1.13	0.53	0.12	0.67	1.37
FeO	6.61	14.10	14.73	11.35	2.43	12.94	7.06	12.95
MnO	0.35	0.02	1.18	1.14	0.03	0.03	0.00	0.03
Cr ₂ O ₃	0.01	0.02	0.00	0.01	0.04	0.02	0.08	0.04
O=F	-0.45	-0.07	-0.04	-0.29	0.00	0.00	-0.01	-0.08
O=Cl	0.00	0.00	0.00	0.00	0.00	0.00	0.00	0.00
Total	86.35	87.09	87.21	86.93	87.03	87.63	87.39	86.90

4.3.2 Laser ablation parameters

A solid state 213 nm UV Nd:YAG (New Wave Research, UP213) laser ablation system was used in this study. The laser was operated at a 10 Hz repetition rate with a laser spot diameter of 50 μm in rastering mode (200 μm line, 10 $\mu\text{m}/\text{s}$ speed and 5 passes over the same raster line). The laser fluence was in the range of 1–3 J/cm^2 . Samples were ablated in He atmosphere (1.2 L/min) using a small volume tear drop-shaped ablation cell. The cell washout time was less than 60 s for ¹¹B signal to drop down from 600 mV to the blank level of 2 mV. Gas blank was always measured with laser firing and closed shutter for the initial 30 s of signal acquisition, followed by collection of the ablation signal for additional 100 s. To evaluate the effects of this sampling strategy on the laser-induced isotopic fractionation of B, sample S1 was also analysed

using the same ablation parameters in single laser spot mode. In addition, the NIST 610 glass reference material and tourmaline B4 were also ablated using the rastering mode with laser beam diameters of 30, 50, 80, 105 and 120 μm in order to evaluate the effect of signal intensity on the measured B isotopic ratios.

4.3.3 MC ICP-MS parameters

The boron isotope ratio measurements were carried out on a Thermo Finnigan Neptune high-mass resolution multicollector ICP-MS equipped with 9 Faraday cups. Masses of ^{11}B and ^{10}B were measured on the outermost collectors H4 and L4, respectively, using a medium mass resolution (mass resolving power of $M/\Delta M \approx 5500$). Isotopic ratios for each measurement were collected in a single block of data consisting of 260 cycles (0.5 s integration time per cycle) preceded by 25 s of baseline measurement (10 s wait + 15 s defocus). Using the instrument parameters given in Tab. 4.3, 100 ng/g B solution yielded a signal intensity of 0.16 V for ^{11}B .

Tab. 4.3: Instrument parameters for laser ablation and solution MC ICP-MS analyses

Measured masses	^{11}B , ^{10}B	
Mass resolution	Medium	
Nebulizer	MicroFlow PFA-ST nebulizer: 50 $\mu\text{L}/\text{min}$	
Spray chamber	Combined cyclonic and double pass quartz glass spray chamber	
	Laser	Solution
Operation Power [W]	1250	1250
Cool Gas [l/min]	15	15
Aux Gas [l/min]	0.95	0.95
Sample Gas [l/min]	1.20	1.19
Additional Gas [l/min]	0.60	0.00
Extraction [V]	-2000.00	-2000.00
Focus [V]	-708.00	-708.00
X Deflection [V]	-6.73	-5.86
Y Deflection [V]	1.07	-0.46
Shape	197.00	210.00
Sensitivity [mV]	160 on mass 11 for 100 ppb B	
Background [mV]	1.6 on mass 11	

Data were processed off-line using a LamTool MS Excel spreadsheet (Košler et al., 2008). Following correction of the measured signal intensities for gas blank, the measured $^{11}\text{B}/^{10}\text{B}$ ratio of each unknown was corrected for mass discrimination and instrumental drift using the mean of the two adjacent analyses of the reference material (“standard-sample-standard” bracketing). The drift-corrected ratios were referenced to the published $^{11}\text{B}/^{10}\text{B}$ value of the reference material and the results are reported as $\delta^{11}\text{B}$ values relative to NIST SRM 951 using a certified $^{11}\text{B}/^{10}\text{B}$ value of 4.04362 ± 0.00137 (Catanzaro et al., 1970). Each measured material was treated not only as sample, but it was also used as a reference material in the standard-sample-standard bracketing sequence for purpose of this study, even though none of the materials used here have undergone an ISO-compliant certification of their boron isotope compositions. Published values (Tab. 4.1) were used as reference values for calibration. All data used for $\delta^{11}\text{B}$ calculations were obtained during one analytical session using identical instrument tuning parameters.

The rate of isotopic fractionation was calculated as the slope of the blank-corrected isotope ratio vs. time (Košler et al., 2002b) using the least square linear fit and the method of (Sylvester and Ghaderi, 1997). Identical signal lengths, corresponding to 800 laser pulses (equivalent to 80 seconds of ablation), were used to calculate the fractionation slopes for all analyses to ensure validity of inter-analysis comparison.

4.3.4 SIMS parameters

All samples were analysed for boron isotope ratios using the Cameca ims 6f SIMS at the Helmholtz Centre Potsdam. A $^{16}\text{O}^-$ primary ion beam employing a nominal accelerating voltage of 12.5 kV with a total an ion current of 800 pA was used to produce positive secondary ions. The beam was focused to $\sim 5 \mu\text{m}$ diameter at the sample surface. A secondary extraction voltage of 10 kV was used. The instrument was operated at a mass resolution $M/\Delta M \approx 1150$ to ensure full separation between the $^{11}\text{B}^+$ and the isobaric $^{10}\text{B}^1\text{H}^+$ mass peaks. Measured isotopic ratios were based on five blocks of 20 cycles of measurement consisting of 2 and 1s integrations of $^{10}\text{B}^+$ and $^{11}\text{B}^+$ respectively. During the two days of data collection we found no time-dependent trend in the measured values on the four calibrants (dravite, elbaite, schorl and B4), the overall fractionation of the SIMS method was defined by the simple average of the observed fractionation during the two days of data acquisition ($n = 29$).

4.3.5 Data comparison and uncertainty calculations

It is not the aim of this study to present a comparison between figures of merit of LA MC ICP-MS and SIMS, mainly because different data acquisition and reduction methods developed for the two techniques make the comparison of analytical uncertainties difficult. The terminology and definitions follow the recommendation by Potts (Potts, 1997). Briefly, the analysis of boron isotopic composition by LA MC ICP-MS was based on the standard-sample-standard bracketing data acquisition procedure that corrects for mass discrimination and instrumental drift. Uncertainties of individual reference material and sample measurements were combined to estimate measurement repeatability and, accordingly, only three consecutive measurements contribute to the calculation of the uncertainty of the individual $\delta^{11}\text{B}$ values. Weighted mean of $\delta^{11}\text{B}$ values for each sample with corresponding standard deviation was used to assess the trueness (accuracy) of the measurement.

The SIMS boron isotope data acquisition and reduction followed the procedures routinely used in the Helmholtz Centre Potsdam SIMS laboratory (Esmaily et al., 2009; Galbraith et al., 2009; Krienitz et al., 2008; Trumbull et al., 2009; Trumbull et al., 2008; Xavier et al., 2008). The SIMS data were corrected for mass discrimination and instrumental drift using the instrument mass discrimination factor (Δ_{inst}) calculated as a ratio between the measured and reference $^{11}\text{B}/^{10}\text{B}$ values. This factor was determined from the mean of all ($n = 29$) analyses of the four tourmaline reference materials used in this study. Because all sample data were corrected by a single Δ_{inst} factor, the repeatability of the reported $\delta^{11}\text{B}$ values includes also possible isotopic heterogeneities and differences in chemical composition of the reference materials, any influence derived from sample changing and over-night machine shutdown. Compared to the LA MC ICP-MS procedure, this approach results in somewhat larger uncertainty estimates and represents a somewhat more robust method.

In order to improve the LA MC ICP-MS technique comparison with SIMS, we have also recalculated the data using the SIMS approach and the results of this comparison are discussed later.

4.4 Results

The mass spectrum from a 100 ng/g standard solution of SRM 951 was scanned at three

different mass resolutions to evaluate potential effects of spectral interferences on the measured isotopic ratios Fig 4.1A. No interferences were detected at mass 11, in contrast there was an interference detected on the low mass side of the ^{10}B peak. However, when operating the MC ICP-MS at medium mass resolution (MR), the ^{10}B peak was fully resolved from the interference. The relative signal intensity of the interfering species was related to plasma temperature since varying the sample gas flow rates between 1.115 and 1.295 L/min was clearly linked to variations in the intensity of the interfering peak. The data compiled in Fig. 4.1B show that the relative intensity of interference decreases with increasing sample gas flow and that the optimum sample gas flow for minimum interference overlap with the ^{10}B peak and sufficient B signal intensity during this experiment is ca. 1.2 L/min.

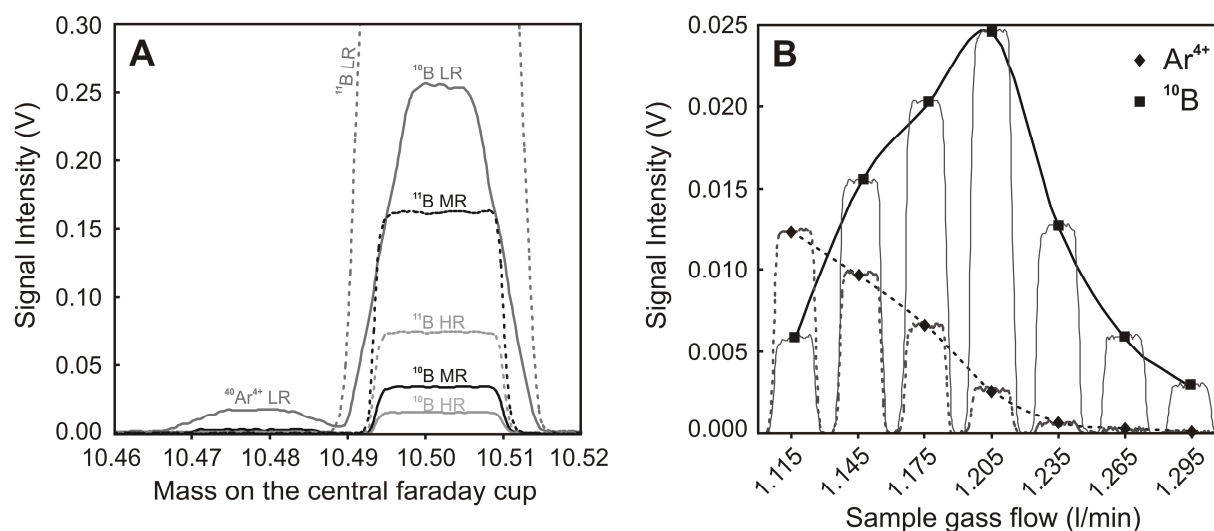


Fig. 4.1: A. Mass scans of 100 ppb B SRM 951 solution at three different mass resolutions showing adjacent interfering peak on mass 10 and its separation from ^{10}B peak (LR – low resolution, MR – medium resolution, HR – high resolution). B. Mass scans over interfering $^{40}\text{Ar}^{4+}$ (dashed line) and ^{10}B (solid line) peak in medium mass resolution for different sample gas flow settings.

In order to assess the effect of B concentration (signal intensity) on the measured B isotopic ratios we performed a series of solution (NIST SRM 951) and laser ablation (B4, NIST 610) analyses. The results shown in Fig. 4.2 suggest that with increasing boron concentration in the NIST SRM 951 solution (10, 50, 100, 150, 200, 250, 300, 400 and 500 ng/g), there is a shift towards heavier measured B isotopic ratios, ultimately showing a 3.2% difference between the lowest and highest measured ratio. A corresponding pattern of changing the measured B isotopic composition with changing signal intensity (increasing laser beam diameter in steps 30, 50, 80,

105 and 120 μm) was also observed for laser ablation MC ICP-MS analysis of tourmaline B4 (1.5% difference) and NIST 610 glass (16.7% difference) samples. This effect was more pronounced for low B concentrations and low signal intensities.

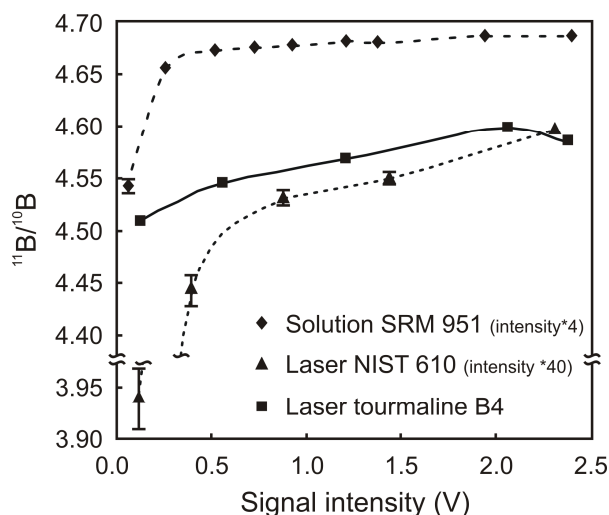


Fig. 4.2: Effect of signal intensity on the measured isotopic ratio in standard solution SRM 951 and laser ablation of NIST 610 and B4 tourmaline. Measured signal intensities of SRM 951 and NIST 610 were multiplied to obtain similar scale as B4 tourmaline for better comparison.

The results of our tourmaline measurements done by laser ablation MC ICP-MS are summarized in Tab. 4.4, the calculated $\delta^{11}\text{B}$ values (relative to NIST SRM 951) for the samples normalised with the bracketing approach are given in Tabs 4.5 and 4.6 for sample mounts S1 and S2, respectively. It should be noted that the resulting B isotopic composition for a particular sample is influenced by the specific tourmaline calibration material used for normalization. With bracketing procedure, where even number analyses are treated as unknown samples and odd number analyses of the same material are treated as calibration runs, the following weighted average $\delta^{11}\text{B}$ values with corresponding repeatabilities were obtained for the Palmer and Slack tourmaline samples: EZ-272 $-14.24 (\pm 0.28\%, 1s, n=2)$, JS-82N-1 $-1.79 (\pm 0.45\%, 1s, n=2)$, with single $\delta^{11}\text{B}$ values and their uncertainty on the JS-82A-1A $-19.02 (\pm 0.1\%, 1s)$ and EB-67-90 $10.76 (\pm 0.1\%, 1s)$. The following weighted average $\delta^{11}\text{B}$ values with repeatability were obtained on the 98144 elbaite $-10.45 (\pm 0.28\%, 1s, n=6)$, 108796 dravite $-6.64 (\pm 0.22\%, 1s, n=6)$, 112566 schorl $-12.41 (\pm 0.25\%, 1s, n=4)$ and B4 $-8.77 (\pm 0.41\%, 1s, n=4)$ tourmaline reference materials.

Tab. 4.4: *Compilation of all LA MC ICP-MS data measured during this study. Reported raw $^{11}\text{B}/^{10}\text{B}$ ratios are corrected for gas blank only.*

Sample	Sample mount S1		Sample	Sample mount S2	
	$^{11}\text{B}/^{10}\text{B}$	2SE		$^{11}\text{B}/^{10}\text{B}$	2SE
elbaite	4.5738	0.0006	elbaite	4.5732	0.0008
	4.5777	0.0006		4.5720	0.0009
	4.5791	0.0007		4.5682	0.0006
	4.5751	0.0006		4.5673	0.0008
	4.5750	0.0007		4.5675	0.0008
	4.5777	0.0006	dravite	4.5985	0.0010
	4.5800	0.0006		4.5989	0.0008
	4.5745	0.0006		4.5975	0.0008
	4.5713	0.0007		4.5966	0.0010
	4.5723	0.0006		4.5961	0.0007
dravite	4.5969	0.0007	EZ-272	4.5635	0.0006
	4.6021	0.0007		4.5620	0.0011
	4.6013	0.0006		4.5635	0.0007
	4.5978	0.0008		4.5608	0.0008
	4.5985	0.0007		4.5575	0.0006
	4.6016	0.0007	JS-82N-1	4.6201	0.0005
	4.5998	0.0007		4.6187	0.0007
	4.5970	0.0007		4.6155	0.0006
	4.5971	0.0008		4.6150	0.0006
	4.5967	0.0009		4.6186	0.0005
schorl	4.5671	0.0006	JS-82A-1A	4.5369	0.0005
	4.5695	0.0006		4.5343	0.0008
	4.5688	0.0006		4.5320	0.0006
	4.5683	0.0006	EB-67-90	4.6789	0.0008
	4.5682	0.0007		4.6785	0.0005
	4.5708	0.0007		4.6754	0.0006
	4.5659	0.0005			
	4.5661	0.0006			
	4.5660	0.0006			
	4.5645	0.0006			
B4	4.5874	0.0007	Sample mount S1 spot		
	4.5894	0.0007	Sample	$^{11}\text{B}/^{10}\text{B}$	2SE
	4.5871	0.0008	elbaite	4.5722	0.0009
	4.5855	0.0008		4.5701	0.0009
	4.5869	0.0009	dravite	4.5948	0.0014
	4.5897	0.0007		4.5937	0.0012
	4.5851	0.0006	schorl	4.5607	0.0011
	4.5855	0.0006		4.5632	0.0010
	4.5853	0.0006	B4	4.5814	0.0010
	4.5839	0.0007		4.5826	0.0010

Tab. 4.5: Calculated $\delta^{11}\text{B}$ values (relative to NIST SRM 951) for the samples contained in mount S1 as determined by LA ICP-MS. The samples were normalised by “standard-sample-standard” bracketing. The mean values represent weighted average of $\delta^{11}\text{B} \pm 1s$.

Sample	Normalized by							
	elbait		dravite		schorl		B4	
	$\delta^{11}\text{B}$	2s	$\delta^{11}\text{B}$	2s	$\delta^{11}\text{B}$	2s	$\delta^{11}\text{B}$	2s
elbait	-10.1	0.2	-11.3	0.2	-10.5	0.2	-11.0	0.2
	-10.8	0.2	-11.5	0.2	-10.4	0.2	-10.7	0.2
	-10.4	0.2	-11.9	0.2	-11.1	0.2	-11.1	0.2
	-10.7	0.2	-11.6	0.2	-11.1	0.2	-11.1	0.2
			-11.4	0.2	-10.7	0.2	-11.0	0.2
			-11.1	0.2	-10.0	0.2	-10.3	0.2
			-11.7	0.2	-10.7	0.2	-11.1	0.2
			-12.2	0.2	-11.4	0.2	-11.8	0.2
			-11.9	0.2	-11.0	0.2	-11.4	0.2
Mean	-10.5 ± 0.3		-11.6 ± 0.3		-10.7 ± 0.4		-11.0 ± 0.4	
Difference	1.1		0.2		0.5			
dravite	-5.8	0.2	-6.5	0.2	-5.2	0.2	-5.7	0.2
	-5.3	0.2	-6.8	0.2	-5.5	0.2	-5.9	0.2
	-5.2	0.2	-6.7	0.2	-6.2	0.2	-6.2	0.2
	-5.5	0.2	-6.9	0.2	-6.0	0.2	-6.0	0.2
	-5.6	0.2			-5.6	0.2	-5.8	0.2
	-5.5	0.2			-5.7	0.2	-6.0	0.2
	-5.5	0.2			-5.8	0.2	-6.2	0.2
	-5.2	0.2			-5.8	0.2	-6.2	0.2
	-4.9	0.2			-5.7	0.2	-6.1	0.2
Mean	-5.4 ± 0.3		-6.7 ± 0.2		-5.7 ± 0.3		-6.0 ± 0.2	
Difference	-1.3		-1.0		-0.7			
schorl	-12.3	0.2	-13.6	0.2	-12.4	0.2	-12.8	0.2
	-12.3	0.2	-13.6	0.2	-12.7	0.2	-12.9	0.2
	-12.2	0.2	-13.2	0.2	-12.1	0.2	-12.6	0.2
	-11.8	0.2	-13.0	0.2	-12.5	0.2	-12.6	0.2
	-12.1	0.2	-13.5	0.2			-12.5	0.2
	-12.1	0.2	-13.1	0.2			-13.4	0.2
	-12.9	0.2	-13.6	0.2			-12.9	0.2
	-11.9	0.2	-13.3	0.2			-12.9	0.2
	-11.6	0.2	-13.3	0.2			-13.1	0.2
Mean	-12.2 ± 0.4		-13.4 ± 0.2		-12.4 ± 0.2		-12.9 ± 0.3	
Difference	-0.2		1.0		0.5			
B4	-7.9	0.2	-9.2	0.2	-8.4	0.2	-8.2	0.2
	-8.0	0.2	-9.2	0.2	-8.1	0.2	-9.0	0.2
	-8.2	0.2	-9.3	0.2	-8.5	0.2	-9.2	0.2
	-8.1	0.2	-9.3	0.2	-8.8	0.2	-8.6	0.2
	-8.1	0.2	-9.4	0.2	-8.7	0.2		
	-8.1	0.2	-9.0	0.2	-7.9	0.2		
	-8.7	0.2	-9.5	0.2	-8.4	0.2		
	-7.7	0.2	-9.1	0.2	-8.3	0.2		
	-7.5	0.2	-9.1	0.2	-8.2	0.2		
Mean	-8.0 ± 0.4		-9.2 ± 0.2		-8.3 ± 0.3		-8.8 ± 0.4	
Difference	-0.8		0.5		-0.5			

Tab. 4.5: Calculated $\delta^{11}\text{B}$ values (relative to NIST SRM 951) for the samples contained in mount S2 as determined by LA ICP-MS. The samples were normalised by “standard-sample-standard” bracketing. The mean values represent weighted average of $\delta^{11}\text{B} \pm 1s$.

Sample	Normalized by											
	elbaite		dravite		EZ 272		JS-82N-1		JS-82A-1A		EB-67-90	
	$\delta^{11}\text{B}$	2s	$\delta^{11}\text{B}$	2s	$\delta^{11}\text{B}$	2s	$\delta^{11}\text{B}$	2s	$\delta^{11}\text{B}$	2s	$\delta^{11}\text{B}$	2s
elbaite	-10.1	0.2	-12.1	0.2	-12.2	0.2	-11.9	0.2	-11.1	0.2	-12.6	0.2
	-10.5	0.2	-12.3	0.2	-13.0	0.2	-12.2	0.2	-11.4	0.2	-13.0	0.2
			-12.8	0.2	-13.0	0.2	-12.0	0.2				
			-12.9	0.2	-12.4	0.2	-12.3	0.2				
Mean	-10.3 ± 0.3		-12.5 ± 0.4		-12.7 ± 0.4		-12.1 ± 0.2		-11.3 ± 0.2		-12.9 ± 0.3	
Difference			2.2		2.4		1.8		1.0		2.5	
dravite	-4.7	0.2	-6.4	0.2	-6.4	0.2	-6.0	0.2	-5.3	0.2	-6.8	0.2
	-4.5	0.2	-6.7	0.3	-6.7	0.2	-5.9	0.2	-5.1	0.2	-6.7	0.2
	-4.2	0.3			-6.7	0.3	-5.7	0.3				
	-4.2	0.2			-6.2	0.2	-6.1	0.2				
Mean	-4.4 ± 0.3		-6.5 ± 0.2		-6.4 ± 0.3		-6.0 ± 0.2		-5.2 ± 0.2		-6.7 ± 0.1	
Difference	-2.1				0.1		-0.5		-1.3		0.2	
EZ 272	-12.4	0.2	-14.2	0.2	-14.5	0.3	-14.0	0.3	-13.3	0.3	-14.7	0.3
	-12.2	0.3	-14.4	0.3	-14.1	0.2	-13.2	0.2	-12.4	0.2	-14.0	0.2
	-11.3	0.2	-13.9	0.2			-13.4	0.2				
	-11.8	0.2	-14.3	0.2			-14.5	0.2				
Mean	-11.9 ± 0.5		-14.2 ± 0.2		-14.2 ± 0.3		-13.8 ± 0.5		-12.7 ± 0.5		-14.3 ± 0.5	
Difference	-2.4		-0.1				-0.4		-1.5		0.0	
JS-82N-1	-0.1	0.2	-2.0	0.2	-1.8	0.2	-1.4	0.2	-1.0	0.2	-2.5	0.2
	0.1	0.2	-2.2	0.2	-2.1	0.2	-2.1	0.2	-1.2	0.2	-2.8	0.2
	-0.1	0.2	-2.6	0.2	-2.6	0.2						
	-0.1	0.2	-2.6	0.2	-2.1	0.2						
Mean	-0.1 ± 0.1		-2.3 ± 0.3		-2.1 ± 0.4		-1.8 ± 0.4		-1.1 ± 0.1		-2.7 ± 0.2	
Difference	-1.8		0.5		0.4				-0.7		0.9	
JS-82A-1A	-18.1	0.2	-20.0	0.2	-19.8	0.2	-19.5	0.1	-19.0	0.2	-20.7	0.2
	-18.2	0.2	-20.4	0.2	-20.3	0.2	-19.5	0.2			-20.9	0.2
	-18.2	0.2	-20.7	0.2	-20.7	0.2	-19.7	0.2				
Mean	-18.1 ± 0.0		-20.3 ± 0.4		-20.2 ± 0.5		-19.5 ± 0.1		-19.0 ± 0.1		-20.8 ± 0.1	
Difference	-0.9		1.3		1.2		0.5				1.8	
EB-67-90	12.6	0.2	10.7	0.2	10.9	0.2	11.2	0.2	12.0	0.2	10.8	0.1
	13.1	0.2	10.7	0.2	10.8	0.2	11.7	0.1	12.5	0.2		
	12.9	0.2	10.3	0.2	10.3	0.2	11.4	0.2				
Mean	12.9 ± 0.2		10.6 ± 0.2		10.6 ± 0.3		11.5 ± 0.2		12.3 ± 0.3		10.8 ± 0.1	
Difference	-2.1		0.2		0.1		-0.7		-1.5			

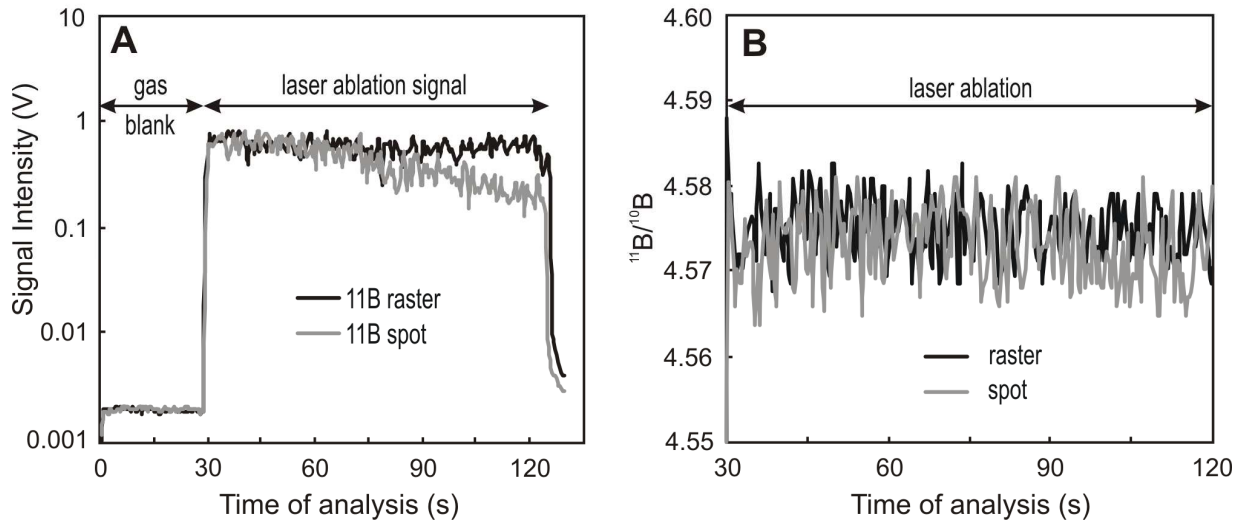


Fig. 4.3: A. Laser ablation signal for raster sampling (black line) and spot ablation (grey line). B. $^{11}\text{B}/^{10}\text{B}$ ratio of measured signals showing no significant isotopic fractionation (change of isotopic ratio during analysis) for raster sampling (black line) and spot ablation (grey line).

Boron isotopic fractionation during laser ablation analysis, expressed as slope of the time-resolved isotope ratio measurement, reveals no laser induced fractionation (systematic change of the measured isotopic ratio with number of laser pulses applied to the sample) for both laser ablation sampling strategies (raster and single spot). The time resolved isotope ratio patterns for raster and single spot laser ablation are similar (Fig. 4.3).

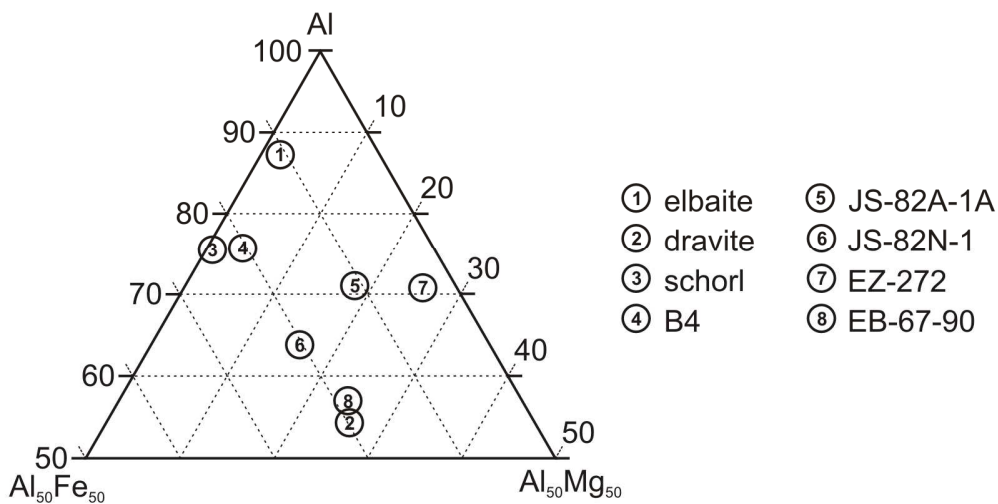


Fig. 4.4: Al- $Fe_{(tot)}$ -Mg diagram showing the samples composition based on EMPA analyses.

Electron microprobe analyses (Tab. 4.2) revealed three compositionally distinct tourmaline groups within the Al-Fe_(tot)-Mg ternary diagram (Fig. 4.4): (1) 98144 elbaite from a granitic pegmatite, (2) the schorl group consisting of 112566 schorl from a granitic pegmatite and B4 tourmaline from a monzogranitic pegmatite, and (3) the chemically uniform dravite group consisting of the 108796 dravite of uncertain origin (detrital source) and metamorphic (amphibolite facies) tourmaline EB-67-90. The chemical compositions of the other metamorphic tourmalines classified as dravite EZ-272 (amphibolite facies), dravite JS-82A-1A (granulite facies) and schorl JS-82N-1 (greenschist facies) (Taylor and Slack, 1984) differ significantly from the rest of samples analyzed in this study.

Results from SIMS measurements are summarized in Tab.4.7. The SIMS technique used in Potsdam is routinely used for measurements of B isotopes. Because of its spatial resolution trueness and reproducibility that are comparable to those achieved by LA MC ICP-MS for analysis of tourmaline, it is better suited for inter-technique comparison than the bulk sample TIMS measurements.

4.5 Discussion

4.5.1 Laser ablation MC ICP-MS

Isobaric interferences, such as those caused by molecular ions generated within the ICP source, can affect both the trueness and precision of the isotope ratio determination. The observed interference on the low mass side of the ¹⁰B peak (Fig. 4.1) has been attributed to ⁴⁰Ar⁴⁺ (Aggarwal et al., 2009; Feldmann et al., 1994; Gäbler and Bahr, 1999; Park, 2002). Although le Roux *et al.* (2004) reported that similar interferences can be caused by ²⁰Ne²⁺, we did not observe any significant traces of Ne during our experiments. The production of ⁴⁰Ar⁴⁺ is, to a large extent, controlled by plasma temperature, which in turn is affected by parameters such as RF power, sample gas flow, solvent loading and RF generator characteristics (e.g., frequency) (Mermet, 2006). Gäbler and Bahr (1999) reported that the intensity of ⁴⁰Ar⁴⁺ interference can be reduced by using a lower radio frequency setting, which is one of the fundamental parameters that influence the ICP temperature. The results of our study are consistent with (Gäbler and Bahr, 1999) in that the ability of plasma to form quadruply charged Ar ions appears to be mainly influenced by the

ICP temperature. This is in agreement with the observed change in the $^{40}\text{Ar}^{4+}$ intensity relative to the intensity of ^{10}B with varying sample gas flow (Fig. 4.1B).

The increase in isotopic ratios with increasing signal intensity (concentration of ions in the ICP, Fig. 4.2) is attributed mainly to the space charge effects due to electrostatic interactions between positively charged ions in the ICP and interface region. It is influenced by the density and composition of the ion cloud, and is therefore related to the composition of sample matrix and concentration of the analyte (Andren et al., 2004). The only observed exception from this trend is the last measured point on the B4 tourmaline sample (120 μm laser beam diameter) that shows a slight decrease of the measured B isotopic ratio for the highest signal intensity. While there is no laser induced fractionation (Fig. 4.3) that could possibly explain this decrease, it may be consistent with effects of plasma mass load. Previously published data (Kroslakova and Günther, 2007) suggest that an increase in the mass loading of the ICP leads to a decrease in the measured intensity ratios; it can therefore be concluded that accurate analyses should only be carried out using identical laser settings for calibration materials and unknown samples.

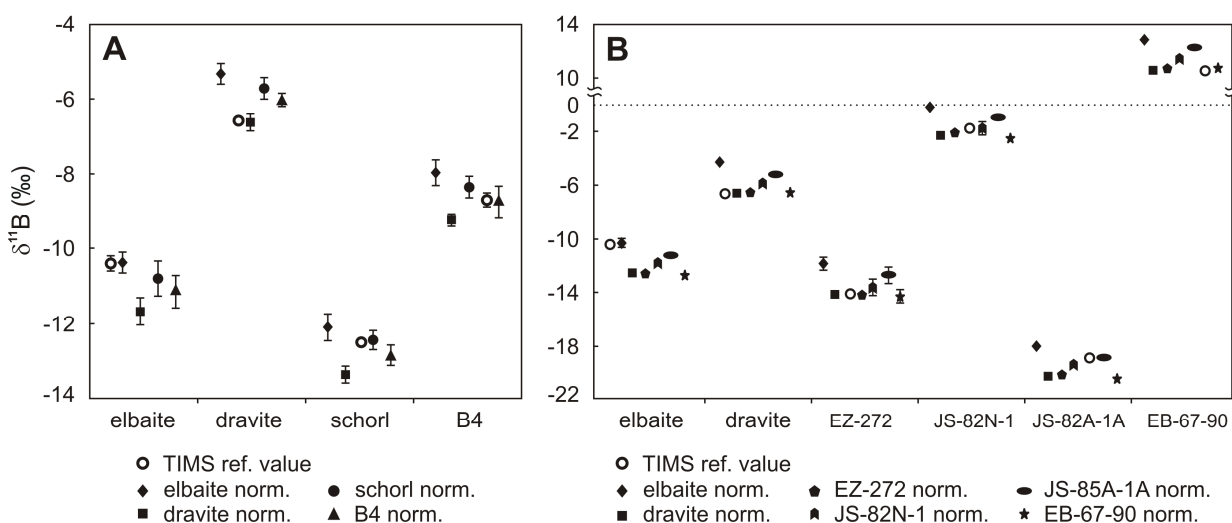


Fig. 4.5: Variations of $\delta^{11}\text{B}$ in tourmaline samples for different compositions of tourmaline standard in the standard-sample-standard analysis strategy (each material was normalised by all other measured materials) for sample mount S1 (A) and S2 (B). Error bars represent 1 σ uncertainty of the mean value. TIMS reference values are discussed in the text.

Results of our experiments revealed an apparent variation in the B isotopic composition of tourmalines which is a function of the different reference materials used for calibration. When calibrated against a tourmaline reference material of similar chemical composition, the isotopic

composition agreed with the expected values (Fig. 4.5). The offset between the measured and expected $\delta^{11}\text{B}$ values (in ‰) correlates with the composition of the reference material which is highly suggestive of a systematic chemical matrix effect. Relation between the offset from expected value and composition of the standard matrix remains same for all measured samples as can be seen from similar offset patterns in Fig. 4.5. The maximum difference of 2.5‰ was observed between elbaite and dravite tourmalines (Fig. 4.5B, Tab. 4.6) and the smallest difference of ca. 0.1‰ (i.e., within analytical uncertainty) was observed between the dravite tourmalines (Fig. 4.5B, Tab. 4.6).

In light of the highly complex solid-solutions possible in the tourmaline system with theoretical formula $(\text{Na,Ca})(\text{Mg,Fe,Mn,Li,Al})_3(\text{Al,Mg,Fe}^{3+})_6(\text{Si}_6\text{O}_{18})(\text{BO}_3)_3(\text{O,OH})_3(\text{OH,F})$ (Deer et al., 1992), it is difficult to assign the observed matrix effect to a particular parameter of chemical composition. Chaussidon and Albarède (1992) reported for their SIMS measurements a systematic decrease in $\delta^{11}\text{B}$ from the Li-rich tourmalines to the Mg-rich and the Fe-rich tourmalines. When comparing the chemical composition of tourmaline (Fig. 4.4) with results of the measured isotopic ratios (Tab. 4.5, Tab. 4.6), it appears that the $\delta^{11}\text{B}$ values for our sample are mainly influenced by Al content in the calibrating tourmaline (the observed $\delta^{11}\text{B}$ values decreases with increasing Al content in the tourmaline calibration material). Though we would not necessarily predict concordant behavior between laser- and ion-based sampling approaches, our observation seems to be consistent with results of Chaussidon and Albarède (1992) because the compositional field of Li-rich tourmalines in Al–Fe_(tot)–Mg ternary diagram is the closest one to the Al apex. In addition, when Al contents in the sample and the calibrating tourmaline are similar, there is a significant correlation between increasing Fe/(Fe+Mg) ratio and the shift in $\delta^{11}\text{B}$ towards isotopically lighter compositions. All tourmalines from the dravite group with similar Mg contents (dravite, EB-67-90, EZ-272) show similar matrix effects, despite substantial differences in composition between EZ-272 and the rest of the group.

The boron isotopic composition of the four tourmaline reference materials (98144 elbaite, 108796 dravite, 112566 schorl and B4), shown graphically in Fig.4.6., suggests that the matrix-matched laser ablation MC ICP-MS data obtained in this study are in good agreement with the previously published P-TIMS values for the isotopic composition of these reference samples by Tonarini *et al.* (2003), Dyar *et al.* (2001), Leeman and Tonarini (2001) and Gonfiantini *et al.* (2003) Fig. 4.7A.

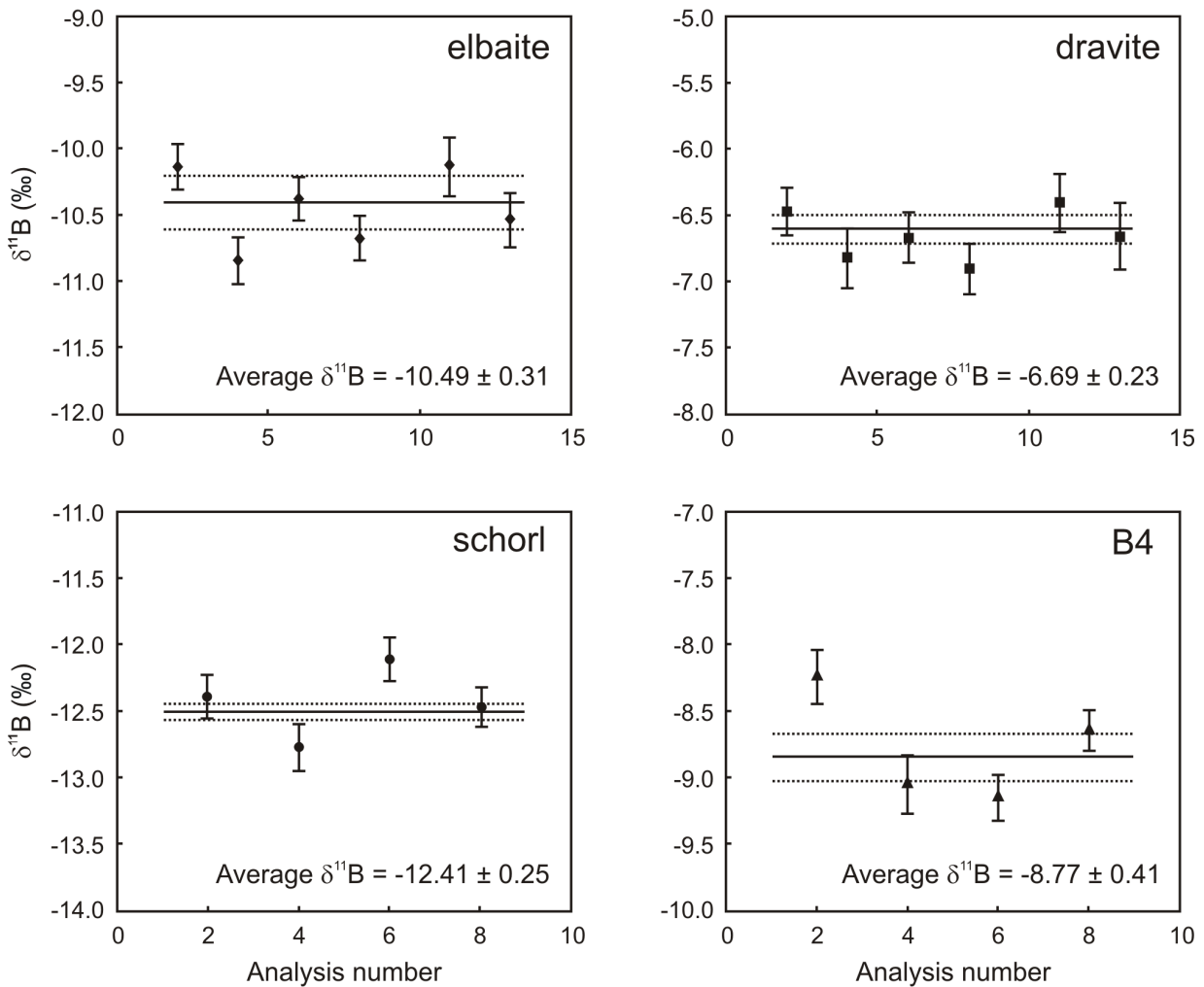


Fig. 4.6: $\delta^{11}\text{B}$ values for four tourmaline reference materials showing 1 σ uncertainty and trueness of laser ablation data calculated by standard-sample-standard procedure (even number analyses are treated as unknown samples and odd number analyses of the same material are treated as calibration runs), with the weighted average $\delta^{11}\text{B}$ value for the whole data set. Solid lines represent the mean TIMS values previously published for these materials with 1 σ uncertainty interval shown by dashed lines.

Tiepolo *et al.* (2006) used laser ablation MC ICP-MS for boron isotopic analysis of various geological materials. With the exception of tourmaline sample B4, all other analysed materials were in the form of a glass and, similar to this study, the data were corrected using a “standard-sample-standard” bracketing technique, while using NIST SRM 610 glass as a calibration material. Tiepolo *et al.* (2006) obtained a mean $\delta^{11}\text{B}$ value of $-8.24 (\pm 0.22\text{‰}, 1\text{s})$ for the B4 tourmaline which is slightly offset towards a heavier value relative to our results and the

reference value provided by Tonarini *et al.* (2003). It is possible that this 0.6‰ offset might be the result of using a non matrix-matched reference material for instrument calibration.

4.5.2 SIMS

The SIMS boron isotope data from the two days of data acquisition for the four reference materials are reported in Tab. 4.7 which represents the most detailed record of analytical results for tourmaline reference materials reported to date for this method. The instrument mass discrimination (Δ_{inst}), defined as the ratio between the measured $^{11}\text{B}/^{10}\text{B}$ and the reference $^{11}\text{B}/^{10}\text{B}$ values, was determined from the mean of $n = 29$ analyses on the four tourmaline reference materials analysed in this study. All measured data were corrected by this single overall Δ_{inst} value of 0.98002 and are reported as $\delta^{11}\text{B}$ values relative to NIST SRM 951. The reproducibility for the Δ_{inst} during the analytical session was 1.34 ‰ (1 s), which is typical for this method. It should be noted that this value for the reproducibility of Δ_{inst} contains components related both to the reliability of the assigned values for each of the four reference materials as well as any possible sample-specific variations in isotopic fractionation. This value for the overall reproducibility of Δ_{inst} should be taken as the limit to which such a data set could be interpreted. The repeatabilities of the results for each reference material are in the range of 0.8 (dravite and schorl) and 1.2 ‰ (elbaite and B4) (Tab. 4.7). We note that the 1.3‰ standard deviation of B4 tourmaline can be attributed to the last three measurements obtained from this material which show a consistently lighter isotopic composition compared to the rest of analyses on this sample.

The results obtained by the SIMS technique employing reference values obtained from TIMS measurements (Fig. 4.7B) suggest that some SIMS data are systematically biased. Lower $\delta^{11}\text{B}$ values were obtained for elbaite and dravite, while both schorl samples (schorl and B4) were shifted towards higher than expected $\delta^{11}\text{B}$ values. Here we note a general observation that other boron isotope studies (Chaussidon and Albarède, 1992) have detected a bias of 1 ‰ to at most 2 ‰ towards lighter ratios for the elbaite reference material as compared to the schorl and dravite reference materials. Until more Li-rich tourmaline reference materials become available, it will not be possible to conclude whether this phenomenon is related to a chemistry-specific matrix effect or to yet unidentified issue related to the reference value of this single specimen. This apparent bias of the elbaite results is similar in direction but substantially less in magnitude to the SIMS matrix effect reported by Chaussidon and Albarède (1992).

Tab. 4.7: *Compilation of SIMS data from the four tourmaline reference materials. The indicated uncertainties are 1s of the reported populations. Δ_{inst} - instrument mass discrimination. Measured values marked by asterisk were obtained during second day of analytical session.*

Sample	measured $^{11}\text{B}/^{10}\text{B}$	Δ_{inst}	corrected $^{11}\text{B}/^{10}\text{B}$	$\delta^{11}\text{B}$	1s
elbaite	3.916	0.97866	3.996	-11.8	0.4
	3.910	0.97716	3.990	-13.3	0.3
	3.911	0.97741	3.991	-13.1	0.3
	3.916	0.97866	3.996	-11.8	0.3
	3.920*	0.97966	4.000	-10.8	0.3
	3.923*	0.98041	4.003	-10.0	0.3
	3.919*	0.97941	3.999	-11.1	0.3
Mean	0.97876 ± 0.00118		-11.7 ± 1.2		
dravite	3.940	0.98086	4.020	-5.8	0.4
	3.933	0.97911	4.013	-7.5	0.3
	3.934	0.97936	4.014	-7.3	0.6
	3.933*	0.97911	4.013	-7.5	0.4
Mean	0.97961 ± 0.00083		-7.0 ± 0.8		
schorl	3.916	0.98069	3.996	-11.8	0.3
	3.912	0.97969	3.992	-12.8	0.4
	3.919*	0.98144	3.999	-11.1	0.3
	3.914*	0.98019	3.994	-12.3	0.4
	3.914*	0.98019	3.994	-12.3	0.4
	3.920*	0.98169	4.000	-10.8	0.4
Mean	0.98065 ± 0.00078		-11.9 ± 0.8		
B4	3.928	0.98009	4.008	-8.8	0.4
	3.935	0.98184	4.015	-7.0	0.4
	3.934	0.98159	4.014	-7.3	0.4
	3.931*	0.98084	4.011	-8.0	0.4
	3.923*	0.97884	4.003	-10.0	0.4
	3.921*	0.97834	4.001	-10.6	0.4
	3.933*	0.98134	4.013	-7.5	0.3
	3.937*	0.98233	4.017	-6.5	0.4
	3.934*	0.98159	4.014	-7.3	0.4
	3.926*	0.97959	4.006	-9.3	0.3
	3.928*	0.98009	4.008	-8.8	0.4
	3.929*	0.98034	4.009	-8.5	0.4
	Mean	0.98057 ± 0.00124		-8.3 ± 1.3	
Overall mean	0.98002 ± 0.00131				

4.5.3 Relative Merits of Laser ablation and SIMS

The main advantages of the LA MC ICP-MS and SIMS techniques over wet chemical methods are their high spatial resolution and small sample size required for analysis. The usual amount of sample consumed by SIMS (of the order of 100 pg total sample mass) is at least two

orders of magnitude smaller than for LA MC ICP-MS. The analyzed mass of the sample during LA MC ICP-MS is approximately two orders of magnitude smaller compared to the bulk analysis by TIMS. The major advantage of LA MC ICP-MS over SIMS lies in its speed of measurement and simple sample handling due to ablation under atmospheric pressure. During this study one LA MC ICP-MS analysis took ca. 2.5 minutes while 11 minutes were needed for a SIMS analysis.

As the focus of this study was the evaluation of the LA MC ICP-MS analyses of $\delta^{11}\text{B}$ determinations of tourmaline and as the SIMS technique has been well established in the Potsdam laboratory, we did not investigate the influence of analytical parameters on the quality of our SIMS data. In order to obtain more directly comparable results and to cancel out effect of different data treatment, we have recalculated raw laser ablation data in the same way as the SIMS measurements. The results are presented in Fig. 4.7A (grey symbols) and show the shift of final LA MC ICP-MS values caused by different data treatment. Such a pattern might be the result of a matrix effect as the most affected data are from the elbaite and dravite materials, which also showed the greatest difference with the same shift direction if used for intercalibration (Fig. 4.5). The offset between the laser ablation results relative to the TIMS values (Fig. 4.7A grey symbols) shows a similar pattern for elbaite, schorl and B4, while dravite shows the opposite trend compared to SIMS results (Fig. 4.7B). However, it shall be noted, that all laser ablation and TIMS results are overlapped by 1s uncertainty interval of SIMS results.

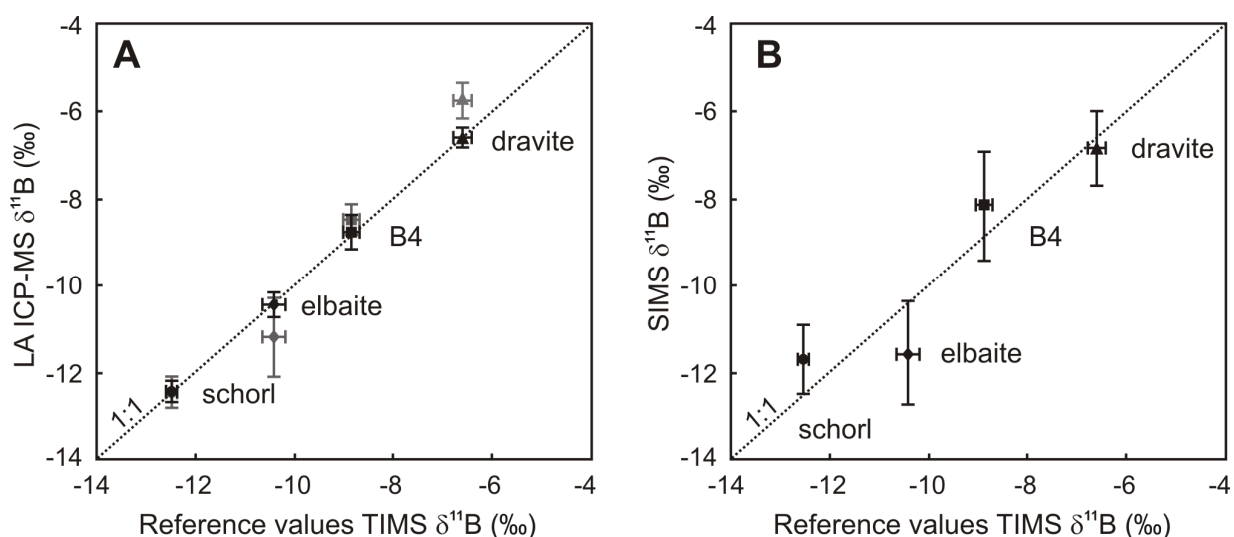


Fig. 4.7: **A.** Comparison of LA MC ICP-MS data (i) normalized by the bracketing with calibration material of the same composition (black symbols), (ii) normalized the same way as SIMS results (grey symbols) with TIMS reference values, error bars represent 1s uncertainty. **B** Comparison of SIMS data with TIMS reference values, error bars represent 1s uncertainty.

The results obtained during this study suggest that the overall repeatability provided by SIMS data treatment for LA MC ICP-MS estimated at 0.8‰ (1s, n=47) is better than that of SIMS 1.3‰ (1s, n=29). Even with equivalent data treatment, laser ablation compares favourably with SIMS. The worst precision recorded by both analytical techniques was for tourmaline B4, for which a non-homogeneous chemical composition (banding detected by cathodoluminescence) has been reported previously (Tonarini *et al.*, 2003). It is also noted that the B4 sample was the only multi-grain material, whereas the other three samples from (Dyar *et al.*, 2001) were fragments from single large monocrystals.

4.6 Conclusion

The results of this study suggest that laser ablation MC ICP-MS analysis of boron isotopes in tourmaline is subject to significant matrix effects that can impact the overall data trueness at ~2.5 ‰ level. The chemical composition of individual tourmaline samples has a systematic effect on the calculated $\delta^{11}\text{B}$ values depending on calibration material used for data normalization. With matrix-matched calibration and standard-sample-standard data reduction, the overall repeatability of LA MC ICP-MS is estimated to be at ca. 0.5‰ (1 s) level. The laser ablation-measured $\delta^{11}\text{B}$ values are close to those obtained by Tonarini *et al.* (2003) and Gonfiantini *et al.* (2003) for the same samples using P-TIMS technique. Furthermore, these results compare favourably with the overall reproducibility of about 1.3‰ (1 s) which is routinely obtained by the SIMS method.

The choice of both laser and MC ICP-MS instrument parameters has significant effect on the measured $^{11}\text{B}/^{10}\text{B}$ ratios, in particular as a result of different signal intensities and $^{40}\text{Ar}^{4+}$ spectral interferences on the ^{10}B mass peak. These interferences can be suppressed by optimizing mass resolution of the instrument. Laser induced isotopic fractionation of B was negligible for single spot and raster sampling strategies during this study, allowing for a choice of optimal sampling mode depending on the size, shape and homogeneity of the samples.

4.3 Acknowledgements

The authors would like to thank John Slack for kindly providing his tourmaline samples for our study.

Chapter 5: Summary and outlook

This dissertation presents an extensive dataset providing a new insight to processes causing fractionation and matrix effects, which compromise accuracy and precision of laser ablation measurements. Experiments were focused on elements and isotopic systems of high importance in geosciences. They include U–Pb system used for geochronological determinations based on radioactive decay of uranium to lead in the accessory mineral zircon (ZrSiO_4), alkali elements that are utilized in geochronology (Rb-Sr, K-Ar) and thermobarometry as well as for correcting for variations in ablation yield (as internal standards) in analyses of other lithophile elements and boron isotopic composition of tourmaline that can be used to study origin and evolution of tourmaline bearing rocks.

Data presented in this thesis indicate that particles generated by laser ablation during course of laser ablation analysis of silicates vary in their size and composition (not only chemical in NIST 612, but also phase in zircon 91 500) and that fractionation during laser ablation ICP-MS analysis takes place also at the ablation site. Different silicate samples under identical experimental conditions can produce aerosols with different size distributions of particles. The release of different particle size fractions during laser ablation experiment changes with prolonged time of laser-sample interaction. Experimental data produced by ablation of NIST 612 glass and zircon 91 500 reference material suggest that large (> 200 nm) particles are formed by melt droplets while small (~ 5 nm) particles are probably condensates from vapour phase. Different mechanisms that produce different particle size fractions generation seem to be responsible for their different composition. Only some particles (zircon)/particle fractions (NIST 612) produced by laser ablation have a chemical composition corresponding to that of the original solid sample. Accordingly, the ablated sample has to be transported to the ICP in a quantitative or representative fashion. In some cases it may be possible to select the size fraction of particles that most closely matches the bulk composition of the target sample for transport and analysis in the ICP-MS using screening particle separation devices. Also due to different nature of analyzed samples (glass NIST 612 vs. crystalline zircon 91 500) it seems that different mechanisms are responsible for Pb/U fractionation during ablation of silicate glass and zircon (and other crystalline and non-crystalline phases). Pb-U decoupling during the ablation of zircon is probably caused by the thermal decomposition of zircon (ZrSiO_4) to baddeleyite (ZrO_2) and

SiO₂. Although the link between the formation of different phases and elemental fractionation can be demonstrated for crystalline samples (zircon), this relationship remains difficult to prove for amorphous materials such as the NIST silicate glasses, where the phase composition of ablated particles may be the same as that of the original sample.

Data on fractionation behavior of alkali elements are in agreement with observations presented for U-Pb in NIST-612 and zircon 91 500. The significant part of the fractionation also takes place on the ablation site during laser-sample interaction and demonstrated thermal alteration of the sample results in variations in the chemical composition as a function of the size of aerosol particles. The rate of fractionation varies with properties of major element used for corrections of ablation yield and also with concentration of individual alkali elements if samples having the same matrix are compared. However, the fractionation rate is also controlled by the sample matrix. In addition, crystallographic orientation relative to the incident laser beam may influence elemental fractionation during laser ablation. This can be attributed to variable heat transfer during laser ablation in different crystallographic orientations. An important conclusion of this study is that chemical composition and spatial distribution of elements below the bottom of laser crater is strongly influenced by thermal effects. The effects of laser ablation on element redistribution below the bottom of the laser pits can be detected down to the depth of tens to first hundreds nm. This effect is significant not only for alkali elements but also for elements that are commonly used in quantitative analysis of silicate geological samples for corrections of ablation yield (isotopes of Si and Ca). Their behavior during laser ablation analysis is different (Si behaves similar to alkali elements, while Ca often shows an opposite fractionation pattern). The choice of the internal standard has an important effect of precision and accuracy of laser ablation ICP-MS analyses. In conclusion, the combination of thermally driven diffusion process within the sample, different mechanisms of particle formation, different chemical composition of produced particle size fractions and nature of sample matrix all seem to be related to observed elemental fractionation.

The matrix effects on precision and accuracy of boron isotopic analyses were studied on a set of tourmaline samples. Because tourmalines are good tracers of geochemical transfer and mixing processes and are difficult to digest chemically without boron loss, laser ablation ICP-MS is a method of choice for their isotopic study. Only a negligible boron isotopic fractionation during laser ablation analysis was observed, allowing for better evaluation of the potential matrix effects.

Different types of tourmalines were analysed and processed using “standard-sample-standard” bracketing approach where even number analyses were treated as unknown samples and odd number analyses were treated as calibration runs. Each tourmaline sample served as calibration material as well as unknown sample. This approach reveals that the compositions of individual tourmaline samples had effect on the calculated $\delta^{11}\text{B}$ values depending on calibration material used for data normalization. The results show that under identical analytical conditions, the matrix effects can contribute to the overall data accuracy at ca. 2.5 ‰ level, while with matrix-matched calibration, the overall precision of LA MC ICP-MS is estimated to be at ca. 0.5‰ (1 s) level. There seems to be a systematic relationship between differences of chemical compositions (especially the element on the octahedral position) of reference material vs. analyzed tourmaline and offset of calculated $\delta^{11}\text{B}$ values. However, more data are needed to establish relations between chemical composition and $\delta^{11}\text{B}$, at least for some of the end members of tourmaline complex solid-solutions.

The results of this thesis point to the importance of matrix matched external calibration in cases where highly precise and accurate laser ablation ICP-MS data are required. Although this thesis answers some of the questions, some still remain open and constitute a topic for future research. Especially important at the present level of understanding is linking the chemical and phase changes during laser-sample interaction to the formation of particles in the laser aerosol and its properties that control particle behaviour in the ICP.

References:

- Aeschliman, D. B., Bajic, S. J., Baldwin, D. P. and Houk, R. S. (2003) High-speed digital photographic study of an inductively coupled plasma during laser ablation: comparison of dried solution aerosols from a microconcentric nebulizer and solid particles from laser ablation. *Journal of Analytical Atomic Spectrometry*, **18**, 1008-1014.
- Aggarwal, J. K., Sheppard, D., Mezger, K. and Pernicka, E. (2003) Precise and accurate determination of boron isotope ratios by multiple collector ICP-MS: origin of boron in the Ngawha geothermal system, New Zealand. *Chemical Geology*, **199**, 331-342.
- Aggarwal, J., Bohm, F., Foster, G., Halas, S., Honisch, B., Jiang, S. Y., Košler, J., Liba, A., Rodushkin, I., Sheehan, T., Shen, J. J. S., Tonarini, S., Xie, Q. L., You, C. F., Zhao, Z. Q. and Zuleger, E. (2009) How well do non-traditional stable isotope results compare between different laboratories: results from the interlaboratory comparison of boron isotope measurements. *Journal of Analytical Atomic Spectrometry*, **24**, 825-831.
- Andren, H., Rodushkin, I., Stenberg, A., Malinovsky, D. and Baxter, D. C. (2004) Sources of mass bias and isotope ratio variation in multicollector ICP-MS: optimization of instrumental parameters based on experimental observations. *Journal of Analytical Atomic Spectrometry*, **19**, 1217-1224.
- Becker, J. S. (2002) Applications of inductively coupled plasma mass spectrometry and laser ablation inductively coupled plasma mass spectrometry in materials science. *Spectrochimica Acta Part B-Atomic Spectroscopy*, **57**, 1805-1820.
- Becker, J. S. and Dietze, H. J. (2000) Inorganic mass spectrometric methods for trace, ultratrace, isotope, and surface analysis. *International Journal of Mass Spectrometry*, **197**, 1-35.
- Becker, J. S., Pickhardt, C. and Dietze, H. J. (2000) Laser ablation inductively coupled plasma mass spectrometry for determination of trace elements in geological glasses. *Mikrochimica Acta*, **135**, 71-80.
- Bleiner, D. (2002) PhD Dissertation nr 14665. *ETH Zurich*.
- Bleiner, D. (2005) Mathematical modelling of laser-induced particulate formation in direct solid microanalysis. *Spectrochimica Acta Part B-Atomic Spectroscopy*, **60**, 49-64.
- Bleiner, D. and Bogaerts, A. (2006) Computer simulations of laser ablation sample introduction for plasma-source elemental microanalysis. *Journal of Analytical Atomic Spectrometry*, **21**, 1161-1174.
- Bleiner, D. and Bogaerts, A. (2007) Computer simulations of sample chambers for laser ablation-inductively coupled plasma spectrometry. *Spectrochimica Acta Part B-Atomic Spectroscopy*, **62**, 155-168.
- Bleiner, D. and Gasser, P. (2004) Structural features of laser ablation particulate from Si target, as revealed by focused ion beam technology. *Applied Physics A-Materials Science & Processing*, **79**, 1019-1022.
- Bleiner, D. and Gunther, D. (2001) Theoretical description and experimental observation of aerosol transport processes in laser ablation inductively coupled plasma mass spectrometry. *Journal of Analytical Atomic Spectrometry*, **16**, 449-456.
- Bleiner, D., Lienemann, P. and Vonmont, H. (2005) Laser-induced particulate as carrier of analytical information in LA-ICPMS direct solid microanalysis. *Talanta*, **65**, 1286-1294.
- Borisov, O. V., Mao, X. L. and Russo, R. E. (2000) Effects of crater development on fractionation and signal intensity during laser ablation inductively coupled plasma mass spectrometry. *Spectrochimica Acta Part B-Atomic Spectroscopy*, **55**, 1693-1704.
- Butterman, W. C. and Foster, W. R. (1967) Zircon Stability and ZrO₂-SiO₂ Phase Diagram. *American Mineralogist*, **52**, 880-885.
- Catanzaro, E. J., Champion, C. E., Garner, E. L., Marienko, K. M., Sappenfield, K. M. and Shield, W. R. (1970) Boric Acid: Isotopic and Essay Standard Reference Materials. Special Publication 260-17, 70. *US National Bureau of Standards*.

- Chapman, H. J. and Roddick, J. C. (1994) Kinetics of Pb Release During the Zircon Evaporation Technique. *Earth and Planetary Science Letters*, **121**, 601-611.
- Chaussidon, M. and Albarède, F. (1992) Secular Boron Isotope Variations in the Continental-Crust - An Ion Microprobe Study. *Earth and Planetary Science Letters*, **108**, 229-241.
- Chaussidon, M. and Albarède, F. (1998) Li-7/Li-6 and B-11/B-10 variations in chondrules from the Semarkona unequilibrated chondrite. *Earth and Planetary Science Letters*, **164**, 577-589.
- Chaussidon, M., Robert, F., Mangin, D., Hanon, P. and Rose, E. F. (1997) Analytical procedures for the measurement of boron isotope compositions by ion microprobe in meteorites and mantle rocks. *Geostandards Newsletter-the Journal of Geostandards and Geoanalysis*, **21**, 7-17.
- Cox, R. A., Wilton, D. H. C. and Košler, J. (2003) Laser-ablation U-Th-Pb in situ dating of zircon and allanite: An example from the October Harbour granite, central coastal Labrador, Canada. *Canadian Mineralogist*, **41**, 273-291.
- Cramer, L. P., Langford, S. C., Hess, W. P. and Dickinson, J. T. (2002) Wavelength dependence of UV laser induced emission of neutral and ionic species from single crystal NaNO₃. *Applied Surface Science*, **197**, 35-40.
- Cromwell, E. F. and Arrowsmith, P. (1995) Fractionation Effects in Laser-Ablation Inductively-Coupled Plasma-Mass Spectrometry. *Applied Spectroscopy*, **49**, 1652-1660.
- Darke, S. A. and Tyson, J. F. (1993) Interaction of Laser-Radiation with Solid Materials and Its Significance to Analytical Spectrometry - A Review. *Journal of Analytical Atomic Spectrometry*, **8**, 145-209.
- Deer, W. A., Howie, R. A., Zussman, J. (1992) *Tourmaline in An Introduction to the Rock-Forming Minerals*. Pearson, 2nd ed., 130-137.
- Durrant, S. F. (1999) Laser ablation inductively coupled plasma mass spectrometry: achievements, problems, prospects. *Journal of Analytical Atomic Spectrometry*, **14**, 1385-1403.
- Dyar, M. D., Wiedenbeck, M., Robertson, D., Cross, L. R., Delaney, J. S., Ferguson, K., Francis, C. A., Grew, E. S., Guidotti, C. V., Hervig, R. L., Hughes, J. M., Husler, J., Leeman, W., McGuire, A. V., Rhede, D., Rothe, H., Paul, R. L., Richards, I. and Yates, M. (2001) Reference minerals for the Microanalysis of light elements. *Geostandards Newsletter-the Journal of Geostandards and Geoanalysis*, **25**, 441-463.
- Eggins, S. M., Kinsley, L. P. J. and Shelley, J. M. G. (1998) Deposition and element fractionation processes during atmospheric pressure laser sampling for analysis by ICP-MS. *Applied Surface Science*, **127**, 278-286.
- Esmaeily, D., Trumbull, R. B., Haghaziar, M., Krienitz, M. S. and Wiedenbeck, M. (2009) Chemical and boron isotopic composition of hydrothermal tourmaline from scheelite-quartz veins at Nezamabad, western Iran. *European Journal of Mineralogy*, **21**, 347-360.
- Evans, E. H. and Giglio, J. J. (1993) Interferences in Inductively Coupled Plasma Mass-Spectrometry - A Review. *Journal of Analytical Atomic Spectrometry*, **8**, 1-18.
- Feldmann, I., Tittes, W., Jakubowski, N., Stuewer, D. and Giessmann, U. (1994) Performance-Characteristics of Inductively-Coupled Plasma-Mass Spectrometry with High-Mass Resolution. *Journal of Analytical Atomic Spectrometry*, **9**, 1007-1014.
- Feng, R., Machado, N. and Ludden, J. (1993) Lead Geochronology of Zircon by Laser Probe-Inductively Coupled Plasma-Mass Spectrometry (LP-ICP-MS). *Geochimica et Cosmochimica Acta*, **57**, 3479-3486.
- Friedlander, S. K. (2000) *Smoke, Dust, and Haze: Fundamentals of Aerosol Dynamics*. Oxford University Press, 2nd ed.
- Frischat, G. H. (1971) Sodium Self-Diffusion in Mixed-Alkali Glasses. *Journal of Materials Science*, **6**, 1229-1231.
- Fryer, B. J., Jackson, S. E. and Longerich, H. P. (1993) The Application of Laser-Ablation Microprobe-Inductively Coupled Plasma-Mass Spectrometry (LAM-ICP-MS) to In-Situ (U)-Pb Geochronology. *Chemical Geology*, **109**, 1-8.

- Fryer, B. J., Jackson, S. E. and Longerich, H. P. (1995) Design, Operation and Role of the Laser-Ablation Microprobe Coupled with An Inductively-Coupled Plasma - Mass-Spectrometer (LAM-ICP-MS) in the Earth-Sciences. *Canadian Mineralogist*, **33**, 303-312.
- Gabler, H. E. and Bahr, A. (1999) Boron isotope ratio measurements with a double-focusing magnetic sector ICP mass spectrometer for tracing anthropogenic input into surface and ground water. *Chemical Geology*, **156**, 323-330.
- Gackle, M. and Merten, D. (2004) Modelling the temporal intensity distribution of laser ablation inductively coupled plasma mass spectrometry in single shot mode. *Spectrochimica Acta Part B-Atomic Spectroscopy*, **59**, 1893-1905.
- Gackle, M. and Merten, D. (2005) Modelling the temporal intensity distribution in laser ablation-inductively coupled plasma-mass spectrometry (LA-ICP-MS) using scanning and drilling mode. *Spectrochimica Acta Part B-Atomic Spectroscopy*, **60**, 1517-1530.
- Galbraith, C. G., Clarke, D. B., Trumbull, R. B., and Wiedenbeck, M., 2009, Assessment of Tourmaline Compositions as an Indicator of Emerald Mineralization at the Tsa da Glisza Prospect, Yukon Territory, Canada. *Economic Geology*, **104**, 713-731.
- Garcia, C. C., Lindner, H. and Niemax, K. (2007) Transport efficiency in femtosecond laser ablation inductively coupled plasma mass spectrometry applying ablation cells with short and long washout times. *Spectrochimica Acta Part B-Atomic Spectroscopy*, **62**, 13-19.
- Garcia, C. C., Walle, M., Lindner, H., Koch, J., Niemax, K. and Günther, D. (2008) Femtosecond laser ablation inductively coupled plasma mass spectrometry: Transport efficiencies of aerosols released under argon atmosphere and the importance of the focus position. *Spectrochimica Acta Part B-Atomic Spectroscopy*, **63**, 271-276.
- Gedeon, O., Hulinsky, V. and Jurek, K. (2000) Microanalysis of glass containing alkali ions. *Mikrochimica Acta*, **132**, 505-510.
- Gedeon, O. and Jurek, K. (2004) Relaxation of alkali glass exposed to an electron beam. *Microchimica Acta*, **145**, 49-52.
- Geertsen, C., Briand, A., Chartier, F., Lacour, J. L., Mauchien, P., Sjoström, S. and Mermet, J. M. (1994) Comparison Between Infrared and Ultraviolet-Laser Ablation at Atmospheric-Pressure - Implications for Solid Sampling Inductively-Coupled Plasma Spectrometry. *Journal of Analytical Atomic Spectrometry*, **9**, 17-22.
- Giletti, B. J. and Shanahan, T. M. (1997) Alkali diffusion in plagioclase feldspar. *Chemical Geology*, **139**, 3-20.
- Gonfiantini, R., Tonarini, S., Groning, M., Adorni-Braccesi, A., Al Ammar, A. S., Astner, M., Bachler, S., Barnes, R. M., Bassett, R. L., Cocherie, A., Deyhle, A., Dini, A., Ferrara, G., Gaillardet, J., Grimm, J., Guerrot, C., Krahenbuhl, U., Layne, G., Lemarchand, D., Meixner, A., Northington, D. J., Pennisi, M., Reitznerova, E., Rodushkin, I., Sugiura, N., Surberg, R., Tonn, S., Wieclenbeck, M., Wunderli, S., Xiao, Y. K. and Zack, T. (2003) Intercomparison of boron isotope and concentration measurements. Part II: Evaluation of results. *Geostandards Newsletter-the Journal of Geostandards and Geoanalysis*, **27**, 41-57.
- Gonzalez, J., Mao, X. L., Roy, J., Mao, S. S. and Russo, R. E. (2002) Comparison of 193, 213 and 266 nm laser ablation ICP-MS. *Journal of Analytical Atomic Spectrometry*, **17**, 1108-1113.
- Gray, A. L. (1985) Solid Sample Introduction by Laser Ablation for Inductively Coupled Plasma Source-Mass Spectrometry. *Analyst*, **110**, 551-556.
- Guillong, M. and Günther, D. (2002) Effect of particle size distribution on ICP-induced elemental fractionation in laser ablation-inductively coupled plasma-mass spectrometry. *Journal of Analytical Atomic Spectrometry*, **17**, 831-837.
- Guillong, M., Horn, I. and Günther, D. (2003a) A comparison of 266 nm, 213 nm and 193 nm produced from a single solid state Nd:YAG laser for laser ablation ICP-MS. *Journal of Analytical Atomic Spectrometry*, **18**, 1224-1230.
- Guillong, M., Kuhn, H. R. and Günther, D. (2003b) Application of a particle separation device to reduce inductively coupled plasma-enhanced elemental fractionation in laser ablation-inductively coupled plasma-mass spectrometry. *Spectrochimica Acta Part B-Atomic Spectroscopy*, **58**, 211-220.

- Günther, D. and Heinrich, C. A. (1999) Enhanced sensitivity in laser ablation-ICP mass spectrometry using helium-argon mixtures as aerosol carrier - Plenary lecture. *Journal of Analytical Atomic Spectrometry*, **14**, 1363-1368.
- Günther, D., Frischknecht, R., Heinrich, C. A. and Kahlert, H. J. (1997) Capabilities of an Argon Fluoride 193 nm excimer laser for laser ablation inductively coupled plasma mass spectrometry microanalysis of geological materials. *Journal of Analytical Atomic Spectrometry*, **12**, 939-944.
- Günther, D., Horn, I. and Hattendorf, B. (2000) Recent trends and developments in laser ablation-ICP-mass spectrometry. *Fresenius Journal of Analytical Chemistry*, **368**, 4-14.
- Günther, D., Jackson, S. E. and Longerich, H. P. (1999) Laser ablation and arc/spark solid sample introduction into inductively coupled plasma mass spectrometers. *Spectrochimica Acta Part B-Atomic Spectroscopy*, **54**, 381-409.
- Gurevich, E. L. and Hergenroder, R. (2007) A simple laser ICP-MS ablation cell with wash-out time less than 100 ms. *Journal of Analytical Atomic Spectrometry*, **22**, 1043-1050.
- Hanson, B., Delano, J. W. and Lindstrom, D. J. (1996) High-precision analysis of hydrous rhyolitic glass inclusions in quartz phenocrysts using the electron microprobe and INAA. *American Mineralogist*, **81**, 1249-1262.
- Heaman, L. M. and Lecheminant, A. N. (1993) Paragenesis and U-Pb Systematics of Baddeleyite (ZrO₂). *Chemical Geology*, **110**, 95-126.
- Heaman, L. M. and Parrish, R. R. (1991) U-Pb geochronology of accessory minerals. In Applications of Radiogenic Isotope Systems to Problems in Geology. *Mineralogical Association of Canada Short Course Handbook*, **19**, 59-102.
- Hemming, N. G. and Hanson, G. N. (1994) A Procedure for the Isotopic Analysis of Boron by Negative Thermal Ionization Mass-Spectrometry. *Chemical Geology*, **114**, 147-156.
- Heumann, K. G. (2004) Isotope-dilution ICP-MS for trace element determination and speciation: from a reference method to a routine method? *Analytical and Bioanalytical Chemistry*, **378**, 318-329.
- Hirata, T. (1997) Soft ablation technique for laser ablation inductively coupled plasma mass spectrometry. *Journal of Analytical Atomic Spectrometry*, **12**, 1337-1342.
- Hirata, T. (2003) Chemically assisted laser ablation ICP mass spectrometry. *Analytical Chemistry*, **75**, 228-233.
- Hirata, T. and Nesbitt, R. W. (1995) U-Pb Isotope Geochronology of Zircon - Evaluation of the Laser Probe-Inductively Coupled Plasma-Mass Spectrometry Technique. *Geochimica et Cosmochimica Acta*, **59**, 2491-2500.
- Hoefs, J. (2009) Boron in Stable Isotope Geochemistry. *Springer*, 6th ed., 45-47.
- Horn, I., Guillong, M. and Günther, D. (2001) Wavelength dependant ablation rates for metals and silicate glasses using homogenized laser beam profiles - implications for LA-ICP-MS. *Applied Surface Science*, **182**, 91-102.
- Horn, I. and Günther, D. (2003) The influence of ablation carrier gasses Ar, He and Ne on the particle size distribution and transport efficiencies of laser ablation-induced aerosols: implications for LA-ICP-MS. *Applied Surface Science*, **207**, 144-157.
- Horn, I., Rudnick, R. L. and McDonough, W. F. (2000) Precise elemental and isotope ratio determination by simultaneous solution nebulization and laser ablation-ICP-MS: application to U-Pb geochronology. *Chemical Geology*, **164**, 281-301.
- Horn, I. and von Blanckenburg, F. (2005) 196 nm femtosecond laser ablation: Applications to trace element and radiogenic isotope ratio determinations. *Geochimica et Cosmochimica Acta*, **69**, A54.
- Horn, I., von Blanckenburg, F., Schoenberg, R., Steinhoefel, G. and Markl, G. (2006) In situ iron isotope ratio determination using UV-femtosecond laser ablation with application to hydrothermal ore formation processes. *Geochimica et Cosmochimica Acta*, **70**, 3677-3688.
- Humphreys, M. C. S., Kearns, S. L. and Blundy, J. D. (2006) SIMS investigation of electron-beam damage to hydrous, rhyolitic glasses: Implications for melt inclusion analysis. *American Mineralogist*, **91**, 667-679.
- Ishikawa, T. and Nakamura, E. (1990) Suppression of Boron Volatilization from A Hydrofluoric-Acid Solution Using A Boron-Mannitol Complex. *Analytical Chemistry*, **62**, 2612-2616.

- Jackson, S. E. and Günther, D. (2003) The nature and sources of laser induced isotopic fractionation in laser ablation-multicollector-inductively coupled plasma-mass spectrometry. *Journal of Analytical Atomic Spectrometry*, **18**, 205-212.
- Jackson, S. E., Horn, I., Longrich, H. P. and Dunning, G. R. (1996) The application of laser ablation microprobe (LAM)-ICP-MS to in situ U-Pb zircon geochronology. *Journal of Conference Abstracts*, **1**, 238.
- Jackson, S. E., Longrich, H. P., Dunning, G. R. and Fryer, B. J. (1992) The Application of Laser-Ablation Microprobe - Inductively Coupled Plasma - Mass-Spectrometry (LAM-ICP-MS) to In situ Trace-Element Determinations in Minerals. *Canadian Mineralogist*, **30**, 1049-1064.
- Jackson, S. E., Pearson, N. J., Griffin, W. L. and Belousova, E. A. (2004) The application of laser ablation-inductively coupled plasma-mass spectrometry to in situ U-Pb zircon geochronology. *Chemical Geology*, **211**, 47-69.
- Jeffries, T. E., Jackson, S. E. and Longrich, H. P. (1998) Application of a frequency quintupled Nd : YAG source ($\lambda = 213$ nm) for laser ablation inductively coupled plasma mass spectrometric analysis of minerals. *Journal of Analytical Atomic Spectrometry*, **13**, 935-940.
- Jeffries, T. E., Perkins, W. T. and Pearce, N. J. G. (1995) Comparisons of Infrared and Ultraviolet-Laser Probe Microanalysis Inductively-Coupled Plasma-Mass Spectrometry in Mineral Analysis. *Analyst*, **120**, 1365-1371.
- Jeong, S. H., Borisov, O. V., Yoo, J. H., Mao, X. L. and Russo, R. E. (1999) Effects of particle size distribution on inductively coupled plasma mass spectrometry signal intensity during laser ablation of glass samples. *Analytical Chemistry*, **71**, 5123-5130.
- Jolliff, B. L., Papike, J. J. and Shearer, C. K. (1986) Tourmaline As A Recorder of Pegmatite Evolution - Ingersoll, Bob Pegmatite, Black Hills, South-Dakota. *American Mineralogist*, **71**, 472-500.
- Jones, A., Islam, M. S., Mortimer, M. and Palmer, D. (2004) Alkali ion migration in albite and K-feldspar. *Physics and Chemistry of Minerals*, **31**, 313-320.
- Jurek, K. and Gedeon, O. (2003) Analysis of alkali-silicate glasses by electron probe analysis. *Spectrochimica Acta Part B-Atomic Spectroscopy*, **58**, 741-744.
- Klotzli, U. S. (1997) Single zircon evaporation thermal ionisation mass spectrometry: Method and procedures. *Analyst*, **122**, 1239-1248.
- Koch, J., Feldmann, I., Jakubowski, N. and Niemax, K. (2002) Elemental composition of laser ablation aerosol particles deposited in the transport tube to an ICP. *Spectrochimica Acta Part B-Atomic Spectroscopy*, **57**, 975-985.
- Koch, J., Schaldach, G., Berndt, H. and Niemax, K. (2004a) Numerical simulation of aerosol transport. *Analytical Chemistry*, **76**, 130A-136A.
- Koch, J., von Bohlen, A., Hergenröder, R. and Niemax, K. (2004b) Particle size distributions and compositions of aerosols produced by near-IR femto- and nanosecond laser ablation of brass. *Journal of Analytical Atomic Spectrometry*, **19**, 267-272.
- Košler, J., Fonneland, H., Sylvester, P., Tubrett, M. and Pedersen, R. B. (2002a) U-Pb dating of detrital zircons for sediment provenance studies - a comparison of laser ablation ICPMS and SIMS techniques. *Chemical Geology*, **182**, 605-618.
- Košler, J., Frost, L., and Sláma, J. (2008) Lamdate and Lamtool: spreadsheet-based data reduction for laser ablation ICP-MS. in *Laser ablation ICP-MS in the Earth sciences: current practices and outstanding issues*, ed. Sylvester, P., *Mineral. Assoc. Can. short course series*, 2008, **40**, 315-317.
- Košler, J., Longrich, H. P. and Tubrett, M. N. (2002b) Effect of oxygen on laser-induced elemental fractionation in LA-ICP-MS analysis. *Analytical and Bioanalytical Chemistry*, **374**, 251-254.
- Košler, J., Pedersen, R. B., Kruber, C. and Sylvester, P. J. (2005a) Analysis of Fe isotopes in sulfides and iron meteorites by laser ablation high-mass resolution multi-collector ICP mass spectrometry. *Journal of Analytical Atomic Spectrometry*, **20**, 192-199.
- Košler, J. and Sylvester, P. J. (2003) Present trends and the future of zircon in geochronology: Laser ablation ICPMS. *Reviews in Mineralogy and Geochemistry*, **53**, 243-275.

- Košler, J., Tubrett, M. N. and Sylvester, P. J. (2001) Application of laser ablation ICP-MS to U-Th-Pb dating of monazite. *Geostandards Newsletter-the Journal of Geostandards and Geoanalysis*, **25**, 375-386.
- Košler, J., Wiedenbeck, M., Wirth, R., Hovorka, J., Sylvester, P. and Míková, J. (2004) Effects of size, chemical and phase composition of ablated particles on elemental fractionation during ICPMS analysis. *Winter Conference on Plasma Spectrochemistry Abstracts*, 166.
- Košler, J., Wiedenbeck, M., Wirth, R., Hovorka, J., Sylvester, P. and Míková, J. (2005b) Chemical and phase composition of particles produced by laser ablation of silicate glass and zircon - implications for elemental fractionation during ICP-MS analysis. *Journal of Analytical Atomic Spectrometry*, **20**, 402-409.
- Kozlov, B., Saint, A. and Skroce, A. (2003) Elemental fractionation in the formation of particulates, as observed by simultaneous isotopes measurement using laser ablation ICP-oe-TOFMS. *Journal of Analytical Atomic Spectrometry*, **18**, 1069-1075.
- Krienitz, M. S., Trumbull, R. B., Hellmann, A., Kolb, J., Meyer, F. M. and Wiedenbeck, M. (2008) Hydrothermal gold mineralization at the Hira Buddini gold mine, India: constraints on fluid evolution and fluid sources from boron isotopic compositions of tourmaline. *Mineralium Deposita*, **43**, 421-434.
- Kroslakova, I. and Günther, D. (2007) Elemental fractionation in laser ablation-inductively coupled plasma-mass spectrometry: evidence for mass load induced matrix effects in the ICP during ablation of a silicate glass. *Journal of Analytical Atomic Spectrometry*, **22**, 51-62.
- Kuhn, H. R., Guillong, M. and Günther, D. (2004) Size-related vaporisation and ionisation of laser-induced glass particles in the inductively coupled plasma. *Analytical and Bioanalytical Chemistry*, **378**, 1069-1074.
- Kuhn, H. R. and Günther, D. (2003) Elemental fractionation studies in laser ablation inductively coupled plasma mass spectrometry on laser-induced brass aerosols. *Analytical Chemistry*, **75**, 747-753.
- Kuhn, H. R. and Günther, D. (2004) Laser ablation-ICP-MS: particle size dependent elemental composition studies on filter-collected and online measured aerosols from glass. *Journal of Analytical Atomic Spectrometry*, **19**, 1158-1164.
- le Roux, P. J., Shirey, S. B., Benton, L., Hauri, E. H. and Mock, T. D. (2004) In situ, multiple-multiplier, laser ablation ICP-MS measurement of boron isotopic composition ($\delta B-11$) at the nanogram level. *Chemical Geology*, **203**, 123-138.
- Leach, A. M. and Hieftje, G. M. (2002) Factors affecting the production of fast transient signals in single shot laser ablation inductively coupled plasma mass spectrometry. *Applied Spectroscopy*, **56**, 62-69.
- Leeman, W. P. and Sisson, V. B. (1996) Geochemistry of boron and its implications for crustal and mantle processes. In *Boron: Mineralogy, Petrology and Geochemistry*, Grew, E. S. and Anovitz, L. M. (eds), *Reviews in Mineralogy and Geochemistry*, **33**, 645-707.
- Leeman, W. P. and Tonarini, S. (2001) Boron isotopic analysis of proposed borosilicate mineral reference samples. *Geostandards Newsletter-the Journal of Geostandards and Geoanalysis*, **25**, 399-403.
- Leeman, W. P., Vocke, R. D., Beary, E. S. and Paulsen, P. J. (1991) Precise Boron Isotopic Analysis of Aqueous Samples - Ion-Exchange Extraction and Mass-Spectrometry. *Geochimica et Cosmochimica Acta*, **55**, 3901-3907.
- Lemarchand, D., Gaillardet, J., Gopel, C. and Manhès, G. (2002) An optimized procedure for boron separation and mass spectrometry analysis for river samples. *Chemical Geology*, **182**, 323-334.
- Lin, T. H. and Yund, R. A. (1972) Potassium and Sodium Self-Diffusion in Alkali Feldspar. *Contributions to Mineralogy and Petrology*, **34**, 177-184.
- Liu, C. Y., Mao, X. L., Gonzalez, J. and Russo, R. E. (2005) Study of particle size influence on laser ablation inductively coupled plasma mass spectrometry using an in-line cascade impactor. *Journal of Analytical Atomic Spectrometry*, **20**, 200-203.
- Liu, H. C., Borisov, O. V., Mao, X. L., Shuttleworth, S. and Russo, R. E. (2000) Pb/U fractionation during Nd : YAG 213 nm and 266 nm laser ablation sampling with inductively coupled plasma mass spectrometry. *Applied Spectroscopy*, **54**, 1435-1442.

- London, D., Morgan, G. B. and Wolf, M. B. (1996) Boron in granitic rocks and their contact aureoles. In *Boron: Mineralogy, Petrology and Geochemistry*, Grew, E. S. and Anovitz, L. M. (eds), *Reviews in Mineralogy and Geochemistry*, **33**, 299-330.
- Longerich, H. P., Günther, D. and Jackson, S. E. (1996a) Elemental fractionation in laser ablation inductively coupled plasma mass spectrometry. *Fresenius Journal of Analytical Chemistry*, **355**, 538-542.
- Longerich, H. P., Jackson, S. E. and Günther, D. (1996b) Laser ablation inductively coupled plasma mass spectrometric transient signal data acquisition and analyte concentration calculation. *Journal of Analytical Atomic Spectrometry*, **11**, 899-904.
- Loucks, R. R., Eggins, S. M., Shelley, L. M. G., Kinsley, L. P. J. and Ware, N. G. (1995) Development of the inductively coupled-plasma mass spectrometry ultraviolet laser trace element micro-analyzer (ICP MS-ULTEMA). *ANU Research School of Earth Sciences - Annual Report*, 138-140.
- Mank, A. J. G. and Mason, P. R. D. (1999) A critical assessment of laser ablation ICP-MS as an analytical tool for depth analysis in silica-based glass samples. *Journal of Analytical Atomic Spectrometry*, **14**, 1143-1153.
- Marton, Z., Landstrom, L., Boman, M. and Heszler, P. (2003) A comparative study of size distribution of nanoparticles generated by laser ablation of graphite and tungsten. *Materials Science & Engineering C-Biomimetic and Supramolecular Systems*, **23**, 225-228.
- Mermet, J. M. (2006) Fundamental Principles of Inductively Coupled Plasmas. In *Inductively Coupled Plasma Spectrometry and its Applications*, Hill, S. J. (ed), *Blackwell Publishing*, 27-50.
- Moenke-Blankenburg, L. (1993) Laser-ICP-Spectrometry. *Spectrochimica Acta Reviews*, **15**, 1-37.
- Moenke-Blankenburg, L., Gackle, M., Günther, D. and Kammel, J. (1989) Plasma Source Mass Spectrometry. *Royal Society of Chemistry, Cambridge*.
- Monticelli, D., Gurevich, E. L. and Hergenröder, R. (2009) Design and performances of a cyclonic flux cell for laser ablation. *Journal of Analytical Atomic Spectrometry*, **24**, 328-335.
- Motelica-Heino, M., Le Coustumer, P. and Donard, O. F. X. (2001) Micro- and macro-scale investigation of fractionation and matrix effects in LA-ICP-MS at 1064 nm and 266 nm on glassy materials. *Journal of Analytical Atomic Spectrometry*, **16**, 542-550.
- Nakamura, E., Ishikawa, T., Birck, J. L. and Allegre, C. J. (1992) Precise Boron Isotopic Analysis of Natural Rock Samples Using A Boron Mannitol Complex. *Chemical Geology*, **94**, 193-204.
- Outridge, P. M., Doherty, W. and Gregoire, D. C. (1996) The formation of trace element-enriched particulates during laser ablation of refractory materials. *Spectrochimica Acta Part B-Atomic Spectroscopy*, **51**, 1451-1462.
- Outridge, P. M., Doherty, W. and Gregoire, D. C. (1997) Ablative and transport fractionation of trace elements during laser sampling of glass and copper. *Spectrochimica Acta Part B-Atomic Spectroscopy*, **52**, 2093-2102.
- Overwijk, M. H. F., Vandenheuvel, F. C. and Bulleliuwma, C. W. T. (1993) Novel Scheme for the Preparation of Transmission Electron-Microscopy Specimens with A Focused Ion-Beam. *Journal of Vacuum Science & Technology B*, **11**, 2021-2024.
- Palmer, M. R. and Slack, J. F. (1989) Boron Isotopic Composition of Tourmaline from Massive Sulfide Deposits and Tourmalinites. *Contributions to Mineralogy and Petrology*, **103**, 434-451.
- Palmer, M. R. and Swihart, G. H. (1996) Boron isotope geochemistry: An overview. In *Boron: Mineralogy, Petrology and Geochemistry*, Grew, E. S. and Anovitz, L. M. (eds), *Reviews in Mineralogy and Geochemistry*, **33**, 709-744.
- Park, C. J. (2002) Determination of boron in steel by isotope-dilution inductively coupled plasma mass spectrometry after matrix separation. *Bulletin of the Korean Chemical Society*, **23**, 1541-1544.
- Parrish, R. R., Nowell, G., Noble, S. R., Horstwood, M., Timmerman, H., Shaw, P. and Bowen, I. J. (1999) LA-PIMMS: A new method of U-Th-Pb geochronology using micro-sampling techniques. *Journal of Conference Abstracts*, **4**, 799.

- Pederson, L. R. (1982) Are Neutral Sodium Atoms Produced on Glass Surfaces by Electron-Bombardment. *Surface Science*, **119**, L307-L313.
- Plotnikov, A., Vogt, C. and Wetzig, K. (2002) An approach to the reconstruction of true concentration profile from transient signal in spatially resolved analysis by means of laser ablation ICP MS. *Journal of Analytical Atomic Spectrometry*, **17**, 1114-1120.
- Poitrasson, F., Freydier, R., Mao, X., Mao, S. S. and Russo, R. E. (2005) Femtosecond laser ablation ICP-MS analysis of trace elements in solids. *Geochimica et Cosmochimica Acta*, **69**, A54.
- Poitrasson, F., Mao, X. L., Mao, S. S., Freydier, R. and Russo, R. E. (2003) Comparison of ultraviolet femtosecond and nanosecond laser ablation inductively coupled plasma mass spectrometry analysis in glass, monazite, and zircon. *Analytical Chemistry*, **75**, 6184-6190.
- Potts, P. J. (1997) A glossary of terms and definitions used in analytical chemistry. *Geostandards Newsletter*, **21**, 157-161.
- Preining, O. (1998) The physical nature of very, very small particles and its impact on their behaviour. *Journal of Aerosol Science*, **29**, 481-495.
- Riondato, J., Vanhaecke, F., Moens, L. and Dams, R. (2000) Fast and reliable determination of (ultra-)trace and/or spectrally interfered elements in water by sector field ICP-MS. *Journal of Analytical Atomic Spectrometry*, **15**, 341-345.
- Russo, R. E. (1995) Laser-Ablation. *Applied Spectroscopy*, **49**, A14-A28.
- Russo, R. E., Mao, X. L., Borisov, O. V. and Liu, H. C. (2000) Influence of wavelength on fractionation in laser ablation ICP-MS. *Journal of Analytical Atomic Spectrometry*, **15**, 1115-1120.
- Russo, R. E., Mao, X. L., Gonzalez, J. J. and Mao, S. S. (2002) Femtosecond laser ablation ICP-MS. *Journal of Analytical Atomic Spectrometry*, **17**, 1072-1075.
- Ruzicka, J. and Hansen, E. H. (1988) *Flow-Injection Analysis*. Wiley, New York.
- Saetveit, N. J., Bajic, S. J., Baldwin, D. P. and Houk, R. S. (2008) Influence of particle size on fractionation with nanosecond and femtosecond laser ablation in brass by online differential mobility analysis and inductively coupled plasma mass spectrometry. *Journal of Analytical Atomic Spectrometry*, **23**, 54-61.
- Sahoo, S. K. and Masuda, A. (1995) Simultaneous Measurement of Lithium and Boron Isotopes As Lithium Tetraborate Ion by Thermal Ionization Mass-Spectrometry. *Analyst*, **120**, 335-339.
- Sasaki, T., Terauchi, S., Koshizaki, N. and Umehara, H. (1998) The preparation of iron complex oxide nanoparticles by pulsed-laser ablation. *Applied Surface Science*, **127**, 398-402.
- Shen, J. J. S. and You, C. F. (2003) A 10-fold improvement in the precision of boron isotopic analysis by negative thermal ionization mass spectrometry. *Analytical Chemistry*, **75**, 1972-1977.
- Slack, J. F. (1996) Tourmaline associations with hydrothermal ore deposits. In *Boron: Mineralogy, Petrology and Geochemistry*, Grew, E. S. and Anovitz, L. M. (eds), *Reviews in Mineralogy and Geochemistry*, **33**, 559-643.
- Stormer, J. C., Pierson, M. L. and Tacker, R. C. (1993) Variation of F-X-Ray and Cl-X-Ray Intensity Due to Anisotropic Diffusion in Apatite During Electron-Microprobe Analysis. *American Mineralogist*, **78**, 641-648.
- Sylvester, P. J. and Ghaderi, M. (1997) Trace element analysis of scheelite by excimer laser ablation inductively coupled plasma mass spectrometry (ELA-ICP-MS) using a synthetic silicate glass standard. *Chemical Geology*, **141**, 49-65.
- Taylor, B. E. and Slack, J. F. (1984) Tourmalines from Appalachian-Caledonian Massive Sulfide Deposits - Textural, Chemical, and Isotopic Relationships. *Economic Geology*, **79**, 1703-1726.
- Telouk, P., Rose-Koga, E. F. and Albarède, F. (2003) Preliminary results from a new 157 nm laser ablation ICP-MS instrument: New opportunities in the analysis of solid samples. *Geostandards Newsletter-the Journal of Geostandards and Geoanalysis*, **27**, 5-11.
- Tiepolo, M., Bouman, C., Vannucci, R. and Schwieters, J. (2006) Laser ablation multicollector ICPMS determination of delta B-11 in geological samples. *Applied Geochemistry*, **21**, 788-801.

- Tonarini, S., Pennisi, M., Adorni-Braccesi, A., Dini, A., Ferrara, G., Gonfiantini, R., Wiedenbeck, M. and Groning, M. (2003) Intercomparison of boron isotope and concentration measurements. Part 1: Selection, preparation and homogeneity tests of the intercomparison materials. *Geostandards Newsletter-the Journal of Geostandards and Geoanalysis*, **27**, 21-39.
- Tonarini, S., Pennisi, M. and Gonfiantini, R. (2009) Boron isotope determinations in waters and other geological materials: Analytical techniques and inter-calibration of measurements. *Isotopes in Environmental and Health Studies*, **45**, 169-183.
- Tonarini, S., Pennisi, M. and Leeman, W. P. (1997) Precise boron isotopic analysis of complex silicate (rock) samples using alkali carbonate fusion and ion-exchange separation. *Chemical Geology*, **142**, 129-137.
- Trumbull, R. B., Krienitz, M. S., Gottesmann, B. and Wiedenbeck, M. (2008) Chemical and boron-isotope variations in tourmalines from an S-type granite and its source rocks: the Erongo granite and tourmalinites in the Damara Belt, Namibia. *Contributions to Mineralogy and Petrology*, **155**, 1-18.
- Trumbull, R. B., Krienitz, M. S., Grundmann, G. and Wiedenbeck, M. (2009) Tourmaline geochemistry and delta B-11 variations as a guide to fluid-rock interaction in the Habachtal emerald deposit, Tauern Window, Austria. *Contributions to Mineralogy and Petrology*, **157**, 411-427.
- Ullmann, M., Friedlander, S. K. and Schmidt-Ott, A. (2002) Nanoparticle formation by laser ablation. *Journal of Nanoparticle Research*, **4**, 499-509.
- Vandecasteele, C., Nagels, M., Vanhoe, H. and Dams, R. (1988) Suppression of Analyte Signal in Inductively-Coupled Plasma Mass-Spectrometry and the Use of An Internal Standard. *Analytica Chimica Acta*, **211**, 91-98.
- Vanhaecke, F., Vanhoe, H., Dams, R. and Vandecasteele, C. (1992) The Use of Internal Standards in ICP-MS. *Talanta*, **39**, 737-742.
- Watson, E. B., Cherniak, D. J., Hanchar, J. M., Harrison, T. M. and Wark, D. A. (1997) The incorporation of Pb into zircon. *Chemical Geology*, **141**, 19-31.
- Wiedenbeck, M., Alle, P., Corfu, F., Griffin, W. L., Meier, M., Oberli, F., von Quadt, A., Roddick, J. C. and Spiegel, W. (1995) 3 Natural Zircon Standards for U-Th-Pb, Lu-Hf, Trace-Element and Ree Analyses. *Geostandards Newsletter*, **19**, 1-23.
- Wilson, S. A. (1997) The collection, preparation and testing of USGS reference material BCR-2, Columbia River, Basalt. *U.S. Geological Survey Open-File Report 98-00x*.
- Xavier, R. P., Wiedenbeck, M., Trumbull, R. B., Dreher, A. M., Monteiro, L. V. S., Rhede, D., de Araujo, C. E. G. and Torresi, I. (2008) Tourmaline B-isotopes fingerprint marine evaporites as the source of high-salinity ore fluids in iron oxide copper-gold deposits, Carajas Mineral Province (Brazil). *Geology*, **36**, 743-746.

Curriculum Vitae

Date and place of birth: 20. 11. 1974, Prague

Education:

1995-1998 Bc. (BSc. degree) - Geology, Faculty of Science, Charles University
1998-2000 Mgr. (MSc. degree) - Geochemistry, Faculty of Science, Charles University
MSc. Thesis - Acid Mine Drainage and its manifestations in the biosphere
Since 2003 PhD. study - Geochemistry, Faculty of Science, Charles University
PhD. Thesis – Use and limitations of laser ablation ICP-MS in geoscience applications

Current & past jobs:

2000-2004 Laboratory assistant in the ICP-MS laboratory at Institute of Geochemistry, Mineralogy and Mineral Resources, Charles University
2005-2007 Researcher at Radiogenic Isotopes Laboratory, Czech Geological Survey
Since 2008 Head of Ultra trace Laboratory, Czech Geological Survey

Professional experience:

02/2004 - 07/2004 Pre-doctoral research fellow in the ICP-MS laboratory at Department of Earth Science, University of Bergen, Norway
04/2007 – 12/2007 visiting scientist, Centre for Geobiology and Department of Earth Science, University of Bergen, Norway

Short courses & Workshops:

- 6th European Workshop on Laser Ablation in Elemental and Isotopic Analysis, Utrecht, 2002
- Summer School: Isotopic tracing of geological processes, Třeš' Chateau, Czech republic, 2003
- Short course on ICP spectrometry, Ioannes Marcus Marci Spectroscopic Society, Brno, 2004
- Short course on Secondary Ion Mass Spectrometry in the Earth Sciences, GeoForschungsZentrum Potsdam, Germany, 2005
- Short course on ICP-Mass Spectrometry I: Introduction and ICP-Mass Spectrometry II. Advanced Topics, R. S. Houk, Winter Conference on Plasma Spectrochemistry, Tucson, 2006
- Short course on Preparing Your Laboratory for Trace Level Analysis, E. Bakowska, Winter Conference on Plasma Spectrochemistry, Tucson, 2006
- 8th European Workshop on Laser Ablation in Elemental and Isotopic Analysis, ETH Zürich, 2006
- Short course on laser ablation, Ioannes Marcus Marci Spectroscopic Society, Nová Olešná, 2008
- 9th European Workshop on Laser Ablation in Elemental and Isotopic Analysis, Prague, 2008 (organizer)
- Course on ICP spectrometry, Ioannes Marcus Marci Spectroscopic Society, Brno, 2009
- 10th European Workshop on Laser Ablation in Elemental and Isotopic Analysis, Kiel, 2010

Personal participation on international conferences:

- Winter Conference on Plasma Spectrochemistry, Budapest, 2005
- 6th International Symposium on Applied Isotope Geochemistry, Prague, 2005
- Winter Conference on Plasma Spectrochemistry, Tucson, 2006
- European Geosciences Union General Assembly 2010 Vienna, Austria, 2010

Conference abstracts:

Košler J., Wiedenbeck M., Hovorka J., Tubrett M., Sylvester P., Míková J. (2003): Size and composition of particles produced by laser ablation - effects on elemental fractionation during ICPMS analysis. *Geoanalysis 2003*, Rovaniemi.

Tubrett M., Míková J., Sylvester P., Košler J. (2003): Trace element composition and homogeneity of MASS-1 sulphide calibration standard. *Geoanalysis 2003*, Rovaniemi.

Košler J., Hovorka J., Wiedenbeck M., Tubrett M., Sylvester P., Míková J. (2003): Size distribution of number, mass and composition of aerosol produced by laser ablation for ICP-MS analysis. *European Aerosol Conference 2003*, Madrid.

Svojtka M., Tagami T., Košler J., Míková J., Buriánková K. (2003): Source and thermal evolution of High Himalayan rocks in the Makalu region interpreted from U-Pb and fission-track dating of zircon. *Goldschmidt 2003*, Kurashiki.

Košler J., Wiedenbeck M., Wirth R., Hovorka J., Sylvester P., Míková J. (2004): Effects of size, chemical and phase composition of ablated particles on elemental fractionation during ICPMS analysis. *2004 Winter Conference on Plasma Spectrochemistry*, Fort Lauderdale.

Míková J., Hovorka J., Košler J. (2005): Charge and transport properties of particles during laser ablation sampling. *2005 Winter Conference on Plasma Spectrochemistry*, Budapest.

Míková J., Košler J., Hovorka J. (2005): Solid sampling of geological materials - properties of particles produced by laser ablation. *6th International Symposium on Applied Isotope Geochemistry*, Prague.

Míková J., Longerich H., Košler J., Wiedenbeck M. (2006): Fractionation of alkali elements during laser ablation ICP-MS analysis of silicate samples. *2006 Winter Conference on Plasma Spectrochemistry*, Tucson.

Míková, J., Longerich, H., Košler, J., Wiedenbeck, M. (2006): Fractionation of alkali elements during laser ablation analysis of silicates. *Geoanalysis 2006*, Beijing, China

Košler, J., Novák, M., Krachler, M., Míková J. (2009): Laser ablation and isotope dilution ICP-MS analysis of Pb in spruce tree rings - a record of atmospheric pollution in NW Bohemia. *2009 Winter Conference on Plasma Spectrochemistry*, Graz

Míková, J., Novák, M., Janoušek, V. (2010): Boron isotopes in tourmaline of dravite-schorl series from granitic pegmatites of the Moldanubian Zone, Czech Republic. *IMA 2010 General Meeting*, Budapest.

Míková, J., Košler, J., Wiedenbeck, M. (2010): Evaluation of matrix effects during laser ablation MC ICP-MS analysis of boron isotopes in tourmaline. *10th European Workshop on Laser Ablation*, Kiel.

Eur. J. Mineral.
2004, 16, 15–22

Laser ablation ICPMS dating of zircons in Erzgebirge orthogneisses: evidence for Early Cambrian and Early Ordovician granitic plutonism in the western Bohemian Massif

JAN KOŠLER^{1,2*}, DONALD R. BOWES³, JIŘÍ KONOPÁSEK⁴ and JITKA MÍKOVÁ²

¹ Department of Earth Sciences, Memorial University of Newfoundland, 300 Prince Philip Drive, St John's, NF A1B 3X5, Canada

² present address: Institute of Geochemistry, Charles University, Albertov 6, CZ-128 43 Prague 2, Czech Republic

*Corresponding author, e-mail: kosler@natur.cuni.cz

³ Division of Earth Sciences, University of Glasgow, Glasgow, G12 8QQ, Scotland, U.K.

⁴ Institute of Petrology and Structural Geology, Charles University, Albertov 6, CZ-128 43 Prague 2, Czech Republic

Abstract: U-Pb isotopic data obtained by laser ablation ICPMS analysis of nine zircons with centre to margin oscillatory growth zones from a K-feldspar-rich augen gneiss in the allochthonous Lower Crystalline Nappe of the Erzgebirge domain of the western part of the Bohemian Massif yield a concordia age of 524 ± 10 Ma (2 sigma). This Early Cambrian age represents the time of magmatic crystallization of the protolith of a representative, from near Měděnec, of the allochthonous "Red gneiss" whose igneous nature is shown by the presence of (deformed) xenoliths. Data from TIMS analysis of zircons with variable proportions of unzoned xenocrystic cores surrounded by oscillatory-zoned overgrowths point to magma derivation from upper Proterozoic, or older, rocks. Data obtained for five zircon grains from another "Red gneiss" in the Lower Crystalline Nappe (in the Klínovec anticline) plot below the concordia with the age of the one point that is near concordant being 519 ± 26 Ma (2 sigma). These data, together with internal features of the zircons, are consistent with Early Cambrian granitic plutonism also in this part of the Erzgebirge but with later Pb loss, possibly associated with considerable fluid movement during thrust nappe development. Another sample of a coarse-grained orthogneiss from the autochthonous St Catherine's dome yielded a significantly younger Early Ordovician age of 480 ± 10 Ma (2 sigma) calculated from eight zircon analyses. However, three zircon grains from the same sample gave a significantly older near-concordant Late Proterozoic age of *ca.* 620 Ma.

Provided that the age difference of *ca.* 40 Ma between orthogneisses from Měděnec – Klínovec and St Catherine's dome holds also for other orthogneisses in the Erzgebirge, zircon U-Pb age data could be used to discriminate between allochthonous and autochthonous units in this region.

The *ca.* 25 Ma difference between the Early Cambrian protolith age of the augen gneiss from near Měděnec determined by the laser ablation ICPMS technique and a previously reported older age of 550 ± 9 Ma for a nearby sample determined by the Pb-Pb evaporation technique is accounted for on the basis of the latter not being adequate for dating zircons with a small xenocrystic component. This study demonstrates the importance of high spatial resolution dating techniques, such as SHRIMP or laser ablation ICPMS, in dating zircons with complex growth history that are common in crustally-derived melts.

Key-words: augen gneiss, Bohemian Massif, Erzgebirge, granitic protolith, laser ablation ICPMS, U-Pb zircon dating, xenocryst.

Introduction

Emplacement ages of plutonic rocks are valuable in constraining the tectonic history of metamorphic domains in orogenic belts, particularly if the intrusions cut across major tectonic boundaries. In addition, corresponding or contrasting emplacement ages and, or, geochemical signatures of magmatic rocks may be used for correlation or to discriminate between different parts of a succession of structural – metamorphic – igneous events. Determination of such emplacement ages that are reliable is possible using zircon U-

Pb chronometry, even if the plutons have experienced penetrative ductile deformation subsequent to their magmatic crystallization (*e.g.* Wayne & Sinha, 1992; Košler *et al.*, 1993), particularly if high spatial resolution dating techniques are used. Laser ablation ICPMS U-Pb analyses reported here give the protolith ages of three orthogneisses from the Erzgebirge (Krušné hory) Mountains in the western part of the Bohemian Massif (Fig. 1).

The augen gneisses are present in the allochthonous Lower Crystalline Nappe (LCN; Konopásek *et al.*, 2001) unit, and also in the structurally lower autochthonous core

Original paper

Hyperpotassic granulites from the Blanský les Massif (Moldanubian Zone, Bohemian Massif) revisited

Vojtěch JANOUŠEK^{1, 2*}, Erwin KRENN³, Fritz FINGER³, Jitka MÍKOVÁ¹, Jiří FRÝDA¹¹Czech Geological Survey, Klárov 3, 118 21 Prague 1, Czech Republic; janousek@cgu.cz²Institute of Petrology and Structural Geology, Charles University, Albertov 6, 128 43 Prague 2, Czech Republic³Division of Mineralogy and Material Science, University of Salzburg, Hellbrunnerstraße 34, A-5020 Salzburg, Austria

*Corresponding author



In the Blanský les granulite Massif (Moldanubian Unit, South Bohemia), built mainly by felsic calc-alkaline HP-HT garnet ± kyanite granulite, occur rare small bodies of hyperpotassic granulite with garnet (Plešovice type) or pyroxene (Lhotka type).

The *Plešovice type* is dominated by slightly perthitic K-feldspar and almandine–pyrope rich garnet, the latter variously retrogressed to biotite ± plagioclase. The other conspicuous euhedral crystals are apatite and zircon. In the rock occur also Zr–Nb-rich rutile and much rarer primary monazite; originally LREE-rich apatites decompose into small Th-poor, MREE-rich monazite grains.

The *Lhotka type* granulites contain pyroxene, often altered to actinolite, instead of garnet. The predominant perthitic K-feldspar encloses a small amount of unmixed celsian. Typical are large euhedral crystals of apatite with small unmixed monazite grains; primary monazite is rare. Noteworthy is the occurrence of secondary Ti phases with high REE, Y and Zr, formed at the expense of the primary pyroxene.

The studied granulite types are highly potassic ($K_2O > 7\%$, up to c. 14%, $K_2O/Na_2O = 3.1\text{--}9.2$ wt. %), silica-poor ($SiO_2 < 65\%$), with low contents of most major- and minor-element oxides, apart from K and P. Characteristic are high concentrations of Cs, Rb, Ba and U at variable enrichments in Zr and Hf. Whole-rock contents some HFSE (Ti, Nb and Ta) are extremely low. The REE patterns show marked negative Eu anomalies and variable LREE enrichments increasing with rising silica due to a conspicuous drop in HREE. The Sr–Nd isotopic ratios document the derivation from mature crustal sources ($\epsilon_{Nd}^{337} \sim -5.5$; $^{87}Sr/^{86}Sr_{337} = 0.7272$ and 0.7279 for the Plešovice and $^{87}Sr/^{86}Sr_{337} = 0.7109$ for the Lhotka types). Apatite saturation temperatures are high (~ 1070 °C), close to the previously estimated conditions of (re)crystallization for both calc-alkaline and hyperpotassic granulites. The zircon saturation temperatures tend to be more variable, some exceeding 1000 °C but many unrealistically low, reflecting effects of disequilibrium melting, heterogeneous distribution of accumulated crystals in the magma and/or sampling bias.

The hyperpotassic granulites are interpreted as Viséan igneous rocks. The parental magma could have originated by low degrees of HP-HT, non-eutectic partial melting. The low-scale melt was most likely expelled close to the HP-HT metamorphic peak or at early stages of decompression from common Moldanubian calc-alkaline granulites. This genetic link is documented by the presumed P-T conditions, similar age and complementary geochemical and Sr–Nd isotopic signatures. Subsequently the magma could have developed by garnet, apatite and zircon dominated fractional crystallization, with or without some crystal accumulation.

Keywords: granulites, alkali feldspar syenites, high-pressure melting, geochemistry, Moldanubian Zone, Bohemian Massif

Received: 29 January 2007; **accepted** 6 June 2007; **handling editor:** M. Novák

1. Introduction

Felsic (granitic) calc-alkaline garnet ± kyanite-bearing high-pressure and high-temperature (HP-HT) granulites form an important constituent of the high-grade Moldanubian Zone, interpreted as an orogenic root of the European Variscan orogen in Central Europe (e.g., Fiala et al. 1987a; Vrána and Šrámek 1999; O'Brien and Rötzler 2003; O'Brien 2006; Kotková this volume). Regardless the attention the classic occurrences of these granulites in South Bohemia, Western Moravia and Lower Austria (Fig. 1a–b) have attracted, their genesis still remains open to debate. They have been interpreted as metamorphosed

older, mostly felsic igneous or volcanosedimentary rocks (e.g., Fiala et al. 1987a; Vellmer 1992). In this case, some amount of trapped high-pressure melt was likely to have been present, even though its proportion is not well constrained yet: less than 10–15 vol. % (Roberts and Finger 1997; Janoušek et al. 2004) or up to 20–30 vol. % (Tropper et al. 2005). Alternatively, some of the felsic granulites were interpreted as separated Viséan (~ 340 Ma) dry, HP-HT ($P > 15$ kbar, $T > 1000$ °C) partial melts of metasedimentary lithologies (Vrána 1989; Jakeš 1997; Kotková and Harley 1999) or of granitoids/acid volcanic rocks (Vrána 1989). As a third, and so far little tested model, Viséan HP metamorphism (P up to 18 kbar,

Original paper

Modified chromatographic separation scheme for Sr and Nd isotope analysis in geological silicate samples

Jitka MÍKOVÁ*, Petra DENKOVÁ

Czech Geological Survey, Klárov 3, 118 21 Prague 1, Czech Republic; jitka.mikova@geology.cz

* Corresponding author



A novel chromatographic separation technique for Sr and Nd separation from geological silicate samples was established and successfully tested for routine use in Laboratory of Radiogenic Isotopes of the Czech Geological Survey. The separation scheme is based on combination and modification of methods published in papers by Christian Pin and his co-workers. This triple column arrangement enables the isolation of pure Sr and Nd fractions (also Sm if required) from bulk-rock solution in a single step during one working day. The Sr and Nd yields are high, while blank levels remain low. This procedure minimizes the acid consumption and time needed for the separation by more than half compared to the traditional ion exchange separation techniques. The calibration of the Ln.Spec columns should be periodically monitored because the elution of REEs shifts after a period of extensive use of the resin. Suitability of this technique for Sr and Nd separation from silicate rock samples was confirmed by repeated measurements of $^{87}\text{Sr}/^{86}\text{Sr}$ and $^{143}\text{Nd}/^{144}\text{Nd}$ isotopic ratios in three international reference materials BCR-1, JA-1 and JB-3.

Keywords: strontium, neodymium, ion exchange chromatography, isotopic analysis, silicate rocks; thermal-ionization mass spectrometry
Received: 12 October 2007; accepted 15 December 2007; handling editor: M. Štemprok

1. Introduction

The measurements of isotopic composition performed by thermal ionization mass spectrometry (TIMS) require chemical separation of the elements of interest. This is important as an impure sample will give both a very poor ion yield and cause beam instability in the mass spectrometer, potentially resulting in a poor analysis. Isobaric interferences, such as $^{87}\text{Rb}^+$ and $^{87}\text{Sr}^+$ must also be minimized for accurate isotopic determination.

This separation is traditionally performed using ion exchange chromatography. Since the early pioneering work of Aldrich et al. (1953), the chromatographic techniques have proven to be the most useful for isolating elements of interest from the sample matrix. Although this technique is widely used in isotope geochemistry, conventional ion exchange resins have a disadvantage of the poor elemental selectivity. In general, chromatographic separation schemes are based on differences in distribution coefficients (the larger the coefficient, the greater the affinity of the ion to the resin, also the larger the ratio of the coefficients of two different ions, the easier it is to separate them using ion exchange). They, therefore, require relatively large ion exchange columns and chemical reagent volumes, depending on the sample size. Previously, we have employed traditional ion exchange separations (Richard et al. 1976) using Bio-Rad AGW X8 (200–400 mesh) resin and decomposed sample in 2.5M HCl solution to separate Rb and Sr. For a sample weight

of c. 100 mg the volumes of reagents required to elute Sr were 60 ml of 2.5M HCl; the Sr fraction was collected in the last c. 15 ml of this volume. Additional 50 ml of 6M HCl were required to elute REEs, which were collected in the last 10 ml of that volume. The REE fraction was then evaporated and dissolved in 0.2M HCl. Finally, Nd was separated by passing the sample through another column packed with BioBeads S-X8, 200–400 mesh beads coated with DEP – bis(2-ethylhexyl) hydrogen phosphate. The total volume of acids required to elute Nd was c. 40 ml.

A new generation of chromatographic resin materials developed at the Argonne National Laboratory (USA) helps to solve many of the difficulties with large amounts of reagents and long time required for separation some of the geochemically important elements. These resins were originally designed for separation of radioactive nuclides from nuclear waste solutions but their high capacity and specificity make them suitable also for environmental and geological applications. Here we present a separation scheme for strontium and neodymium applicable to isotopic analysis of silicate rocks. This separation procedure is based up on combination and slight modification of methods published in papers by Pin et al. (1994) and Pin and Zalduegui (1997). The first paper describes the separation procedure for Sr using the Sr.Spec and the separation of LREEs using the TRU.Spec resins from silicate samples, while the second paper describes the separation of individual light rare elements using the Ln.Spec resin.

Available online at www.sciencedirect.com

Geochimica et Cosmochimica Acta 74 (2010) 4207–4218

**Geochimica et
Cosmochimica
Acta**

www.elsevier.com/locate/gca

Radial distribution of lead and lead isotopes in stem wood of Norway spruce: A reliable archive of pollution trends in Central Europe

Martin Novak^{a,*}, Jitka Mikova^a, Michael Krachler^{b,1}, Jan Kosler^c, Lucie Erbanova^a,
Eva Prechova^a, Iva Jackova^a, Daniela Fottova^a

^a Czech Geological Survey, Geologická 6, 152 00 Prague 5, Czech Republic

^b Institute of Geosciences, University of Heidelberg, Im Neuheimer Feld 236, 69120 Heidelberg, Germany

^c Department of Earth Science and Centre for Geobiology, University of Bergen, Allegaten 41, N-5007 Bergen, Norway

Received 26 January 2009; accepted in revised form 23 April 2010; available online 6 May 2010

Abstract

Annual growth rings of a common hardwood species, *Picea abies* L., were investigated as a potential archive of past atmospheric Pb pollution. Wide distribution of trees in terrestrial settings and straightforward chronology are two advantages of this potential geochemical archive, but several processes described in the literature may obscure the trends in past Pb deposition. These confounding factors include, e.g., radial post-depositional mobility of Pb in xylem, and ecosystem acidification leading to higher bioavailability of Pb. One- to five-year annual wood increments were analyzed for Pb concentrations and ²⁰⁶Pb/²⁰⁷Pb ratios at Jezeri (JEZ), Uhlirka (UHL) and Na Lizu (LIZ), three sites in the Czech Republic, differing in atmospheric Pb loads. Three to four trees per site were included in the study. Distinct Pb concentration maxima between 1960 and 1990 at the two heavily polluted sites (JEZ and UHL) coincided with historical Pb emissions known from inventories of industrial production. No Pb concentration maxima were found at one site, LIZ, situated in a national park 150 km from major pollution sources. Spruce tree rings from JEZ, located just 5 km from coal-burning power stations, contained a large proportion of coal-derived Pb (a high-²⁰⁶Pb/²⁰⁷Pb ratio of 1.19). A coal-related maximum in ²⁰⁶Pb/²⁰⁷Pb in JEZ tree rings was found using two different analytical techniques, laser-ablation multi-collector ICP MS, and single-collector sector-field ICP MS. In a three-isotope graph (²⁰⁶Pb/²⁰⁷Pb vs. ²⁰⁸Pb/²⁰⁷Pb), tree-ring data plotted into the field of ombrotrophic (i.e., rain-fed) peat bogs, suggesting negligible contribution of bedrock-derived Pb in the xylem. We concluded that none of the potential confounding factors played a major role at our sites. Annual growth rings of *P. abies* in Central Europe faithfully recorded historical changes in atmospheric Pb depositions.

© 2010 Published by Elsevier Ltd.

1. INTRODUCTION

The detrimental effect of environmental lead (Pb) on human health is well documented (Nriagu and Pacyna, 1988; Gulson et al., 2006). The toxic behaviour of bioavailable Pb

in ecosystems has also attracted much attention (Adriano, 2001). Long-term exposure to Pb can be equally dangerous to fauna and flora as short-term episodes of intense pollution (Gulson et al., 2004). In the 1980s, direct monitoring of atmospheric Pb inputs via rainfall and dry deposition began in many industrial countries of the world (Bollhoffer and Rosman, 2001). In order to assess the cumulative effect of anthropogenic Pb on organisms, however, the time-series of these direct measurements are too short. Fortunately, several geochemical archives of historical trends in Pb pollution have been identified, extending our knowledge

* Corresponding author. Tel.: +420 251085333.

E-mail address: martin.novak@geology.cz (M. Novak).

¹ Present address: European Commission Joint Research Centre, Institute for Transuranium Elements (ITU), P.O. Box 2340, D-76125 Karlsruhe, Germany.

Charge and transport properties of particles during laser ablation sampling

Jitka Míková, Jan Hovorka and Jan Košler

Department of Geochemistry, Charles University, Prague, Czech Republic * Institute for Environmental Studies, Charles University, Prague, Czech Republic * Department of Earth Science, University of Bergen, Norway *

Particles produced by laser ablation

THEORY

Aerosol particles produced by laser ablation of solid samples are usually charged. Normally, a high level of electrical charge is undesirable because it increases the particle loss to the walls of transport and sampling systems, especially when these are made from non-conductive materials such as glass or plastics (e.g. PFA Teflon). Different transport of ablated particles, together with processes that occur at the ablation site and in the ICP, can result in decoupling of elements and isotopes, a process that is observed as elemental or isotopic fractionation during LA ICP-MS analysis. The size distribution of particles produced during laser ablation is thought to possess a significant control on the nature and size of elemental fractionation. It has also been demonstrated that chemical and phase compositions of ablated particles can vary with their sizes. An outstanding issue is whether laser ablation of different sample matrices produces particles with different charge-size distributions and whether such variations have a significant effect on the particle transport properties.

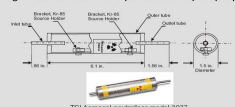


Fig. 1 Schematics of the aerosol charge neutralizer used in this study.

Here we report results of a series of laser ablation experiments with an aerosol charge neutralizer to test the effect of particle charge on the transport properties of ablated particles. The aerosol charge neutralizer (TSI model 3077, Fig. 1) uses a radioactive beta-source (2 millicuries of Kr-85, 0.67 MeV) to ionize the He carrier gas into positive and negative ions.

Particles carrying a high charge can discharge by capturing ions of opposite polarity. After a sufficient residence time, the particles reach charge equilibrium such that the aerosol carries an equilibrium bipolar Boltzman charge size distribution. We then compare the signal intensities and element fractionation rates measured by ICP-MS with and without the employment of the neutralizer. We also compare the effects of using a conductive and non-conductive aerosol transport systems on the rate of elemental fractionation and signal intensity.

EXPERIMENTAL

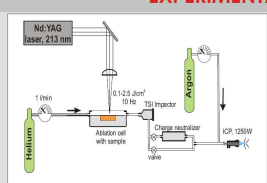


Fig. 2 Schematics of the experimental setup used in this study



Fig. 3 Laser ablation ICP-MS facility at Bergen University

We have used a 213 nm Nd:YAG laser (New Wave, UP213) connected to the Element 2 Thermo Finnigan single collector ICP-MS at Bergen University, Norway Fig. 3.

We have ablated NIST-612 (silicate glass with nominal element concentration of 50 ppm) and zircon 91500 (natural ZrSiO₄ that contains 81 ppm U, 29 ppm Th, and 15 ppm Pb) samples in He atmosphere (1 l/min). The laser was fired at 10 Hz repetition rate, using 80 μm spot diameter and energy density of 3.5 J/cm². A single stage stainless steel TSI impactor was set to cut off particles larger than 350 nm. It was mounted on the He carrier gas line between the ablation cell and the ICP torch. The gas line was made of flexible conductive tubing (or, alternatively, of non-conductive Nalgene PFA tubing). A stainless steel aerosol charge neutralizer was employed in some experiments after the impactor. He gas line was recombined with Ar gas line in a T-piece at the back end of the ICP torch. The ICP-MS was operated in peak jumping mode with one point measured per peak (10 ms dwell time) for masses 206 (Pb), 208 (Pb), 232 (Th) and 238 (U). Data were acquired in time resolved acquisition mode. Gas blank was measured for the initial 60 seconds of each analysis, followed by measurement of 120 seconds of laser ablation signal.

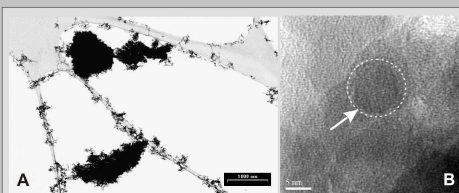


Fig. 6 High resolution TEM images of (A) particle clusters produced by laser ablation of the NIST 612 silicate glass, (B) single particle within a particle cluster.

RESULTS

The results of this experiment are summarized in Table 1 and on Fig. 5. The elemental fractionation is described here by the slope of the regression line fitted to the time resolved trace of a corresponding elemental ratio (Fig. 4).

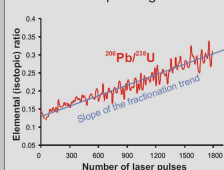


Fig. 4 Definition of the fractionation rate as the slope of the regression line fitted to the time resolved trace of a corresponding elemental ratio

Fractionation slope	NIST 612		Zircon 91500	
	With neutraliser	Without neutraliser	With neutraliser	Without neutraliser
Conductive tubing	2.2	4.0	0.2	0.2
Non-conductive tubing	1.8	2.0	0.3	0.2
Signal intensity	15 000	9 500	40 500	26 000
	8 000	7 800	7 700	15 000

Table 1 Summary of results of the laser ablation experiments for different experimental arrangements, fractionation refers to the change in the slope of the ²⁰⁶Pb/²⁰⁸Pb ratio with the number of laser pulses applied, signal intensity refers to the measured intensity of ²⁰⁸Pb in cps.

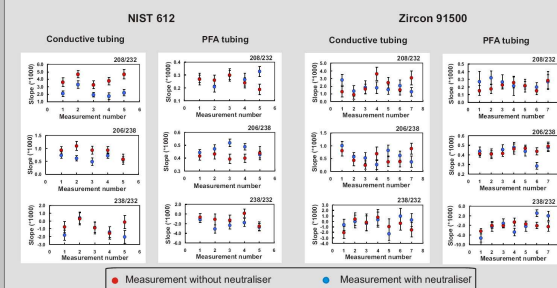


Fig. 5 Results of the laser ablation experiments for different experimental arrangements

DISCUSSION

The mechanisms that may be responsible for the loss of some of the fine and ultra-fine particles (< 350 nm) during the transport of ablated aerosol to the ICP include (1) diffusion and (2) adhesion to the walls of transport system and predominantly to walls of tubing due to induced electrostatic charge. The later mechanism can be influenced by the employment of charge neutralizer and conductive tubing. Previous studies have demonstrated that particles produced during a UV nanosecond laser ablation form by phase explosion (mostly large particles), melt splashing due to hydrodynamic instabilities (mostly large and fine particles) and condensation from supersaturated vapor (fine and ultra-fine particles). Some of the fine (nm-sized) particles usually aggregate and form electrically neutral clusters already in the ablation cell (Fig. 6). Results of the present experiment (Fig. 5) suggest that (1) laser ablation of different sample matrices (silicate glass and zircon) produces particles < 350 nm that have different distribution of charge, (2) the aerosol that leaves the ablation cell is only weakly charged because there is no significant difference between the conductive and non-conductive transport system in cases, when the charge neutralizer was not employed and (3) the use of charge neutralizer emphasizes the different aerosol transport efficiencies in conductive and non-conductive tubing and it also has an effect on the rate of elemental fractionation in the aerosol produced by ablation of silicate glass. The increase of particle transmission, as a result of the use of charge neutralizer, can be attributed to aerosol coagulation in the neutralizer which suppresses diffusional losses in the tubing.

CONCLUSIONS

- Charge distribution of particles produced by nanosecond UV lasers varies subject to the composition of the sample matrix.
- Fine and ultra-fine particles that leave the ablation cell are only weakly charged, probably due to their aggregation into larger clusters.
- Use of conductive tubing and aerosol charge neutralizer can affect the transmission of particles from the ablation cell to the ICP source of a mass spectrometer.

FRACTIONATION OF ALKALI ELEMENTS DURING LASER ABLATION ICP-MS ANALYSIS OF SILICATE SAMPLES

Jitka Míková, Henry Longrich, Jan Košler and Michael Wiedenbeck

Charles University, Prague, Czech Republic; Memorial University, St John's, Canada; University of Bergen, Norway; Geoforschungszentrum Potsdam, Germany

THEORY

Alkali element analysis in geological silicate samples is a real impediment for various rock-forming processes, age dating and thermobarometry. Alkali elements (Li, Na, K, Rb and Cs) are commonly present in silicate rocks, but they are often difficult to analyze by microbeam techniques, such as laser ablation (LA) ICP-MS. Sample inhomogeneity or ion suppression (SIMS) can result in element re-distribution, formation of chemical gradient in the sample and fractionation of alkali elements. These mechanisms are usually not known and it is often assumed that various diffusion mechanisms are involved in this process. It is difficult to differentiate between these mechanisms, as well as reflect the ionic radius and charge of the ions, as well as chemical composition and structure of the sample [1] and sample-beam interaction. Our better understanding of the elemental fractionation during LA ICP-MS is desirable not only to improve the precision and accuracy of alkali elements in correcting for ablation yield (as internal standards) in analyses of other lithophile elements that are present in silicate rocks, but also to improve the accuracy of SIMS. Here we present results of alkali element measurements in synthetic silicate glasses (NIST-610, BCR-2) and natural crystalline alkali by LA ICP-MS, EMP and SIMS. These results are compared with the theoretical fractionation mechanisms that may be related to the alkali element fractionation during laser ablation.

A. Laser ablation experiment

We have used a 213 nm Nd:YAG laser (Wave LP-213) connected to an Element 2 Thermo Finnigan single collector ICP-MS at Bergen to analyze silicate and alkali silicate samples (NIST-610 and BCR-2 glasses and mineral albite NaAlSi₃O₈).

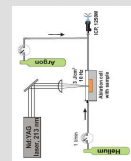


Fig. 1 Experimental setup at Bergen

The laser was fired at 10 Hz with a pulse width of 30 ns and a density of 3 J/cm². Laser beam diameter was 30 μm. The measured time resolved signal intensity ratios of the alkali elements to Si and Ca were used to correct for the fractionation trends (Fig. 2).

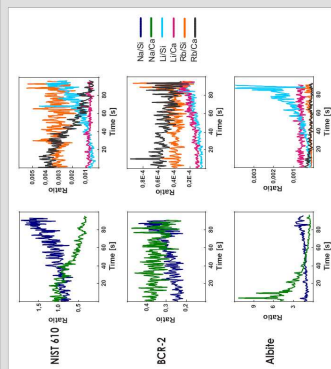


Fig. 2 Laser ablation ICP-MS measured signal intensity ratios of alkali elements, Si and Ca for NIST-610, BCR-2 and albite samples. Data are not corrected for blank, interferences, and mass discrimination.

EXPERIMENTAL AND RESULTS - LASER ABLATION

Chemical maps of SIMS in Potsdam were used to measure the chemical composition of the NIST-610 sample. The shape of the ejecta can be affected by the dynamics of the gas flow during the ablation but commonly maintains a structure that consists of larger (~5 μm) particles being concentrated adjacent to the ablation crater and smaller (sub-μm or nm sized) particles being deposited in the outer part of the crater. The primary beam accelerating voltage was immediately at the edge of the laser ablation pit radially outwards to beyond the edge of the ejecta deposit (Fig. 4). The primary beam accelerating voltage was 12.5 kV with an ion beam current of 0.5 nA. Beam spot size was 5 μm with a secondary extraction voltage of 10 kV.

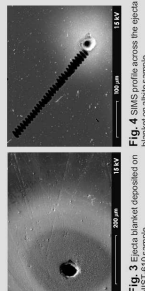


Fig. 3 Ejecta blanket deposited on NIST-610 sample.

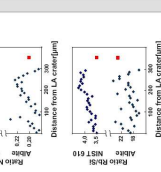


Fig. 4 SIMS profiles across the ejecta blanket on albite sample.

Analyses of the NIST-610 ejecta blanket show a depletion of Na relative to the composition of the particles with increasing distance from the laser pit. The relative intensity of Rb signal (Fig. 5) suggest a relative increase in Rb/Si ratio towards the edge of the ejecta. Similar composition trends were found for the alkali elements, except for the Na/Si ratio that shows a more complex variation.

EXPERIMENTAL AND RESULTS - OTHER MICROBEAM TECHNIQUES

B. Electron microprobe and ion probe experiments

Electron microprobe and ion probe (SIMS) analyses of clean NIST-610 and BCR-2 glasses were conducted to compare the behavior of alkali elements during laser ablation and other microbeam techniques. We have used a Cameca SX100 at the Masaryk University in Brno; the accelerating voltage was 15 kV and the beam current was 10 and 20 nA. The time course of an analysis at different rates, depending on the electron beam current and sample composition (Fig. 7). A corresponding experiment on SIMS yielded an increasing Na/Si ratio in NIST-610 but an opposite fractionation trend during the analysis of BCR-2 (Fig. 9).

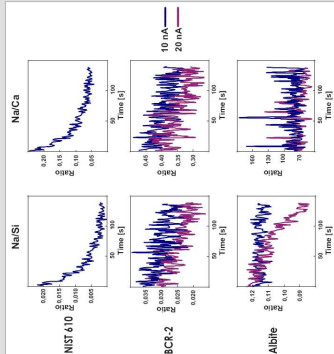


Fig. 7 Fractionation of alkali elements during analysis of NIST-610, BCR-2 and albite by an electron microprobe.

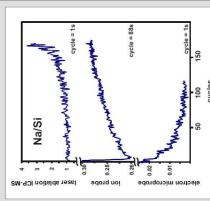


Fig. 9 Summary of Na behavior during analysis of NIST-610 by laser ablation ICP-MS, ion probe and electron microprobe.

Literature:
 1. T. M. Shawhan, Chem. Geol., 133, 3 (1997).
 2. G. S. L. Fisher, S. L. Johnson, F. J. Fleck, J. Anal. Chem., 55, 538 (1983).
 3. K. Jurek and O. Gabel, Spectrochim. Acta B, 55, 103 (1999).
 4. K. Jurek, J. Wiedenbeck, M. Wirth, R. Hovind, G. S. L. Fisher, P. Míková, J. (2005). JAS 20 (5): 402-404

SUMMARY OF OBSERVATIONS

- The observed fractionation of sodium during laser ablation ICP-MS analysis varied from Na-enrichment relative to the sample matrix composition. Similar consistent behavior for all studied sample matrices was observed for Li but fractionation of Rb relative to Si and Ca was matrix dependent.
- Vertical profiles in alkali element contents in sample adjacent to the bottom of the laser pit and chemical variations measured by SIMS across the ejecta blanket suggest that (i) the fractionation of alkali elements relative to Si and Ca takes place at the ablation site and (ii) that different particle size fractions fractionate alkali element to different extent.
- Electron microprobe and ion probe measurements show generally different fractionation patterns compared to LA ICP-MS, indicating that different mechanisms are likely to be involved in the fractionation of alkali elements during interaction with electrons, ions and photons, respectively (Fig. 9).
- SIMS depth profiling and analysis of the ejecta blanket of NIST-610 suggest that the fractionation of alkali elements may be caused by the observed particle size fractionation of alkali elements from Si and Ca during laser ablation.

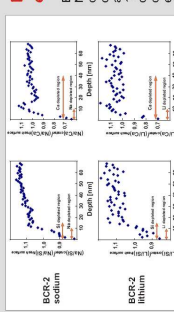


Fig. 6 Results of SIMS depth profiling experiment at bottom of 95 μm wide laser ablation pits in BCR-2 glass. The measured elemental ratios are normalized to analyses of the sample.

We have then conducted a series of SIMS depth profile measurements at the bottom of ca. 95 μm wide laser ablation pits in BCR-2 glass (Fig. 6). The data show changes in the BCR-2 chemical composition in first 20 nanometers below the bottom of the crater. The sample is depleted in Li and Na relative to Si and Ca in the first 15 nm. The depletion in Ca extends up to 40 nm into the sample. This elemental fractionation results in the observed Li and Na signal ratio differences when normalized to Si and Ca, respectively.

Fractionation of alkali elements during laser ablation

FRACTIONATION OF ALKALI ELEMENTS DURING LA ICP-MS ANALYSIS OF SILICATE SAMPLES



Jitka Míková (mikova@cgu.cz)
Department of Geochemistry, Charles University &
Czech Geological Survey
Geologický 6, Prague 5, 152 00, CZECH REPUBLIC



Henry Longerich
Department of Earth Sciences
Memorial University of Newfoundland
300 Prince Philip Drive
St. John's, NL A1B 3X5, CANADA



Jan Košler
Department of Earth Science
University of Bergen,
Allegaten 41
N-5007 Bergen, NORWAY



Michael Wiedenbeck
SIMS Laboratory Section 4.2
Geoforschungszentrum Potsdam
Telegrafenberg C164
D14473 Potsdam, GERMANY

THEORY

Alkali element analysis of silicate samples is of a great importance for studying various rock-forming processes, age dating and thermobarometry. Alkali elements (Li, Na, K, Rb and Cs) are commonly present as major constituents in silicate minerals and natural glasses but they are often difficult to analyze by laser ablation (LA) ICP-MS. Sample interaction with the laser beam can induce element redistributions, formation of chemical gradients in samples and fractionation of alkali elements during the analysis. The exact mechanism and scale of such element redistribution is usually not known and it is often assumed that various diffusion mechanisms are involved in this process. It is expected that diffusion rates of alkali elements would reflect the ionic radius and charge of the ions, as well as chemical composition and structure of the sample and the thermal gradient that results from sample-beam interaction. A better understanding of elemental fractionation during LA ICP-MS is desirable not only to improve the precision alkali element analysis, but also for the potential use of alkali elements in correcting for ablation yield (as internal standards) in analyses of other lithophile elements that occur in geological samples.

Here we present results of alkali element measurements of synthetic silicate glasses (NIST-610, BCR-2) and natural crystalline albite by LA ICP-MS and SIMS. The experiments were designed to reveal some of the mechanisms that may be related to the alkali element fractionation during laser ablation.

EXPERIMENTAL

A. Laser ablation experiment

We have used a 213 nm Nd:YAG laser (New Wave, UP213) connected to an Element 2 Thermo Finnigan single collector ICP-MS at Bergen University (Fig. 1) to ablate silicate samples (NIST-610, BCR-2) and crystalline albite NaAlSi₃O₈. The laser was fired at 10 Hz repetition rate, with energy density of 3 J/cm² and laser spot diameter 30 μm. Samples were ablated in He atmosphere (1 l/min).



Fig. 1 Laser ablation ICP-MS facility at Bergen University

For the SIMS depth profiling measurements we utilized laser craters produced by 5 and 10 shots on each sample. Roughness of their bottoms and crater depth determinations were studied by Dektak 3 stylus profilometer. The laser parameters were 1Hz repetition rate, energy density 5 J/cm² and 80 μm spot diameter.

B. Ion probe experiments

Cameca ims 6f SIMS at Geoforschungszentrum Potsdam (Fig. 2) was used to measure the chemical composition of particles deposited in the ejecta blanket (Fig. 5) adjacent to ablation crater on the surface of the NIST-610 and albite samples. Several point profiles were conducted which extend from immediately at the edge of the laser ablation pit radially outwards to beyond the edge of the ejecta deposit (Fig. 6). The primary beam accelerating voltage was 22.5 kV, the ion beam current was 0.5 nA. Beam spot size was 5 μm with a secondary extraction voltage 10 kV. We additionally conducted a series of SIMS depth profile measurements at the bottom of ca. 80 μm wide laser ablation pits. The depth of craters was determined by Dektak 3 stylus profilometer (Fig. 9). The primary beam accelerating voltage was 22.5 kV and the ion beam current was 5 nA. Raster size was 70 μm with a secondary extraction voltage of 10 kV and a 30 μm field-of-view.



Fig. 2 SIMS facility at Geoforschungszentrum in Potsdam

RESULTS

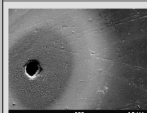


Fig. 5 Ejecta blanket deposited on NIST-610

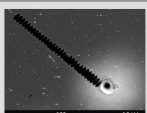


Fig. 6 SIMS profile across the ejecta blanket on albite sample

in the composition of particles with increasing distance from the laser pit. Li, Na and Rb intensity signal ratios relative to Si (Fig. 4) suggest a relative increase in the concentration of alkali elements towards the edge of the ejecta where smaller particles were deposited. Similar composition trends were found for the albite ejecta, except for the Na/Si ratio that shows a more complex variation.

B. Ion probe experiment

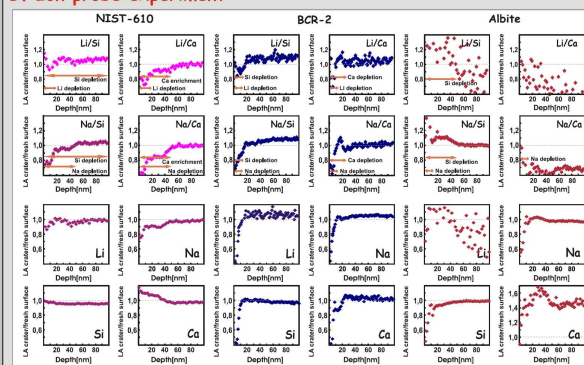


Fig. 7 Results of SIMS depth profiling experiment at bottom of 5 laser shot 80 μm wide laser pits. The measured elemental ratios are normalized to analyses of fresh sample surface.

The results from the SIMS depth profile measurements of the bottom of 80 μm wide laser ablation pits (Fig. 7) reveal changes in the chemical composition in first tens of nanometers below the bottom of the crater.

The **NIST-610** sample below the laser crater is depleted in both Li and Na in the first 20 nm and 50 nm relative to fresh sample surface, respectively. Si is slightly depleted up to the maximum measured depth of 290 nm, but the ratio of Si below laser crater to Si on fresh sample surface is stable. The Ca crater/fresh signal ratio shows the complete opposite trend to other elements and the sample below laser ablation pit seems to be enriched in Ca relative to fresh sample surface. The highest difference of signal ratios for one measured element is ca 30% for Na.

The **BCR-2** sample below laser crater is depleted in Li and Na relative to unaffected fresh sample surface in the first 15 nm below the bottom of the pit; Si is depleted in a zone that is 17 nm deep while the depletion in Ca extends up to 30 nm into the sample. For all elements in BCR-2 a maximum depletion of 60% was observed directly at the base of the laser crater with the degree of depletion decreasing with increasing depth.

The **Albite** sample beneath the laser crater is depleted in Na and Si to depths of 15 nm and 50 nm relative to the fresh sample surface, respectively. Li and Ca are not common constituents of natural albite material. Li signal shows much noise and the Ca signal may reflect inhomogeneity in our natural sample. It could explain strange behavior of those elements signals. The albite sample is the most depleted in Si with a 60% decrease in signal at the laser crater bottom relative to fresh material.

The elemental fractionation results in the observed Li and Na signal ratio differences when normalized to Si and Ca, respectively.

We also made SIMS scanning ion image qualitative distribution maps of laser craters in artificial andesite glasses doped with alkali elements. The images indicate that the laser ablation craters are depleted relative to surrounding area (Fig. 8).

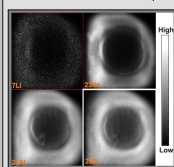


Fig. 8 SIMS measured qualitative distribution maps of laser crater in Na after SIMS depth profiling with depth of crater

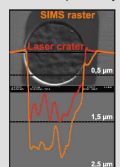


Fig. 9 SEM image of laser crater on NIST-610

RESULTS

A. Laser ablation experiment

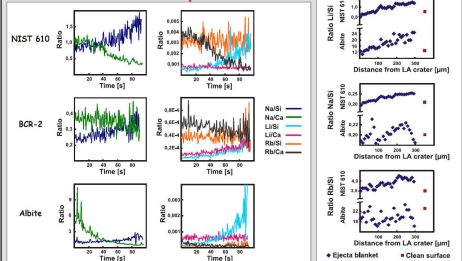


Fig. 3 Laser ablation ICP-MS measured signal intensity ratios of alkali elements, Si and Ca for NIST-610, BCR-2 and albite samples. Data are not corrected for blank, interferences and mass and Si for NIST-610 and albite (not discrimination).

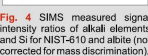


Fig. 4 SIMS measured signal intensity ratios of alkali elements Na/Si, Na/Ca, Li/Si, Li/Ca, Rb/Si, and Rb/Ca for NIST-610 and albite (not corrected for mass discrimination).

The LA ICP-MS measured time resolved signal intensity ratios of the alkali elements to Si and Ca often show opposite fractionation trends (Fig. 3). Analyses of the NIST-610 and albite ejecta blanket show a systematic change

CONCLUSIONS

- ❖ Na during laser ablation ICP-MS analysis consistently showed an enrichment relative to Si and a depletion relative to Ca irrespectively of the sample matrix. The degree of depletion/enrichment was found to be matrix dependent. Similarly consistent behavior for all studied sample matrices was observed for Li but fractionation of Rb relative to Si and Ca was matrix dependent.
- ❖ Variations in alkali element contents in sample adjacent to the bottom of the laser pit and chemical variations measured by SIMS across the ejecta blanket suggest that (i) significant fractionation of alkali elements relative to Si and Ca takes place at the ablation site and (ii) that different particle size fractions fractionate alkali element to different extent.
- ❖ SIMS depth profiles show modifications in the chemical composition of sample in the first tens of nanometers below the bottom of the laser crater not only for alkali elements, but also for matrix elements like Si and Ca. Most elements are depleted and the degree of modification is matrix dependent.
- ❖ SIMS depth profiling and analysis of the ejecta blanket suggest that a complex combination of thermally-driven diffusion and particle size fractionation may be responsible for the observed decoupling of alkali elements from Si and Ca during laser ablation.

Dendrochemical record of Pb pollution

LASER ABLATION AND ISOTOPE DILUTION ICP-MS ANALYSIS OF Pb IN SPRUCE TREE RINGS A RECORD OF ATMOSPHERIC POLLUTION IN NW BOHEMIA

Jan Kosler, Martin Novak, Michael Krachler and Jitka Mikova

Centre for Geobiology, University of Bergen, Norway

Czech Geological Survey, Prague, Czech Republic

Institute of Environmental Chemistry, University of Heidelberg, Germany

jan.kosler@geo.uib.no

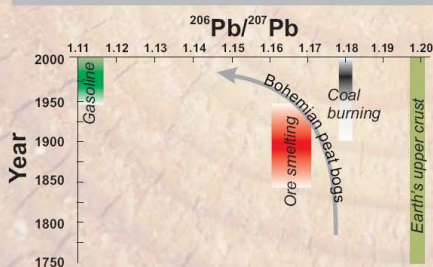


AIM OF THIS STUDY

This study attempts to assess a dendrochemical Pb record along the north-south pollution gradient in the Czech Republic. We compared the Norway spruce (*Picea abies*) tree ring Pb record with the known industrial emission rates during the 20th century, and also with published Pb data from *Sphagnum* peat profiles. Lead pollution in Central Europe is dominated by incineration of soft coal in power stations, which produce extremely small aerosol particles containing Pb. It is assumed that the trees can directly absorb these airborne particles, and deposit them in annual growth rings, making the dendrochemical patterns a reliable archive of past Pb pollution. This study also compares Pb isotope records obtained by two analytical techniques, in-situ analysis of tree rings by laser ablation multi-collector ICP-MS and single-collector ICP-MS analysis of digested xylem.

This study explores the possibilities of using dendrochemical record to study the past Pb atmospheric pollution.

Pb POLLUTION RECORD IN PEAT BOGS



Isotopic composition of Pb in Bohemian peat bogs reflects the temporal changes of sources of atmospheric pollution. (Novak et al., EST 2003, 37, 437-445)

SAMPLES

Samples of Norway spruce were taken from industrially polluted northern Czech Republic (site JEZ "Jedlak" in the Erzgebirge). Reference sample (LIZ) was taken from non-polluted area in southern Czech Republic.



EXPERIMENTAL

Single collector ICP-MS solution measurement

Concentric segments of 5 consecutive tree rings sampled ca 1.5 m above ground were cut from the trunk, homogenized and dried at 60 °C. Samples were digested in a mixture of H₂SO₄, HNO₃, and HF at 200 °C and the digests were analyzed with single collector sector field ICP-MS (Thermo Finnigan Element 2) at UoH. A sample introduction consisted of a microflow PFA nebulizer, a Scott-type PFA spray chamber and a sapphire injector tube. External precision of ²⁰⁶Pb/²⁰⁷Pb and ²⁰⁹Pb/²⁰⁷Pb isotopic measurements were better than 0.05 % and 0.1 % for Pb concentrations of 1 and 0.1 ppm, respectively. Repeat measurements of SRM 981 were used to correct data for instrument mass discrimination.

Laser ablation multicollector ICP-MS measurement

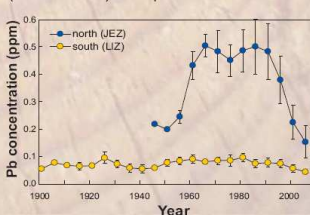
Section of the xylem (4 x 4 x 200 mm) cut perpendicular to the growth rings was mounted in 1 inch epoxy blocks and diamond-polished in ethanol to obtain flat and smooth surfaces. Isotopic composition of Pb in denser latewood segments of the tree rings was measured using an Nd:YAG 213 nm laser (New Wave UP-213) coupled to a Thermo Finnigan Neptune multicollector ICP-MS at UoB. The laser was fired with energy of 3 J/cm², laser beam diameter of 100 microns and repetition rate of 20 Hz. The laser beam was scanned across the sample surface to ablate linear rasters 600 microns long parallel to the tree rings. The ablation cell was flushed with He (0.7 L min⁻¹) that was mixed with Ar gas (1 L min⁻¹) carrying Tl tracer solution which was aspirated to the plasma through an APEX (Elemental Scientific) desolvating nebulizer. The data were corrected for gas blank and Hg interference on ²⁰⁹Pb. Correction for instrument mass discrimination of Pb isotopes utilized the exponential law and measurement of Tl isotopic composition in the tracer solution. In-house wood pressed powder pellet standard (420 ppb Pb) was periodically analyzed during this study for quality control.



Sample mount and laser ablation pits in tree rings (track length is 600 microns).

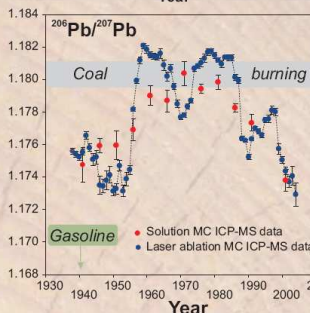
Pb POLLUTION RECORD IN TREE RINGS

Lead concentration and isotope trends determined in Norway spruce (*Picea abies*) from polluted site in the northern Czech Republic shows



a distinct Pb concentration maximum and a ²⁰⁶Pb/²⁰⁷Pb isotope signature close to that of coal Pb (1.18) in the second half of the 20th century, coinciding with elevated industrial Pb emission rates.

Tree rings from a relatively unpolluted site in the southern Czech Republic show no change in their low Pb concentrations over the past 100 years



Laser ablation multicollector ICP-MS and solution single collector ICP-MS provided consistent data sets. However, the laser ablation sampling is faster and yields a time resolution that is potentially better than 1 year.

Picea abies growth rings faithfully record historical changes in atmospheric Pb pollution.

Presented at Plasma Spectrochemistry Winter Conference, Graz, February 2009

www.geobio.uib.no